Published for SISSA by Springer

Received: *September 28, 2021*
Accepted: *January 12, 2022*
Published: *January 28, 2022*

Measurement of double-parton scattering in inclusive production of four jets with low transverse momentum in proton-proton collisions at $\sqrt{s} = 13$ TeV

The CMS collaboration

E-mail: cms-publication-committee-chair@cern.ch

Abstract: A measurement of inclusive four-jet production in proton-proton collisions at a center-of-mass energy of 13 TeV is presented. The transverse momenta of jets within $|\eta| < 4.7$ are required to exceed 35, 30, 25, and 20 GeV for the first-, second-, third-, and fourth-leading jet, respectively. Differential cross sections are measured as functions of the jet transverse momentum, jet pseudorapidity, and several other observables that describe the angular correlations between the jets. The measured distributions show sensitivity to different aspects of the underlying event, parton shower modeling, and matrix element calculations. In particular, the interplay between angular correlations caused by parton shower and double-parton scattering contributions is shown to be important. The double-parton scattering contribution is extracted by means of a template fit to the data, using distributions for single-parton scattering obtained from Monte Carlo event generators and a double-parton scattering distribution constructed from inclusive single-jet events in data. The effective double-parton scattering cross section is calculated and discussed in view of previous measurements and of its dependence on the models used to describe the single-parton scattering background.

Keywords: Hadron-Hadron Scattering , Jets, QCD

ArXiv ePrint: 2109.13822

https://doi.org/10.1007/JHEP01(2022)177

Contents

1 Introduction **1**

2 Observables **3**

3 Measuring jets with the CMS detector **5**

4 Monte Carlo event generators **6**
- 4.1 The PYTHIA8, HERWIG++, and HERWIG7 models 6
- 4.2 Multijet models 7
- 4.3 SPS+DPS samples 8

5 Event selection and unfolding **9**

6 Extraction of the effective cross section **10**

7 Systematic uncertainties **11**

8 Results **13**
- 8.1 The PYTHIA8 and HERWIG models 14
- 8.2 Multijet models 19
- 8.3 SPS+DPS models 21
- 8.4 Extraction of the effective cross section 27

9 Summary **32**

The CMS collaboration **41**

JHEP01(2022)177

1 Introduction

Quantum chromodynamics (QCD), the theory of strong interactions, provides a good description of the production of hadron jets with large transverse momentum (p_{T}) in high-energy proton-proton (pp) collisions. This is achieved by factorizing the cross section into a perturbatively calculable matrix element describing the scattering between partons, and parton distribution functions (PDFs) that provide the probability to find a parton with given properties within the proton. The PDFs cannot be perturbatively calculated and are obtained by fitting available data. This fitting process includes nonperturbative effects such as the underlying event, hadronization, and parton showering. Measurements of the cross section for the production of inclusive high-p_{T} jets have been performed by the CMS collaboration at various center-of-mass energies and show agreement with perturbative QCD predictions at next-to-leading-order (NLO) accuracy [1–3]. However, final

states with multiple jets are not as well understood [4], suggesting a need for additional theoretical treatments of the strong interaction.

Multijet final states can be produced in a single-parton scattering (SPS). Depending on the order of the matrix element in the strong coupling, two or more jets can be produced in SPS. Radiation before and/or after the interaction between the partons, as described by parton shower models, can contribute additional jets to the final state. Thus, predictions for multijet processes in SPS provide an important test of the matching between fixed-order matrix element calculations and the parton-shower formalism. A different approach introduces an additional hard scattering in the pp collision, which also contributes a number of jets to the final state. Such processes are in general referred to as double-parton scattering (DPS), and they represent the simplest case of multiple-parton interactions (MPI). A schematic depiction of inclusive four-jet production through SPS and DPS is shown in figure 1.

The cross section of a DPS process, $\sigma_{\mathrm{A,B}}^{\mathrm{DPS}}$, where A and B denote two processes with their own respective cross sections σ_{A} and σ_{B}, can be expressed as:

$$\sigma_{\mathrm{A,B}}^{\mathrm{DPS}} = \frac{m}{2}\frac{\sigma_{\mathrm{A}}\sigma_{\mathrm{B}}}{\sigma_{\mathrm{eff}}}. \tag{1.1}$$

The factor m is a combinatorial factor, which is equal to 1 for identical processes and 2 for nonidentical processes. The effective cross section (σ_{eff}) reflects how strongly the occurrence of A and B is correlated [5]. For fully uncorrelated production of A and B, σ_{eff} tends to the total inelastic pp cross section, whereas a small σ_{eff} indicates an enhanced simultaneous occurrence of processes A and B. For multijet production, SPS processes often exhibit strong kinematic correlations between all jets, whereas DPS processes will manifest a distinctly different behavior. Indeed, the jets resulting from DPS are more often produced in two independent pairs, each in a back-to-back configuration in the transverse plane. The relevance of DPS rises with increasing center-of-mass energy; at higher energy and for fixed p_{T} of the jets, smaller values of the momentum fraction of the protons carried by the partons are probed, resulting in a strong increase of the gluon density and a larger probability for DPS. A study of the extent to which DPS processes can supplement various SPS models is therefore beneficial for a complete description of hadronic interactions.

Various DPS measurements at different center-of-mass energies and for various final states have been performed. Studies including one or two photons in the final state have been published in refs. [6–10]. Signatures involving one or two vector bosons have been measured by the ATLAS and CMS Collaborations [11–15]. Other studies have opted to include the production of heavy flavors [16–20]. Earlier measurements in the four-jet final state have been performed by the UA2 and CDF experiments [21, 22]. The ATLAS and CMS Collaborations have more recently also performed DPS measurements with four jets [4, 23–25] at a center-of-mass energy of 7 TeV. The CMS Collaboration additionally performed at 7 TeV [26] a measurement of the final state with two b-tagged jets in combination with two light-flavored jets.

This paper presents an analysis of the inclusive production of four-jet events in pp collisions at a center-of-mass energy of 13 TeV. The data correspond to an integrated luminosity of 42 nb^{-1} and were collected with the CMS detector at the CERN LHC in 2016

JHEP01(2022)177

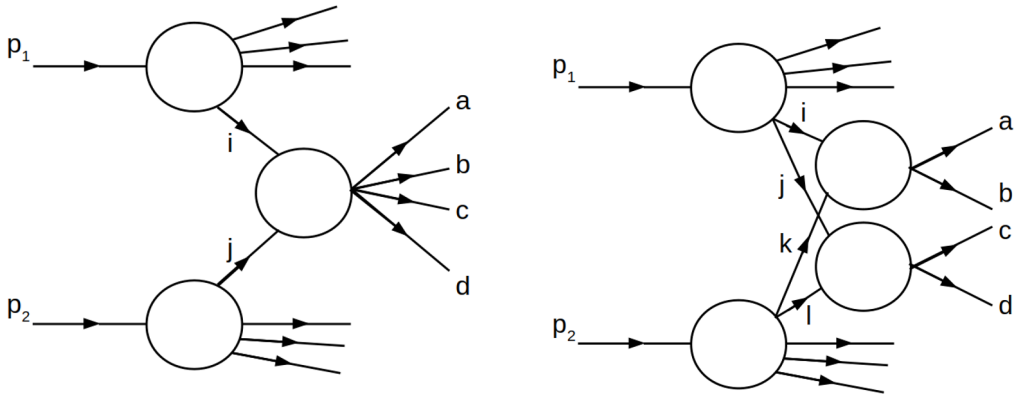

Figure 1. A schematic depiction of inclusive four-jet production through SPS (left) and DPS (right). In the case of SPS, one hard scattering produces the jets a through d, whereas two independent hard scatterings create two jets each in the case of DPS. Since the two jet pairs are created independently in a DPS event, they are expected to show different kinematic correlations compared with the four jets originating from an SPS event.

during a special data-taking period with a low probability for several pp interactions occurring within the same or neighbouring bunch crossings (pileup). This avoids the challenges posed by pileup and enables us to include jets with low p_{T}. As a result of the low-p_{T} jets, a custom calibration of the jet energy scale is required. Data are corrected for detector efficiency and resolution effects by means of an unfolding procedure.

Several aspects of multijet production are studied by comparing the distributions of DPS-sensitive observables predicted by various Monte Carlo (MC) event generators with the distributions measured in data. These observables all exploit differences in the kinematic correlations between the jets expected for SPS and DPS. The DPS cross section is extracted with a template method. A pure DPS signal template is reconstructed from data by randomly mixing two inclusive single-jet events into one inclusive DPS four-jet event. This is then fitted together with several SPS-only background MC models to the distributions obtained from inclusive four-jet data. Finally, the effective cross section is computed using eq. (1.1), with σ_{A} and σ_{B} measured from data.

Tabulated results are provided in the HEPData record for this analysis [27].

This paper is organized as follows. In section 2, the observables of interest are defined. Section 3 gives a brief overview of the CMS detector. The MC models used in the comparison with data are detailed in section 4, whereas the data samples, event selection, and correction procedure are discussed in section 5. The strategy for the extraction of the DPS cross section and σ_{eff} is detailed in section 6. Systematic uncertainties for each of the unfolded observables are discussed in section 7. Section 8 contains a discussion of the results, which are summarized in section 9.

2 Observables

Six observables are defined to study DPS in four-jet production processes. Many of these variables have been used in earlier measurements [4, 6–14, 16–20, 23–26] and in phenomeno-

JHEP01(2022)177

logical studies [28–33]. The four leading jets are ordered with decreasing p_{T}. Based on the azimuthal angle (ϕ), pseudorapidity (η), and transverse momentum vector ($\vec{p}_{\mathrm{T}}$), the variables studied in this paper can be described as follows.

- The azimuthal angular difference between the two softest jets:

$$\Delta\phi_{\mathrm{Soft}} = |\phi_3 - \phi_4|.$$

  The two softest jets are more likely to be in a back-to-back configuration when produced by DPS since there is an increased probability that the two softest jets are produced in an independent scattering from the two hardest jets and since the momentum should be conserved in the transverse plane. The increased probability leads to an enhanced DPS contribution around $\Delta\phi_{\mathrm{Soft}} = \pi$.

- The minimal combined azimuthal angular range of three jets:

$$\Delta\phi_{3\mathrm{j}}^{\mathrm{min}} = \min\left\{|\phi_i - \phi_j| + |\phi_j - \phi_k| | i,j,k \in [1,2,3,4], i \neq j \neq k\right\}.$$

  In DPS, at least two out of three jets are more likely to be in a back-to-back configuration, while SPS processes have a more random distribution in their azimuthal angular difference. Therefore, a DPS process is prone to yield larger values of $\Delta\phi_{3\mathrm{j}}^{\mathrm{min}}$ [33].

- The maximum η difference between two jets:

$$\Delta Y = \max\left\{|\eta_i - \eta_j| | i,j \in [1,2,3,4], i \neq j\right\}.$$

  As the maximum separation in η between two jets becomes larger, the probability for the two jets to originate from two different parton interactions increases.

- The azimuthal angular difference between the jets with the largest η separation:

$$\phi_{ij} = |\phi_i - \phi_j| \quad \text{for} \quad \Delta Y = |\eta_i - \eta_j|$$

  Since the jets with the largest η separation are more likely to be produced in separate DPS subprocesses, a decorrelation in the distribution of the azimuthal angular difference of these jets is expected, whereas the jets will show stronger correlations in a SPS event.

- The transverse momentum balance of the two softest jets:

$$\Delta p_{\mathrm{T,Soft}} = \frac{|\vec{p}_{\mathrm{T},3} + \vec{p}_{\mathrm{T},4}|}{|\vec{p}_{\mathrm{T},3}| + |\vec{p}_{\mathrm{T},4}|}.$$

  When the two softest jets originate from a DPS process, they are more likely to be in a back-to-back configuration rendering the value for $\Delta p_{\mathrm{T,Soft}}$ small. In SPS processes, the two softest jets do not necessarily balance.

JHEP01(2022)177

- The azimuthal angular difference between the hard and the soft jet pairs:

$$\Delta S = \arccos\left(\frac{(\vec{p}_{\mathrm{T},1} + \vec{p}_{\mathrm{T},2}) \cdot (\vec{p}_{\mathrm{T},3} + \vec{p}_{\mathrm{T},4})}{|\vec{p}_{\mathrm{T},1} + \vec{p}_{\mathrm{T},2}|\ |\vec{p}_{\mathrm{T},3} + \vec{p}_{\mathrm{T},4}|}\right).$$

  In a SPS process, the four jets must balance so that the ΔS distribution peaks around π, while in DPS the two jet pairs are more likely to be independently produced, yielding a less correlated ΔS distribution. Thus we anticipate that DPS events tend toward lower values of ΔS.

3 Measuring jets with the CMS detector

The central feature of the CMS apparatus is a superconducting solenoid of 6 m internal diameter, providing a magnetic field of 3.8 T. Within the solenoid volume are a silicon pixel and strip tracker, a lead tungstate crystal electromagnetic calorimeter (ECAL), and a brass and scintillator hadron calorimeter (HCAL), each composed of a barrel and two endcap sections. Forward calorimeters extend the η coverage provided by the barrel and endcap detectors. Muons are detected in gas-ionization chambers embedded in the steel flux-return yoke outside the solenoid.

The silicon tracker measures charged particles within the range $|\eta| < 2.5$. During the LHC running period when the data used in this paper were recorded, the silicon tracker consisted of 1440 silicon pixel and 15 148 silicon strip detector modules.

The ECAL consists of 75 848 lead tungstate crystals, which provide coverage in $|\eta| < 1.48$ in a barrel region and $1.48 < |\eta| < 3.0$ in the two endcap regions. Preshower detectors consisting of two planes of silicon sensors interleaved with a total of $3X_0$ of lead are located in front of each endcap detector.

In the region $|\eta| < 1.74$, the HCAL cells have widths of 0.087 in η and 0.087 in azimuth (ϕ). In the η-ϕ plane, and for $|\eta| < 1.48$, the HCAL cells map on to 5×5 arrays of ECAL crystals to form calorimeter towers projecting radially outwards from close to the nominal interaction point. For $|\eta| > 1.74$, the coverage of the towers increases progressively to a maximum of 0.174 in $\Delta\eta$ and $\Delta\phi$. Within each tower, the energy deposits in ECAL and HCAL cells are summed to define the calorimeter tower energies.

The forward hadron (HF) calorimeter uses steel as an absorber and quartz fibers as the sensitive material. The two halves of the HF are located 11.2 m from the interaction region, one on each end, and together they provide coverage in the range $3.0 < |\eta| < 5.2$. They also serve as luminosity monitors.

Events of interest are selected using a two-tiered trigger system. The first level (L1), composed of custom hardware processors, uses information from the calorimeters and muon detectors to select events at a rate of around 100 kHz within a fixed latency of about 4 μs [34]. The second level, known as the high-level trigger (HLT), consists of a farm of processors running a version of the full event reconstruction software optimized for fast processing, and reduces the event rate to around 1 kHz before data storage [35].

A global event reconstruction (particle flow) algorithm [36] reconstructs and identifies each individual particle in an event, with an optimized combination of all subdetector

JHEP01(2022)177

information. Jets are clustered from these reconstructed particles using the infrared and collinear safe anti-k_{T} algorithm [37, 38] with a distance parameter of 0.4. The jet momentum is determined as the vectorial sum of the momenta of all particles in the jet, and is typically within 5 to 10% of the true momentum over the whole p_{T} spectrum and detector acceptance, based on simulation. Jet-energy corrections are derived from simulation studies so that the average measured energy of jets becomes identical to that of particle-level jets. In situ measurements of the momentum balance in dijet, photon+jet, Z+jet, and multijet events are used to determine any residual differences between the jet-energy scale in data and in simulation, and appropriate corrections are made [39]. Additional selection criteria are applied to each jet to remove those potentially dominated by instrumental effects or reconstruction failures. The jet-energy resolution varies with rapidity and transverse momentum and typically amounts in the central region to 20–25% at 20 GeV, 10% at 100 GeV, and 5% at 1 TeV [39].

A more detailed description of the CMS detector, together with a definition of the coordinate system and the kinematic variables, can be found in ref. [40].

4 Monte Carlo event generators

4.1 The PYTHIA8, HERWIG++, and HERWIG7 models

The PYTHIA8 [41], HERWIG++ [42], and HERWIG7 [43] MC event generators use $2 \to 2$ leading order (LO) matrix elements, matched to a DGLAP evolution [44–46] at leading logarithmic level for the simulation of the parton shower. By default, a p_{T}-ordered parton shower is implemented in PYTHIA8, whereas an angular-ordered parton shower is used in HERWIG++ and HERWIG7 (jointly referred to as HERWIG). For hadronization, PYTHIA8 uses the Lund string model [47], whereas HERWIG relies on the cluster model [48]. The generators are interfaced with different sets of predetermined parameters (or "tunes") for the description of the underlying event, including MPI. These tunes are obtained from fitting predictions to data. Of all the generated samples, two have been passed through the detector simulation program GEANT4 [49]. These two samples will be used to correct the data for detector effects by means of an unfolding procedure. The configurations used in this paper to generate events with PYTHIA8 and HERWIG, are listed below.

- The PYTHIA8.240 generator is interfaced with three different tunes, i.e., the CUETP8M1 tune [50, 51], the CP5 tune [52] and the CDPSTP8S1-4j tune [51].

  The PYTHIA8 sample, interfaced with the CUETP8M1 tune, uses the NNPDF2.3_LO PDFs [53]. The simulation of the detector effects has been applied to these generated events since they will be used to correct the data through an unfolding procedure.

  The PYTHIA8 sample interfaced with the CP5 tune uses the NNPDF3.1 next-to-next-to-leading order (NNLO) PDFs [53].

  The CDPSTP8S1-4j tune [51] is a CMS DPS tune, based on the standard Tune 4C [54], where parameters related to MPI and DPS have been altered to fit predictions to the $\Delta p_{\mathrm{T,Soft}}$ and ΔS distributions obtained from an inclusive four-jet measurement at a center-of-mass energy of 7 TeV [51]. This tune uses the CTEQ6L1 PDFs [55].

JHEP01(2022)177

- An additional PYTHIA8.301 sample is generated with VINCIA [56] activated, which replaces the p_{T}-ordered parton shower from PYTHIA8 with a dipole-antenna shower. The default parameter values of PYTHIA8.301 and the NNPDF2.3_LO PDFs are used.

- The HERWIG++ 2.7.1 generator is used in combination with the CUETHS1 tune [51] and the CTEQ6L1 PDFs. This sample is also passed through the detector simulation program GEANT4 and is used in the unfolding procedure.

- Two tunes are used for the HERWIG 7.1.5 MC event generator.

  The SoftTune is the default tune provided by the HERWIG7 authors and uses the MMHT2014lo68cl PDFs [57].

  The CH3 tune has been obtained by the CMS Collaboration from a study of underlying event measurements [58]. It is used in combination with the NNPDF2.3_NNLO PDF.

4.2 Multijet models

A second group of models, referred to as the multijet models, uses higher-order matrix elements to produce more than two jets in the hard parton scattering. These MC event generators are interfaced with PYTHIA, HERWIG, or CASCADE [59] to include a description of the underlying event. Details of the generated event samples are given below.

- MADGRAPH5_aMC@NLO (version 2.6.5) [60] is a generator with the ability to compute tree-level and NLO matrix elements for arbitrary processes. Two LO samples and one NLO sample are generated, as listed below.

  The LO samples combine a $2 \to 2$, a $2 \to 3$, and a $2 \to 4$ matrix element, referred to as $2 \to 2, 3, 4$. An $H_{\mathrm{T}} > 50\,\mathrm{GeV}$ generation condition is used, where H_{T} is defined as the scalar sum of the transverse momenta of the produced partons, and all partons must have $|\eta| < 5$. For one sample the description of the underlying event, parton shower, and hadronization is handled by PYTHIA8.240, using the CP5 tune, whereas the other sample is interfaced to PYTHIA8.301 with VINCIA. The former uses the NNPDF2.3_NNLO PDFs, whereas the latter uses the NNPDF2.3_LO PDFs. The MLM scheme [61] is used to match jets produced via matrix-element calculations with those from parton showers, using the matching p_{T} scale of 18 GeV, which was optimized by analyzing the differential jet-rate distributions.

  The $2 \to 2$ NLO sample is interfaced with PYTHIA8.240, using the CP5 tune with the NNPDF2.3_NNLO PDFs and an MLM matching scheme. The two leading partons are required to lie within $|\eta| < 5$ and have a p_{T} above 25 and 20 GeV, respectively.

- POWHEGBOX version 3633 (2019.02.25) [62–64] is a framework for implementing NLO corrections in MC event generators. Each event is constructed by producing the Born configuration, on which the real phase space is built afterwards. Two different samples are generated, both are interfaced with PYTHIA8.240, using the CP5 tune along with the NNPDF2.3_NNLO PDFs.

JHEP01(2022)177

A first sample is generated with a $2 \to 2$ NLO matrix element [65]. The factorization and renormalization scales are set to the p_{T} of the underlying Born configuration.

A second sample was generated with a $2 \to 3$ NLO matrix element [66]. The generator-level minimal p_{T} of the underlying Born configuration is set to 10 GeV, and the factorization and renormalization scales are set to $H_{\mathrm{T}}/2$.

- KaTie version 23April2019 [67] is a LO parton-level event generator, based on k_{T}-factorization [68–70], allowing for on-shell and off-shell production. In the case of the latter, the initial partons are generated with a nonzero intrinsic k_{T}, which can alter the momentum balance of the jets, yielding various topologies and correlations between the jets compared with on-shell production. A $2 \to 4$ matrix element is used for all samples generated with KaTie. The generator-level requirements for the p_{T} of the four partons produced by the matrix element are 35, 30, 25, and 20 GeV, and their rapidities are limited to $|\eta| < 5.0$. Since the p_{T} requirements are introduced at parton level, the effective p_{T} thresholds for the resulting hadron-level jets are typically 5 to 10 GeV lower. The factorization and renormalization scales are set to $H_{\mathrm{T}}/2$. Two on-shell and two off-shell samples are produced.

  The two on-shell samples are interfaced with pythia8.240 and herwig 7.1.5, along with the CP5 and CH3 tunes, respectively. Both samples use the NNPDF2.3_NNLO PDFs.

  For the two off-shell samples, the showering and hadronization is handled by Cascade 3.0.01-beta1. Two different transverse-momentum-dependent (TMD) PDFs are used: the MRW-CT10nlo TMD PDFs (MRW) [71] and the PB-NLO-HERAI+II-2018-set2 TMD PDFs (PBTMD) [72].

4.3 SPS+DPS samples

The pythia8.240 and KaTie MC event generators both produce two $2 \to 2$ matrix elements per event, resulting in a pure DPS sample. MPIs are also present as part of the underlying event. In KaTie, σ_{eff} is a parameter that directly determines the size of the DPS contribution relative to the SPS cross section. A value of 21.3 mb for σ_{eff} is adopted, as in [51]. For pythia8, it is not possible to set σ_{eff}, because it is determined by the underlying event parameters, and therefore the second $2 \to 2$ process is simply added with the same kinematic requirements, without any additional scaling of the cross section.

Four samples with an explicit DPS contribution are used in this paper.

- A pythia8.240 sample is generated with the CP5 tune and the NNPDF2.3_NNLO PDFs. It is the aforementioned pythia8 sample to which a pure DPS sample, obtained by overlaying two $2 \to 2$ matrix elements, is added.

- The second pythia8 sample, which includes an explicit DPS contribution, is the one already mentioned in section 4.1, since the CDPSTP8S1-4j tune has been fitted to DPS-sensitive observables.

JHEP01(2022)177

- An on-shell KaTie sample is generated with an explicit DPS contribution that is obtained by overlaying two $2 \to 2$ matrix elements, with the exact same generation parameters as the on-shell KaTie LO sample from the multijet models. Showering and hadronization are handled by pythia8.240 with the CP5 tune and the NNPDF2.3_NNLO PDFs.
- Two off-shell KaTie samples with an explicit DPS contribution are generated using the same TMD PDFs as for the multijet samples. Since Cascade cannot handle two $2 \to 2$ matrix elements, nonperturbative corrections have been derived from the on-shell SPS and DPS KaTie samples, and are applied to the off-shell DPS KaTie parton level sample. The nonperturbative corrections range from 1–4% for all observables, except for the ΔS observable for which corrections up to 11% were found.

5 Event selection and unfolding

This analysis uses data from pp collisions at a center-of-mass energy of 13 TeV, collected during a data taking period at low luminosity, with an average pileup of 1.3 and an integrated luminosity of 42 nb^{-1}. The online selection of multi-jet events was based on four single-jet triggers each requiring the presence of at least one jet with a p_{T} above 30, 50, 80, or 100 GeV, and within $|\eta| < 4.7$. Because the triggers have been prescaled, they are used in disjoint p_{T} ranges. Offline requirements are imposed to ensure that the triggers are fully efficient, except for the trigger with the lowest p_{T} threshold. In this last case, a correction as a function of the jet p_{T} is applied to the selected event, effectively altering its weight. The trigger efficiency was determined by comparing the performance of the jet trigger with a minimum-bias trigger serving as an unbiased reference.

Events are selected offline by requiring exactly one primary vertex, so effects of pileup can be neglected. The correction of the event yield is based on the measurement of the average pileup and has negligible uncertainty. A systematic uncertainty due to a possible contamination of events containing two or more pp collisions is nevertheless included in the results. Two phase space regions defined by selections on jet p_{T} are used. In *Region* I, the four leading jets within $|\eta| < 4.7$ are required to exceed p_{T} thresholds of 35, 30, 25, and 20 GeV. Asymmetric thresholds have been chosen over symmetric ones because the latter tend to dampen the DPS contribution with respect to the SPS fraction, according to higher-order calculations or calculations performed in the k_{T}-factorization framework [31, 33]. The ΔS distribution is obtained in *Region* II, with p_{T} thresholds of 50, 30, 30, and 30 GeV. On the one hand, the resolution of the ΔS observable is improved by imposing higher p_{T} cuts. On the other hand, the ΔS observable can now be used to perform the extraction of σ_{eff}, using the lowest jet-p_{T} trigger threshold of 30 GeV. The second set of selections is needed to obtain the cross sections σ_{A} and σ_{B}, as detailed in section 6.

The measured distributions are corrected for detector effects with the TUnfold program [73, 74], which is based on a least squares fit and Tikhonov regularization [75]. The regularization is necessary to avoid possible instabilities in the inversion of the matrix describing the migrations within the phase space. Bin-to-bin migrations are kept to a minimum by choosing a bin width that is two times larger than the resolution of the considered

JHEP01(2022)177

variable, as obtained from a simulation study with PYTHIA8. The migration matrix, as well as the probabilities for migration into and out of the phase space, are obtained from the PYTHIA8 and HERWIG++ MC models.

6 Extraction of the effective cross section

The DPS formula (1.1) allows the calculation of σ_{eff} if the DPS cross section, as well as the cross sections of the two Processes A and B, are known. In the simplest case, the Processes A and B would both be dijet production, resulting in a four-jet final state with uncorrelated jet pairs, as depicted in figure 1. However, initial- and final-state radiation, and higher-order interactions can produce final states with more than two jets, yielding additional possibilities to form a four-jet topology.

To avoid additional model dependencies, a DPS signal template is constructed from data, following an approach similar to the one laid out in ref. [25]. The Processes A and B are both defined as inclusive single-jet production. Combining two events of Type A and B will result in a multijet final state. Whenever at least four jets are found in the combined final state originating from the same process, the combined event is labeled as SPS process, otherwise the event is labeled as a DPS process.

Region II is used for the extraction of σ_{eff}. The choice is motivated by ref. [31] where it is suggested that such asymmetric cuts could boost the DPS signature. The cross sections of the Processes A and B are defined as inclusive single jet production with

$$\sigma_{\text{A}} = \sigma_{\text{jet}}\,(p_{\text{T}} \geq 50)\,,$$
$$\sigma_{\text{B}} = \sigma_{\text{jet}}\,(p_{\text{T}} \geq 30)\,.$$

Combining two inclusive single-jet processes results in final states with at least four jets in only a fraction of the cases. A "four-jet efficiency" ($\epsilon_{4\text{j}}$) has been obtained from the combined sample as detailed below.

From the event sample with at least one jet with $p_{\text{T}} > 30\,\text{GeV}$, two events are drawn at random with the second event containing at least one jet with $p_{\text{T}} > 50\,\text{GeV}$. The two selected events are combined to form one single event. A combined event is discarded whenever two or more jet axes spatially coincide. This veto condition is formulated as $R_{ij} = ((\phi_i - \phi_j)^2 + (\eta_i - \eta_j)^2)^{1/2} \geq 0.4$, where the indices i and j indicate jets belonging to the first and second event, respectively. The newly constructed combined event sample is then subjected to the four-jet selection criteria of *Region* II. The four-jet efficiency was estimated to be

$$\epsilon_{4\text{j}} = 0.324^{+0.037}_{-0.065}\,(\text{syst}), \tag{6.1}$$

where the statistical uncertainty is negligible and the systematic error is detailed in the next section.

The ΔS observable is chosen for the extraction of the DPS cross section and σ_{eff} because it is the least affected by parton shower effects. The signal template is taken from the combined data sample, which is used to extract the ΔS distribution in exactly the same manner as before, including the correction for detector effects by means of unfolding.

JHEP01(2022)177

The SPS MC models are taken as background templates. To avoid contamination by MPI, additional samples are provided where an event is omitted if it contains a generator level parton with a $p_{\mathrm{T}} > 20\,\mathrm{GeV}$ that originates from a MPI. This selection ensures that no hard jets originating from MPI enter the four-jet analysis, and will be referred to as "hard MPI removed".

The fraction of DPS events, f_{DPS}, is extracted by performing a template fit to the unfolded ΔS distribution, obtained from the original inclusive four-jet sample. The DPS signal and SPS background ΔS distributions are both normalized to the integral of the ΔS distribution obtained from the four-jet events in data. The optimal value of the DPS fraction f_{DPS} is determined with a maximum likelihood technique using Poisson statistics [76]:

$$\sigma^{\mathrm{data}}(\Delta S) = f_{\mathrm{DPS}}\sigma^{\mathrm{data}}_{\mathrm{DPS}}(\Delta S) + (1 - f_{\mathrm{DPS}})\sigma^{\mathrm{MC}}_{\mathrm{SPS}}(\Delta S). \tag{6.2}$$

The cross section $\sigma^{\mathrm{DPS}}_{\mathrm{A,B}}$, needed for the extraction of σ_{eff}, is then given by the integral of the ΔS distribution measured in data, scaled with the DPS fraction f_{DPS}:

$$\sigma^{\mathrm{DPS}}_{\mathrm{A,B}} = f_{\mathrm{DPS}} \int \sigma^{\mathrm{data}}(\Delta S)\mathrm{d}(\Delta S). \tag{6.3}$$

Because of the overlapping p_{T} ranges, the Processes A and B are not always distinguishable and the cross section for Process B has therefore to be rewritten as the sum of the cross section for Process A (σ_{A}) and the difference between the cross sections for Processes B and A ($\sigma_{\mathrm{B}} - \sigma_{\mathrm{A}}$). Taking into account the correct combinatorial factor along with the four-jet efficiency, the DPS formula (1.1) can be reformulated as:

$$\sigma^{\mathrm{DPS}}_{\mathrm{A,B}} = \frac{\epsilon_{4\mathrm{j}}}{\sigma_{\mathrm{eff}}}\left(\frac{1}{2}\sigma^2_{\mathrm{A}} + \sigma_{\mathrm{A}}(\sigma_{\mathrm{B}} - \sigma_{\mathrm{A}})\right) = \frac{\epsilon_{4\mathrm{j}}\sigma_{\mathrm{A}}\sigma_{\mathrm{B}}}{\sigma_{\mathrm{eff}}}\left(1 - \frac{1}{2}\frac{\sigma_{\mathrm{A}}}{\sigma_{\mathrm{B}}}\right). \tag{6.4}$$

The cross sections σ_{A} and σ_{B} are determined by integrating the η spectra for jets with p_{T} above 50 and 30 GeV in data, which are unfolded in exactly the same manner as all other distributions.

7 Systematic uncertainties

Different sources of systematic uncertainties occurring in the data analysis are studied. A summary is given in tables 1 and 2.

Jet energy scale (JES) uncertainty: the low-pileup, low jet-p_{T} data sample used in this analysis necessitates a dedicated JES calibration. The methods discussed in ref. [39] are applied, scaling the four-momentum vectors of the jets by a series of sequential corrections. The JES uncertainty depends on jet p_{T} and η and is smaller than 10% over the whole p_{T} spectrum and detector acceptance. The jet momenta are scaled downwards and upwards by the JES uncertainty to estimate its effect on the measured distributions. The JES uncertainty is the dominant contribution to the total uncertainty for the observables in terms of the absolute cross section and results in a maximal upward (downward) uncertainty of 39 (33)%. It largely cancels in the normalized distributions, never exceeding 16%.

JHEP01(2022)177

Jet energy resolution (JER) uncertainty: the JER obtained from MC simulation differs from the one estimated for data, which would lead to a wrong estimation of the bin-to-bin migrations. An additional smearing of the jet p_{T} at detector level is therefore applied to both MC samples used in the unfolding. To estimate the JER uncertainty, the data-to-simulation smearing factor is varied up and down with its own uncertainty, resulting in migration matrices that differ from the nominal ones. The newly obtained migration matrices are used to unfold the distributions, which are then compared with the nominal distributions for all observables. The JER uncertainty is less than 9%, except for the p_{T} spectrum of the leading jet where it reaches a maximum of 26%.

Trigger uncertainty: an event weight as a function of jet p_{T} is applied to data to correct for the efficiency of the trigger with the lowest threshold. These weights are obtained by fitting the trigger efficiency curve determined in data using a least-squares minimization. Varying the fit parameters by their uncertainty leads to a trigger uncertainty that never exceeds 1%.

Model uncertainty: the data distributions are unfolded using migration matrices from the PYTHIA8 and HERWIG++ models. The averages of the two unfolded distributions are taken as the nominal unfolded distributions and the systematic error is estimated as half of the difference. The model uncertainty varies between 1% and 16%, depending on the observable.

Pileup: events with two pp collisions in the same bunch crossing may be reconstructed with only one vertex if the collision points are separated by less than 0.12 cm along the beam axis. Taking into account the spread of vertices and the relative yields of events with 1 and 2 collisions, the pileup contamination in the data sample is estimated to be 0.28%. No further correction is applied, and a systematic uncertainty is included by reproducing all distributions with a sample of events containing two vertices, normalizing these to 0.28% of the nominal distributions, and estimating the effect of such pileup correction on the data. The systematic uncertainty is smaller than 1% in all bins for all observables.

Integrated luminosity uncertainty: the uncertainty in the integrated luminosity for data collected in 2016 is 1.2% [77].

Because the four-jet efficiency is determined using uncorrected data, it has neither JER or model systematic uncertainty. However, an additional systematic uncertainty is included to cover a possible difference with respect to the true efficiency to be applied on the corrected cross sections. This uncertainty is determined by examining the four-jet efficiency obtained with PYTHIA8 and HERWIG++ at both the detector and generator levels, after a 2-dimensional reweighting as a function of leading-jet p_{T} and jet multiplicity to obtain a better description of the data. A four-jet efficiency of 0.404 and 0.412 is found with PYTHIA8 on detector and generator level, respectively, whereas values of 0.403 and

JHEP01(2022)177

Observable	JES		JER	Model	Trigger	Vertex	Lum.	Stat	Total	
	Upper	Lower							Upper	Lower
Absolute cross section (%)										
$p_{\mathrm{T},1}$	11–39	9–30	2–26	0–16	< 1	< 1	1.2	1–10	11–51	10–44
$p_{\mathrm{T},2}$	11–31	10–24	0–2	0–7	< 1	< 1	1.2	1–8	14–33	11–26
$p_{\mathrm{T},3}$	1–31	7–24	1–3	2–7	< 1	< 1	1.2	2–15	13–33	13–25
$p_{\mathrm{T},4}$	10–25	0–21	1–8	2–7	< 1	< 1	1.2	4–31	14–34	13–32
η_1	22–33	18–28	< 1	1–9	< 1	< 1	1.2	3–5	22–34	19–29
η_2	22–30	18–26	< 1	0–6	< 1	< 1	1.2	3–6	23–31	18–26
η_3	21–29	18–24	< 1	0–7	< 1	< 1	1.2	3–5	22–30	19–25
η_4	19–29	16–24	< 1	1–8	< 1	< 1	1.2	3–4	19–30	17–25
$\Delta\phi_{\mathrm{Soft}}$	21–24	19–20	< 1	1–7	< 1	< 1	1.2	3–4	22–25	20–22
$\Delta\phi_{\mathrm{3j}}^{\mathrm{min}}$	21–28	18–24	< 1	1–6	< 1	< 1	1.2	3–7	21–29	19–25
ΔY	22–25	16–33	< 1	0–6	< 1	< 1	1.2	3–6	23–26	17–34
ϕ_{ij}	23–26	19–22	< 1	0–7	< 1	< 1	1.2	3–4	24–27	19–22
$\Delta p_{\mathrm{T,Soft}}$	22–25	19–20	0–3	2–6	< 1	< 1	1.2	3–4	23–26	19–21
ΔS	4–34	13–20	< 1	0–5	< 1	< 1	1.2	3–13	12–37	15–22
Bin-normalized cross section (%)										
$\Delta\phi_{\mathrm{Soft}}$	0–1	0–1	< 1	0–4	< 1	< 1	—	3–4	3–6	3–6
$\Delta\phi_{\mathrm{3j}}^{\mathrm{min}}$	0–5	0–4	< 1	0–4	< 1	< 1	—	3–7	4–8	3–8
ΔY	0–2	0–18	< 1	0–5	< 1	< 1	—	3–6	3–10	3–21
ϕ_{ij}	0–3	0–2	< 1	0–4	< 1	< 1	—	3–4	3–6	3–6
$\Delta p_{\mathrm{T,Soft}}$	0–2	0–2	0–2	0–2	< 1	< 1	—	3–4	3–5	3–5
ΔS	0–16	0–7	< 1	0–7	< 1	< 1	—	3–13	3–22	3–15

Table 1. Systematic uncertainties, along with the statistical and the total uncertainties for the p_{T} spectra, the η spectra, and the DPS sensitive observables, in percent. The JES uncertainty leads to asymmetric uncertainties (an upper and a lower error), while all other systematic uncertainties, as well as the statistical uncertainty, are symmetric.

0.392 are obtained with HERWIG++, with negligible statistical uncertainty. The systematic uncertainty is therefore conservatively estimated to be smaller than 2%.

8 Results

The total cross sections in the two phase space regions defined by thresholds on the p_{T} of the four leading jets, *Region* I and *Region* II, are obtained by integrating the differential cross section as a function of the leading jet η and the ΔS observable, respectively, yielding:

$$\sigma_{\mathrm{I}}\,(\mathrm{pp}\to 4\mathrm{j}+\mathrm{X}) = 2.77 \pm 0.02\,(\mathrm{stat})\,^{+0.68}_{-0.55}\,(\mathrm{syst})\,\mu\mathrm{b}, \tag{8.1}$$

$$\sigma_{\mathrm{II}}\,(\mathrm{pp}\to 4\mathrm{j}+\mathrm{X}) = 0.61 \pm 0.01\,(\mathrm{stat})\,^{+0.12}_{-0.10}\,(\mathrm{syst})\,\mu\mathrm{b}. \tag{8.2}$$

Tables 3–5 compares the values measured in data with the ones obtained from MC event generators. A discussion of the total and differential cross sections for each of the sets of models introduced in section 4 is presented below.

JHEP01(2022)177

Observable	JES		JER	Model	Trigger	Vertex	Lum.	Stat	Total	
	Upper	Lower							Upper	Lower
Integrated cross section (%)										
σ_{I}	24	19	< 1	4	< 1	< 1	1.2	1	25	20
σ_{II}	17	13	< 1	6	< 1	< 1	1.2	2	20	16
σ_{eff} extraction (%)										
ΔS(DPS template)	7–19	15–24	< 1	0–3	< 1	< 1	1.2	1–2	7–19	15–25
σ_{A}	10	9	< 1	4	< 1	< 1	1.2	1	11	10
σ_{B}	7	9	< 1	4	< 1	< 1	1.2	1	9	10
$\epsilon_{4\mathrm{j}}$	11	20	—	—	< 1	< 1	—	< 1	11	20

Table 2. Systematic uncertainties, along with the statistical and the total uncertainties for the cross sections of the two phase space regions, along with the observables needed for the extraction of $\sigma_{\mathrm{A,B}}^{\mathrm{DPS}}$, in percent. The JES uncertainty leads to asymmetric uncertainties (an upper and a lower error): all other systematic uncertainties, as well as the statistical uncertainty, are symmetric. An additional uncertainty in $\epsilon_{4\mathrm{j}}$ because of possible differences between generator- and detector-level events, is estimated to be 2%.

The cross sections of the inclusive single-jet Processes A and B are determined by integrating the leading jet η distribution for both processes, and are:

$$\sigma_{\mathrm{A}}\,(\mathrm{pp}\to 1\mathrm{j}+\mathrm{X}) = 15.9 \pm 0.1\,(\mathrm{stat})\,^{+1.8}_{-1.6}\,(\mathrm{syst})\,\mu\mathrm{b}, \tag{8.3}$$

$$\sigma_{\mathrm{B}}\,(\mathrm{pp}\to 1\mathrm{j}+\mathrm{X}) = 106 \pm 1\,(\mathrm{stat})\,^{+10}_{-11}\,(\mathrm{syst})\,\mu\mathrm{b}. \tag{8.4}$$

A large increase in cross section is observed when lowering the p_{T} threshold from 50 GeV to 30 GeV, as expected. These cross sections will be used as input to eq. (6.4) for the determination of the DPS cross section and σ_{eff} along with the four-jet efficiency from eq. (6.1).

8.1 The PYTHIA and HERWIG models

The models based on LO $2 \to 2$ matrix elements, PYTHIA8, HERWIG++, and HERWIG7, respectively labeled as P8, H++, and H7 in the figures, are compared with data. Table 3 gives an overview of the event generators, tunes, and PDF sets, along with their respective cross sections. All LO $2 \to 2$ models predict cross sections that are much larger than the measured ones; especially PYTHIA8 with the CDPSTP8S1-4j tune predicts a cross section that is roughly 2.5 times larger than the one observed in data. Figures 2–5 show a comparison of the data to various MC models as a function of p_{T}, η, and the DPS-sensitive observables. Three PYTHIA8 models and one HERWIG7 model are shown in direct comparison with the data. These models employ the most recent CP5 and CH3 tunes, the dedicated DPS tune or combine PYTHIA8 with a dipole-antenna shower provided by VINCIA, while all of the models are represented in the ratio plots.

The p_{T} spectra in figure 2, obtained for *Region* I, show that the much larger integrated cross section of the MC models, compared with the data, comes from an abundance of low-p_{T} jets, whereas for $p_{\mathrm{T}} \gtrsim 100$ GeV the models show agreement within 50% of the data; for

JHEP01(2022)177

Sample	ME	Tune	PDF	σ_{I} (μb)	σ_{II} (μb)
Data	—	—	—	$2.77 \pm 0.02\,^{+0.68}_{-0.55}$	$0.61 \pm 0.01\,^{+0.12}_{-0.10}$
PYTHIA8	LO $2 \to 2$	CUETP8M1	NNPDF2.3_LO	5.03	1.07
PYTHIA8	LO $2 \to 2$	CP5	NNPDF2.3_NNLO	4.07	0.84
PYTHIA8	LO $2 \to 2$	CDPSTP8S1-4j	CTEQ6L1	7.06	1.28
PYTHIA8 +VINCIA	LO $2 \to 2$	Default	NNPDF2.3_LO	4.66	0.97
HERWIG++	LO $2 \to 2$	CUETHS1	CTEQ6L1	4.35	0.83
HERWIG7	LO $2 \to 2$	CH3	NNPDF2.3_NNLO	4.82	0.98
HERWIG7	LO $2 \to 2$	SoftTune	MMHT2014lo68cl	5.34	1.07

Table 3. Cross sections obtained from data and from the PYTHIA8, HERWIG++, and HERWIG7 models in *Region* I and *Region* II of the phase space, where ME stands for matrix element.

HERWIG7 it is even within the total uncertainty. Figure 3, the η spectra, shows that a large part of the excess of low-p_{T} jets is located in the forward η regions.

The distributions in the DPS-sensitive observables are shown in figures 4 and 5, for *Region* II in the case of ΔS and *Region* I for all other observables. To make qualitative statements about the shape, the fully corrected distributions have been normalized to one or more bins where a much reduced DPS contribution is expected. The distribution in $\Delta\phi_{\mathrm{Soft}}$ is normalized to the average of the first five bins, covering the tail of the distribution, which is determined by the jet cone size. The distributions in $\Delta\phi_{3\mathrm{j}}^{\mathrm{min}}$ and ΔY are normalized to the average of their first four bins. Normalizing to the average of multiple bins reduces the effect of statistical fluctuations. The distributions in ϕ_{ij}, $\Delta p_{\mathrm{T,Soft}}$, and ΔS are all normalized to their last bin, since these bins already have a small relative statistical uncertainty.

The $\Delta\phi_{\mathrm{Soft}}$ and $\Delta p_{\mathrm{T,Soft}}$ distributions are relatively well described by all LO $2 \to 2$ models. Deviations from data never exceed 20%, albeit being larger than the total uncertainty in the data points in certain bins for some of the models. Similar results are observed for the predictions of the $\Delta p_{\mathrm{T,Soft}}$ observable from the DPS tune in [15]. Deviations of 10–20% occur between a model employing a similar DPS tune (CDPSTP8S1-WJ) and the data in the Z+jets final state.

The shape of the ΔY distribution predicted by all the LO $2 \to 2$ models differs significantly from data, and the MC-to-data ratio increases towards higher values of ΔY. The overshoot at large ΔY is consistent with the excess of low-p_{T} forward jets.

A distinction between two classes of models becomes apparent in the $\Delta\phi_{3\mathrm{j}}^{\mathrm{min}}$ and ϕ_{ij} distributions. The models implementing a p_{T}-ordered parton shower describe the distribution in $\Delta\phi_{3\mathrm{j}}^{\mathrm{min}}$ well, although yielding a distribution in ϕ_{ij} that is more uncorrelated than observed in data. The slope of the $\Delta\phi_{3\mathrm{j}}^{\mathrm{min}}$ distribution obtained from the models with a p_{T}-ordered shower algorithm going to zero, overshoots the slope of the distribution obtained from data. For models that use an angular-ordered or dipole-antenna parton shower, the $\Delta\phi_{3\mathrm{j}}^{\mathrm{min}}$ correlation is too strong. The slope of the distributions $\Delta\phi_{3\mathrm{j}}^{\mathrm{min}}$ distributions obtained from the models with an angular-ordered shower overshoot the distribution obtained from data when going to π, whereas the shape of the data is described more accurately by ϕ_{ij}. The PYTHIA8+VINCIA model confirms that the parton shower algorithm is responsible for

JHEP01(2022)177

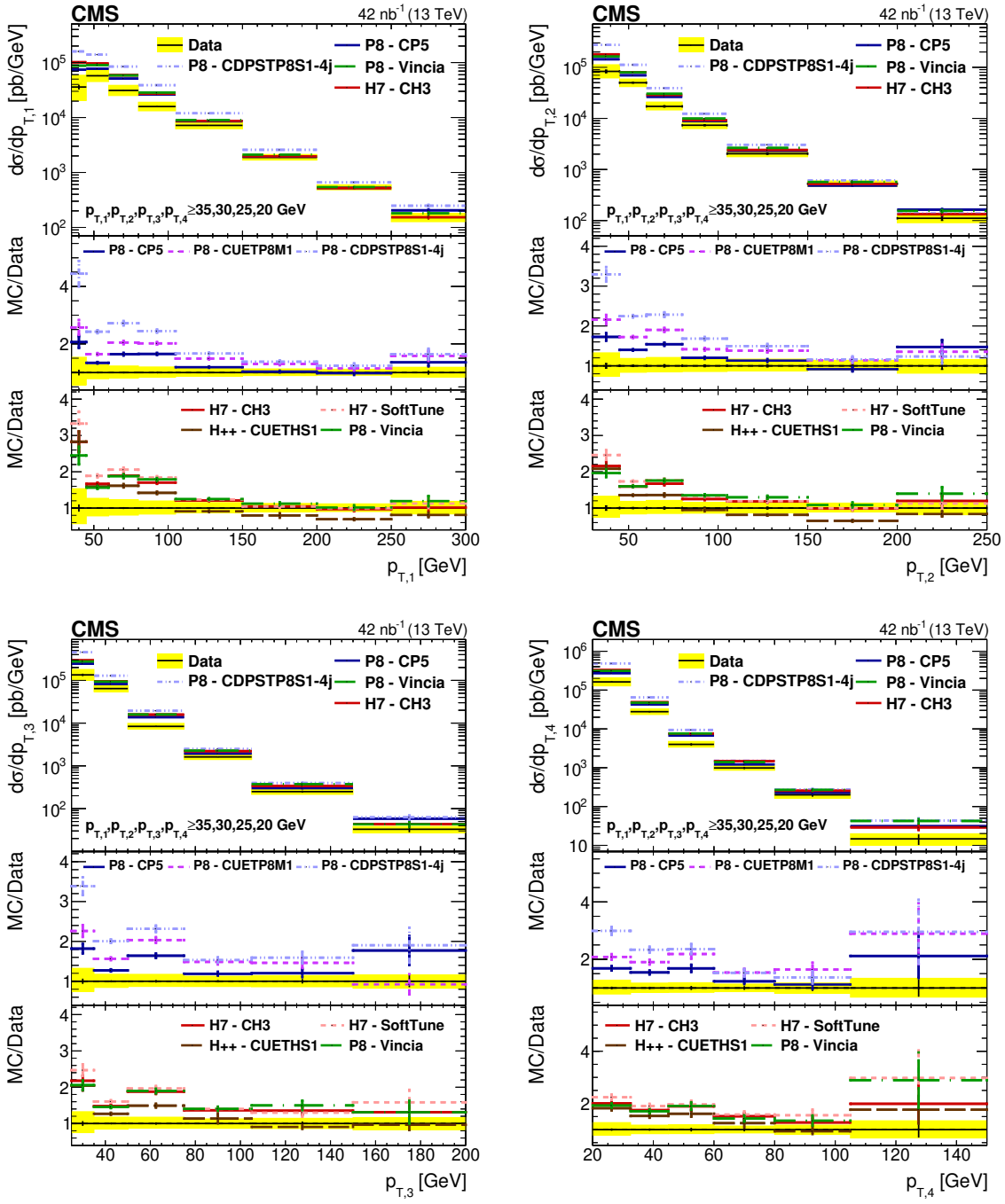

Figure 2. Comparison of the p_T spectra from data to different PYTHIA8 (P8), HERWIG++ (H++), and HERWIG7 (H7) tunes, for the leading (upper left), subleading (upper right), third leading (lower left), and fourth leading (lower right) jet in *Region* I. The error bars represent the statistical uncertainty, and the yellow band indicates the total (statistical+systematic) uncertainty in the measurement.

JHEP01(2022)177

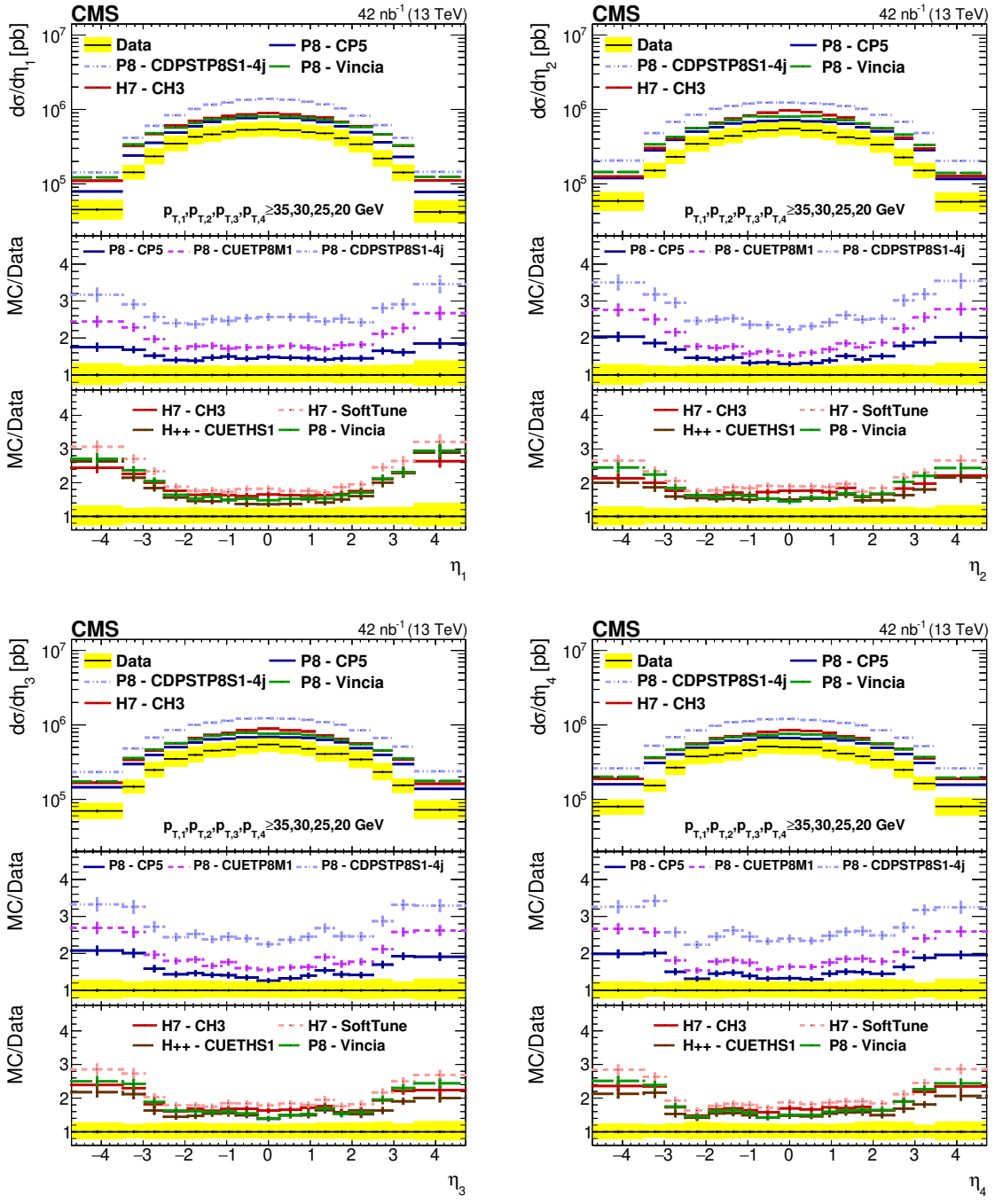

Figure 3. Comparison of the η spectra from data to different PYTHIA8 (P8), HERWIG++ (H++), and HERWIG7 (H7) tunes, for the leading (upper left), subleading (upper right), third leading (lower left), and fourth leading (lower right) jet in *Region* I. The error bars represent the statistical uncertainty, and the yellow band indicates the total (statistical+systematic) uncertainty in the measurement.

JHEP01(2022)177

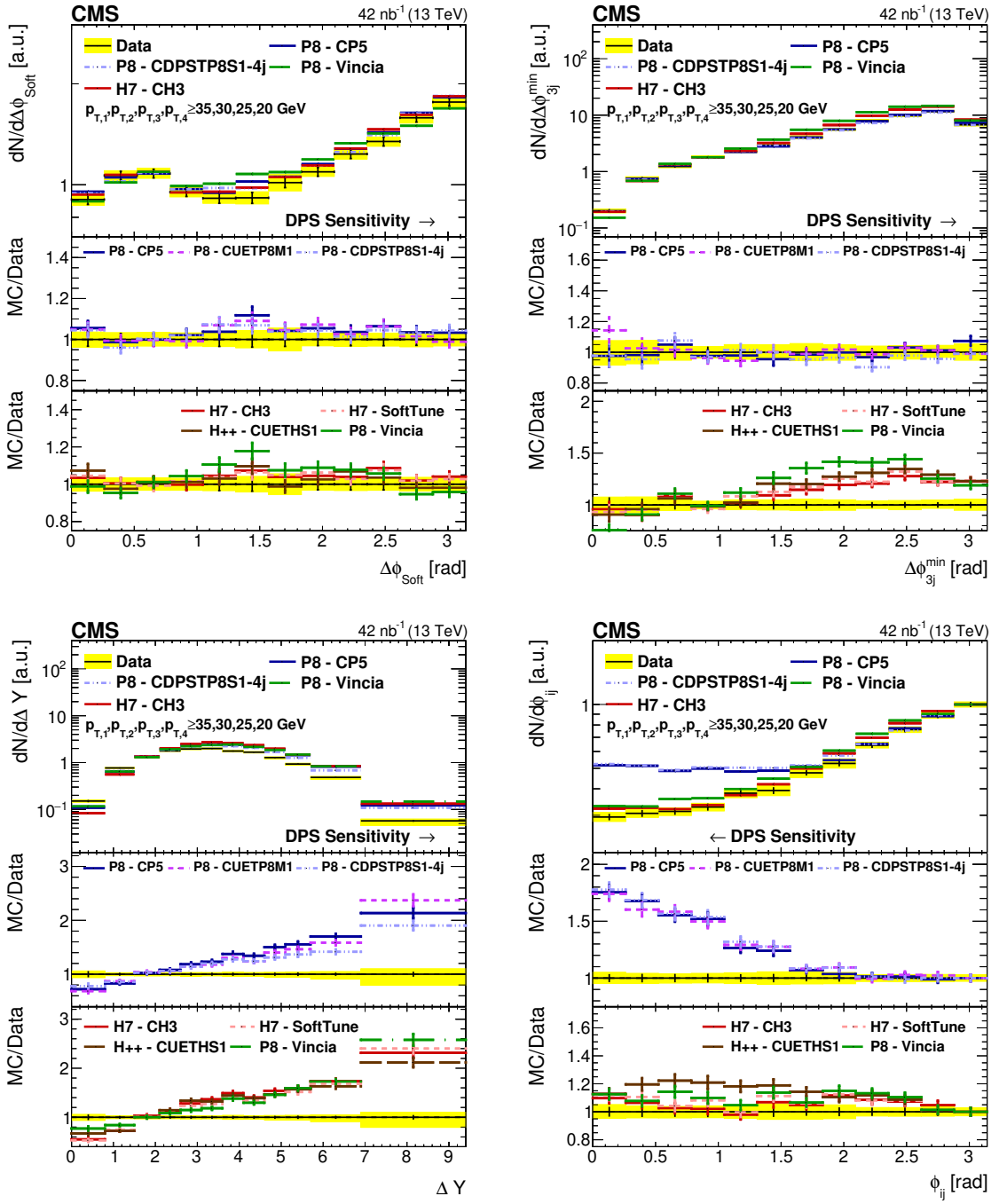

Figure 4. Comparison of the $\Delta\phi_{\mathrm{Soft}}$, $\Delta\phi_{3\mathrm{j}}^{\mathrm{min}}$, ΔY, and ϕ_{ij} distributions from data to different PYTHIA8 (P8), HERWIG++ (H++), and HERWIG7 (H7) tunes in *Region* I. All distributions have been normalized to regions where a reduced DPS contribution is expected. The error bars represent the statistical uncertainty, and the yellow band indicates the total (statistical+systematic) uncertainty in the measurement.

JHEP01(2022)177

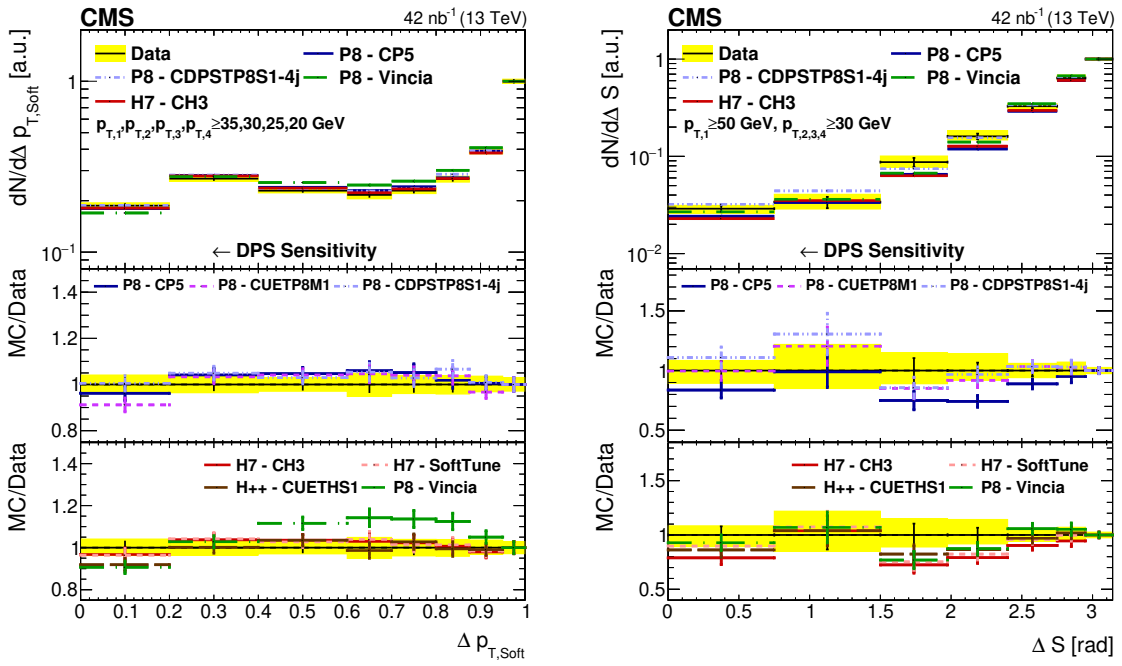

Figure 5. Comparison of the $\Delta p_{\mathrm{T,Soft}}$ and ΔS distributions from data to different PYTHIA8 (P8), HERWIG++ (H++), and HERWIG7 (H7) tunes in *Region* I and *Region* II, respectively. All distributions have been normalized to regions where a reduced DPS contribution is expected. The error bars represent the statistical uncertainty, and the yellow band indicates the total (statistical+systematic) uncertainty in the measurement.

the different tendencies observed for the two classes of models. This observation makes these observables less suitable to untangle SPS and DPS contributions to the cross section.

The ΔS distribution is less affected by different parton shower implementations. The DPS tune CDPSTP8S1-4j agrees very well with the shape of the data, but lies slightly above the data at low values of ΔS, pointing to a potential overestimation of the DPS contribution. All other models underestimate the data at low ΔS, indicating a possible need for more DPS to obtain a proper description of the shape of the ΔS distribution.

8.2 Multijet models

Data distributions are also compared with the multijet samples that are obtained from models based on LO $2 \to n(n \geq 2)$ and NLO $2 \to 2$ and $2 \to 3$ matrix elements. The group of multijet samples includes $2 \to 4$ on-shell and off-shell predictions made by KaTie, two MadGraph5_aMC@NLO LO samples for which $2 \to 2, 3, 4$ matrix element are all included, a MadGraph5_aMC@NLO NLO $2 \to 2$ sample, and two POWHEG NLO samples that use a $2 \to 2$ and a $2 \to 3$ matrix element. Table 4 gives a complete overview of all models, tunes, and PDF sets, along with their respective cross sections. In the figures, the labels KT, PW, and MG5 are used for KaTie, POWHEG, and MadGraph5_aMC@NLO, respectively. Figures 6–9 show a comparison of the data to various MC models as a function of p_{T}, η, and the DPS-sensitive observables. Four models are shown in direct comparison

JHEP01(2022)177

Sample	ME	Tune	PDF/TMD	σ_{I} (μb)	σ_{II} (μb)
Data	—	—	—	$2.77 \pm 0.02\,^{+0.68}_{-0.55}$	$0.61 \pm 0.01\,^{+0.12}_{-0.10}$
KaTie on-shell + pythia8	LO $2 \to 4$	CP5	NNPDF2.3_NNLO	4.23	2.87
KaTie on-shell + herwig7	LO $2 \to 4$	CH3	NNPDF2.3_NNLO	3.56	2.25
KaTie off-shell + Cascade	LO $2 \to 4$	—	MRW	2.40	1.46
KaTie off-shell + Cascade	LO $2 \to 4$	—	PBTMD	2.57	1.56
MadGraph5_aMC@NLO + pythia8	LO $2 \to 2, 3, 4$	CP5	NNPDF2.3_NNLO	2.69	1.26
MadGraph5_aMC@NLO + pythia8+Vincia	LO $2 \to 2, 3, 4$	Default	NNPDF2.3_LO	1.93	0.90
MadGraph5_aMC@NLO + pythia8	NLO $2 \to 2$	CP5	NNPDF2.3_NNLO	2.12	1.03
powheg + pythia8	NLO $2 \to 2$	CP5	NNPDF2.3_NNLO	3.50	1.62
powheg + pythia8	NLO $2 \to 3$	CP5	NNPDF2.3_NNLO	2.55	1.22

Table 4. Cross sections obtained from data and from KaTie, MadGraph5_aMC@NLO, and powheg in region *Region* I and *Region* II of the phase space, where ME stands for matrix element.

with the data. These models include one of the two on- and off-shell KaTie models, the MadGraph5_aMC@NLO LO sample interfaced with the CP5 tune and the powheg NLO $2 \to 2$ sample, while all of the models are represented in the ratio plots.

The predicted cross sections obtained from the on-shell KaTie samples interfaced with pythia8 and herwig7 are larger than the cross sections obtained from data. They sharply decrease when an off-shell matrix element is used, showing agreement within the data uncertainty for *Region* I. The MadGraph5_aMC@NLO LO samples and all the NLO samples predict cross sections that are roughly in agreement with the cross sections obtained from data in *Region* I, but are larger than those from data in *Region* II, as are all the KaTie cross sections in the same region.

Figure 6 compares the p_{T} spectra of the various models with the data. The on-shell KaTie predictions agree with the data in the first bin of each of the p_{T} spectra, but are above the data at higher p_{T}. This may be explained because most jets originate from the $2 \to 4$ matrix element and not from the parton shower. The same effect, but less pronounced, is observed for the off-shell KaTie curves. The different PDF sets used with off-shell KaTie result in small variations. A better description of the p_{T} spectra is given by the MadGraph5_aMC@NLO LO sample, with a p_{T}-ordered parton shower. In this case, some jets must originate from the parton shower, yielding a softer spectrum. The combination of the MadGraph5_aMC@NLO LO $2 \to 2, 3, 4$ sample with the dipole-antenna showering from pythia8+Vincia, results in a lowering of the total cross section. All NLO models give a similar description as the MadGraph5_aMC@NLO sample; the higher-order matrix element, including virtual corrections, contributes to a lower cross section. A comparison of the multi jet data samples to the standard pythia8 and herwig curves from the previous section demonstrates that NLO corrections and the inclusion of multi-leg matrix elements improve the description of the p_{T} spectra.

JHEP01(2022)177

The η spectra are shown in figure 7. The central region is consistently described by all models, even the on-shell KaTie models; the overall cross section is too large but the ratio remains flat for $|\eta| \leq 3.0$. An excess of jets is observed in the forward region, although this is less pronounced than in the case of the pythia8 and herwig models. The excess is also strongest for the leading jet and diminishes for the second, third and fourth leading jet, yielding a good description of the shape for the latter.

Differential cross sections for all other observables are shown in figures 8 and 9. As before, these distributions have been normalized to a region with a much reduced DPS contribution.

The distributions in $\Delta\phi_{\text{Soft}}$ and $\Delta p_{\text{T,Soft}}$ demonstrate that most multijet models leave room for an additional DPS contribution in the regions where this can be expected. The exceptions are the MadGraph5_aMC@NLO LO $2 \to 2, 3, 4$ distributions that describe the shape of the distributions from data reasonably well. This last model contains a LO $2 \to 2$ contribution, and, as observed in Sec 8.1, the LO $2 \to 2$ models describe the $\Delta\phi_{\text{Soft}}$ and $\Delta p_{\text{T,Soft}}$ distributions well.

The ΔY distributions show that some multijet models still have an excess of jets at large rapidity separation.

The distributions in ϕ_{ij} confirm the strong dependence on the parton shower implementation observed with the LO $2 \to 2$ models (as shown, e.g., the MadGraph5_aMC@NLO LO $2 \to 2, 3, 4$ predictions for ϕ_{ij}). Angular-ordered parton showers, reproduced by Vincia and KaTie, describe the shape of the data distributions better. The off-shell KaTie predictions show a depletion in the region where additional DPS is expected. The effect of the parton shower on the $\Delta\phi_{3\text{j}}^{\text{min}}$ distributions is less pronounced in the multijet models compared to the LO $2 \to 2$ models.

The ΔS distributions again show a more robust behavior with respect to the parton shower implementation. The LO MadGraph5_aMC@NLO samples leave less room for an additional DPS contribution compared with the NLO models. Due to the sole use of a $2 \to 4$ matrix element, the p_{T} spectra are far too hard, resulting in a large overestimation of the slope for all the KaTie models.

8.3 SPS+DPS models

The last group of model predictions that are compared with data are those including an explicit DPS contribution, as described in section 4.3. The pythia8 CDPSTP8S1-4j predictions presented in this section are the same as in previous sections; there is no need to add a DPS contribution explicitly, because the underlying event parameters are specifically tuned to include a DPS contribution. All models are labeled as before in the figures.

A comparison of the integrated cross sections obtained from the SPS+DPS samples in table 5 with those from pure SPS samples, shows the expected increase. Only the values of the off-shell KaTie models agree with the measured cross section in *Region* I within the uncertainty. The cross sections predicted for *Region* II are all too high.

Figures 10 and 11 show the p_{T} and η spectra of the four leading jets, respectively. A comparison with the spectra of the pure SPS samples from the previous sections shows

JHEP01(2022)177

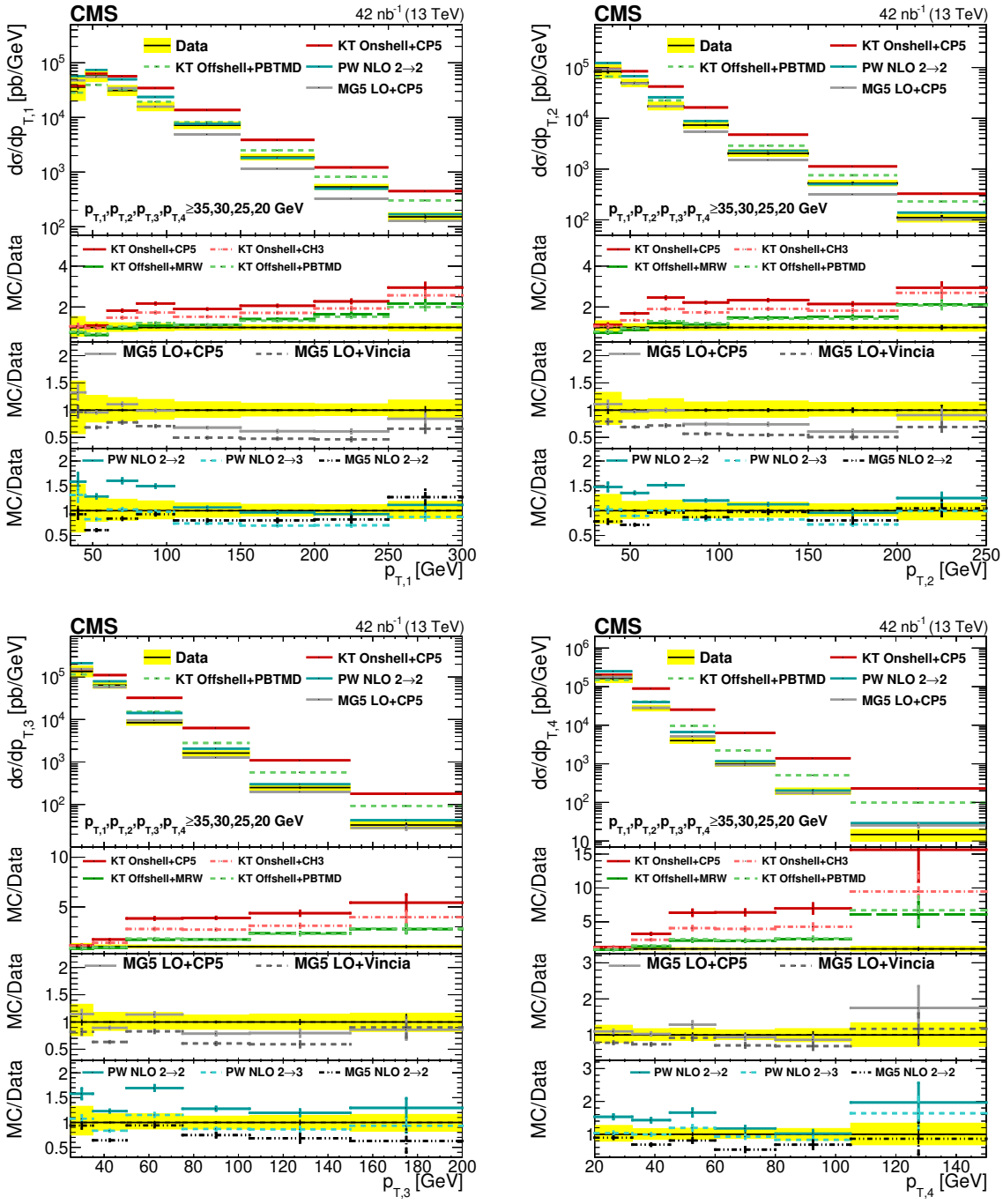

Figure 6. Comparison of the unfolded p_T spectra of data with different KaTie (KT), MadGraph5_aMC@NLO (MG5), and powheg (PW) models, for the leading (upper left), subleading (upper right), third leading (lower left), and fourth leading (lower right) jet in *Region* I. The error bars represent the statistical uncertainty, and the yellow band indicates the total (statistical+systematic) uncertainty in the measurement.

JHEP01(2022)177

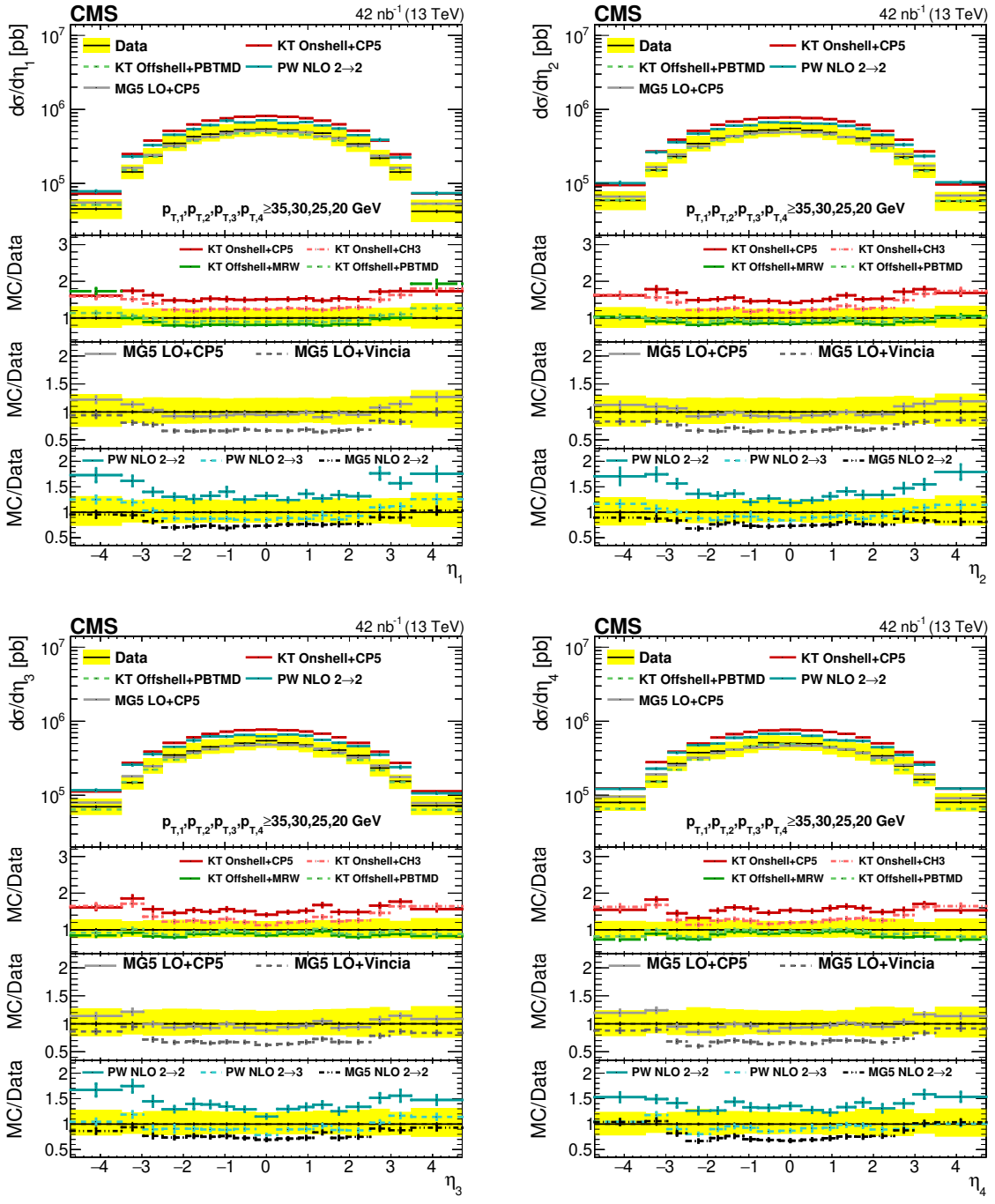

Figure 7. Comparison of the unfolded η spectra of data with different KaTie (KT), MadGraph5_aMC@NLO (MG5), and powheg (PW) models, for the leading (upper left), subleading (upper right), third leading (lower left), and fourth leading (lower right) jet in *Region* I. The error bars represent the statistical uncertainty, and the yellow band indicates the total (statistical+systematic) uncertainty in the measurement.

JHEP01(2022)177

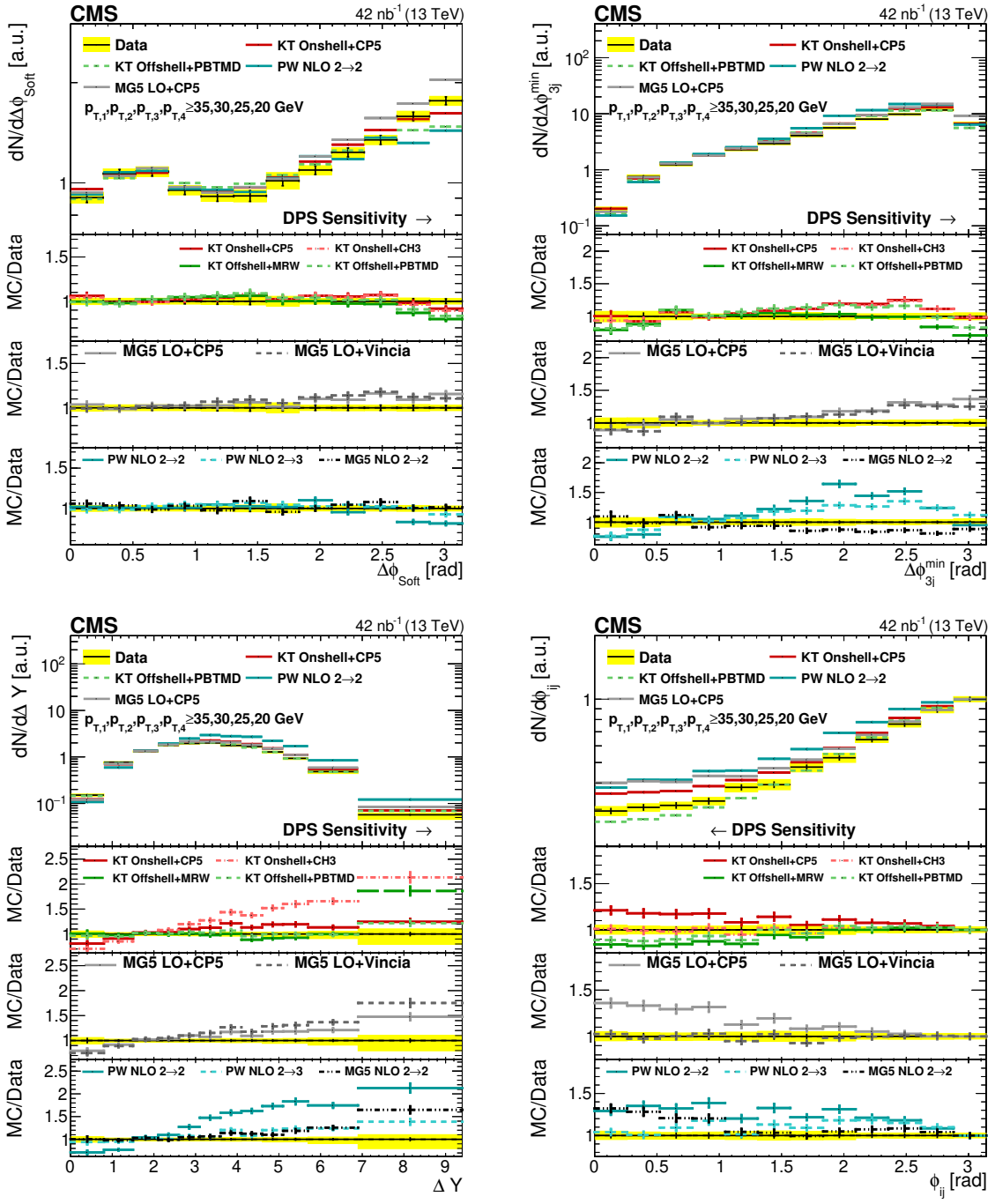

Figure 8. Comparison of the $\Delta\phi_{\text{Soft}}$, $\Delta\phi_{3\text{j}}^{\text{min}}$, ΔY, and ϕ_{ij} distributions from data to different KaTie (KT), MadGraph5_aMC@NLO (MG5), and POWHEG (PW) implementations in *Region* I. All distributions have been normalized to regions where a reduced DPS sensitivity is expected. The error bars represent the statistical uncertainty, and the yellow band indicates the total (statistical+systematic) uncertainty on the measurement.

JHEP01(2022)177

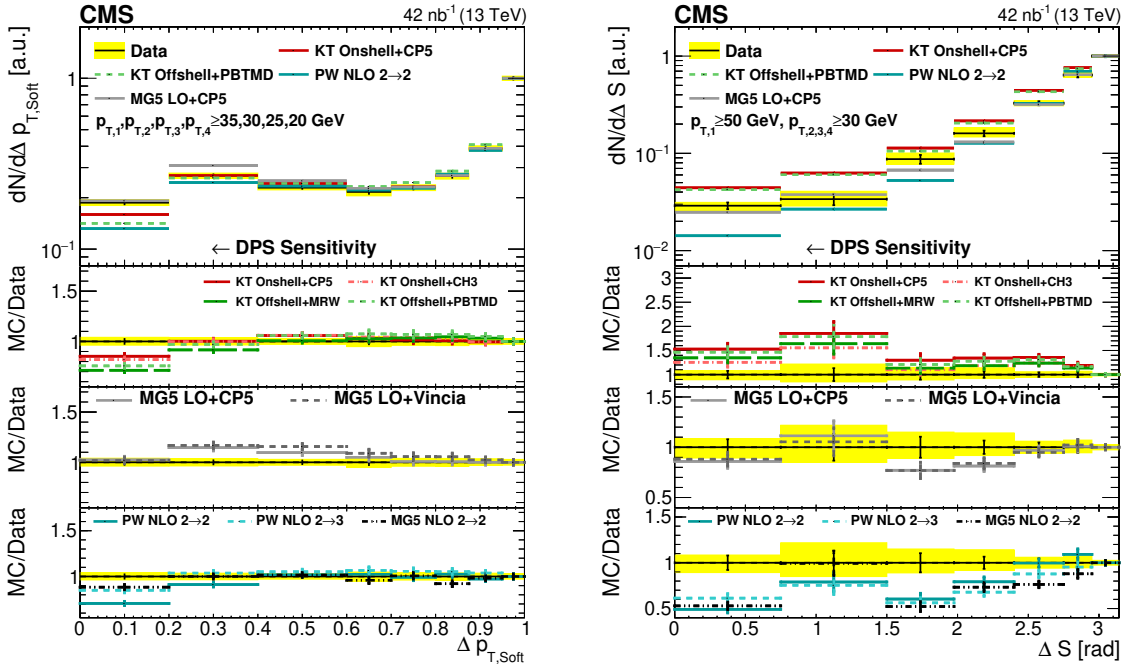

Figure 9. Comparison of the $\Delta p_{\mathrm{T,Soft}}$ and ΔS distributions from data to different KaTie (KT), MadGraph5_aMC@NLO (MG5), and powheg (PW) implementations in *Region* I and *Region* II, respectively. All distributions have been normalized to regions where a reduced DPS sensitivity is expected. The error bars represent the statistical uncertainty, and the yellow band indicates the total (statistical+systematic) uncertainty on the measurement.

Sample	ME	Tune	PDF/TMD	σ_{I} (μb)	σ_{II} (μb)
Data	—	—	—	$2.77 \pm 0.02\,^{+0.68}_{-0.55}$	$0.61 \pm 0.01\,^{+0.12}_{-0.10}$
pythia8	LO $2 \to 2$	CDPSTP8S1-4j	CTEQ6L1	7.06	1.28
SPS+DPS pythia8	LO $2 \to 2$	CP5	NNPDF2.3_NNLO	4.76	0.94
SPS+DPS KaTie on-shell + pythia8	LO $2 \to 4$	CP5	NNPDF2.3_NNLO	5.04	2.14
SPS+DPS KaTie off-shell + Cascade	LO $2 \to 4$	—	MRW	3.11	0.95
SPS+DPS KaTie off-shell + Cascade	LO $2 \to 4$	—	PBTMD	3.12	0.99

Table 5. Cross sections obtained from data and from models with an explicit DPS contribution in *Region* I and *Region* II of the phase space, where ME stands for matrix element.

that the DPS samples contribute in the low-p_{T} region, and mostly in the forward regions of the η spectra.

Normalized distributions in the DPS-sensitive observables are shown in figure 12. Small differences in shape, typically $\sim 5\%$, occur in the DPS-sensitive regions when comparing the SPS+DPS pythia8 sample, interfaced with the CP5 tune, with its pure SPS counterpart in figures 4 and 5. The pythia8 samples give a good description of shape of the distributions in the observables $\Delta\phi_{\mathrm{Soft}}$, $\Delta\phi_{\mathrm{3j}}^{\mathrm{min}}$, $\Delta p_{\mathrm{T,Soft}}$ and ΔS, with the CDPSTP8S1-4j

JHEP01(2022)177

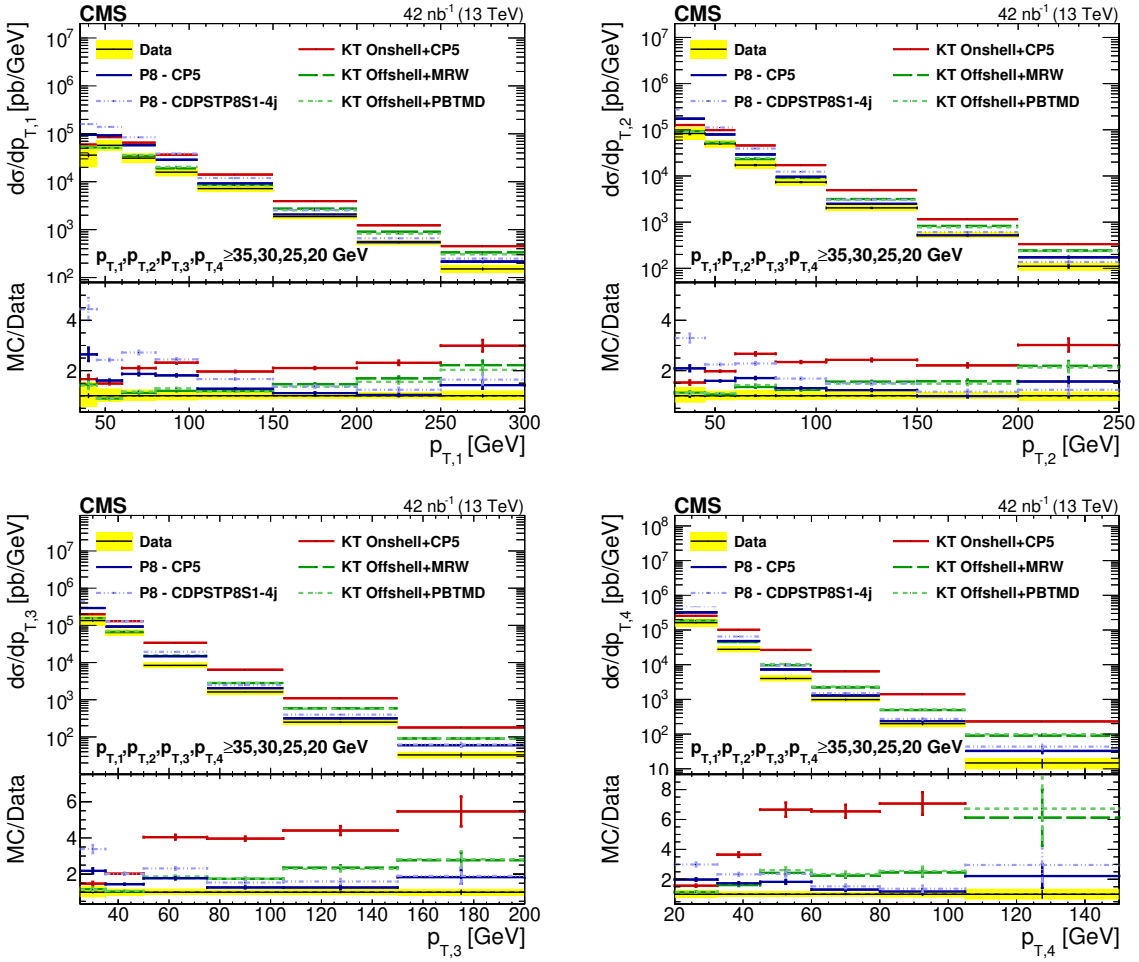

Figure 10. Comparison of the unfolded p_{T} spectra of data with different SPS+DPS KaTie (KT) and pythia8 (P8) models, for the leading (upper left), subleading (upper right), third leading (lower left), and fourth leading (lower right) jet in *Region* I. The error bars represent the statistical uncertainty, and the yellow band indicates the total (statistical+systematic) uncertainty in the measurement.

tune performing slightly better than the pythia8 SPS+DPS sample with the CP5 tune. This might be expected since the CDPSTP8S1-4j tune was obtained by fitting the pythia8 underlying event parameters to distributions in $\Delta\phi_{\mathrm{Soft}}$, $\Delta p_{\mathrm{T,Soft}}$, and ΔS measured with data at a center-of-mass energy of 7 TeV, as detailed in [51].

The KaTie curves show a more noticeable increase where a DPS contribution is expected, especially in the case of the off-shell samples. This is in contrast with the performance of the SPS-only predictions (see figures 8 and 9) where the off-shell KaTie models underestimate the data. This shows that a DPS contribution is needed in the KaTie model to improve the description of the data, but that the value of $\sigma_{\mathrm{eff}} = 21.3\,\mathrm{mb}$ (taken from ref. [51]), is too small for this model based on a $2 \to 4$ matrix element.

All models fail to describe the shape of the ΔY observable, and the ϕ_{ij} observable shows the same tendencies found in the previous sections. The LO $2 \to 2$pythia8 models

JHEP01(2022)177

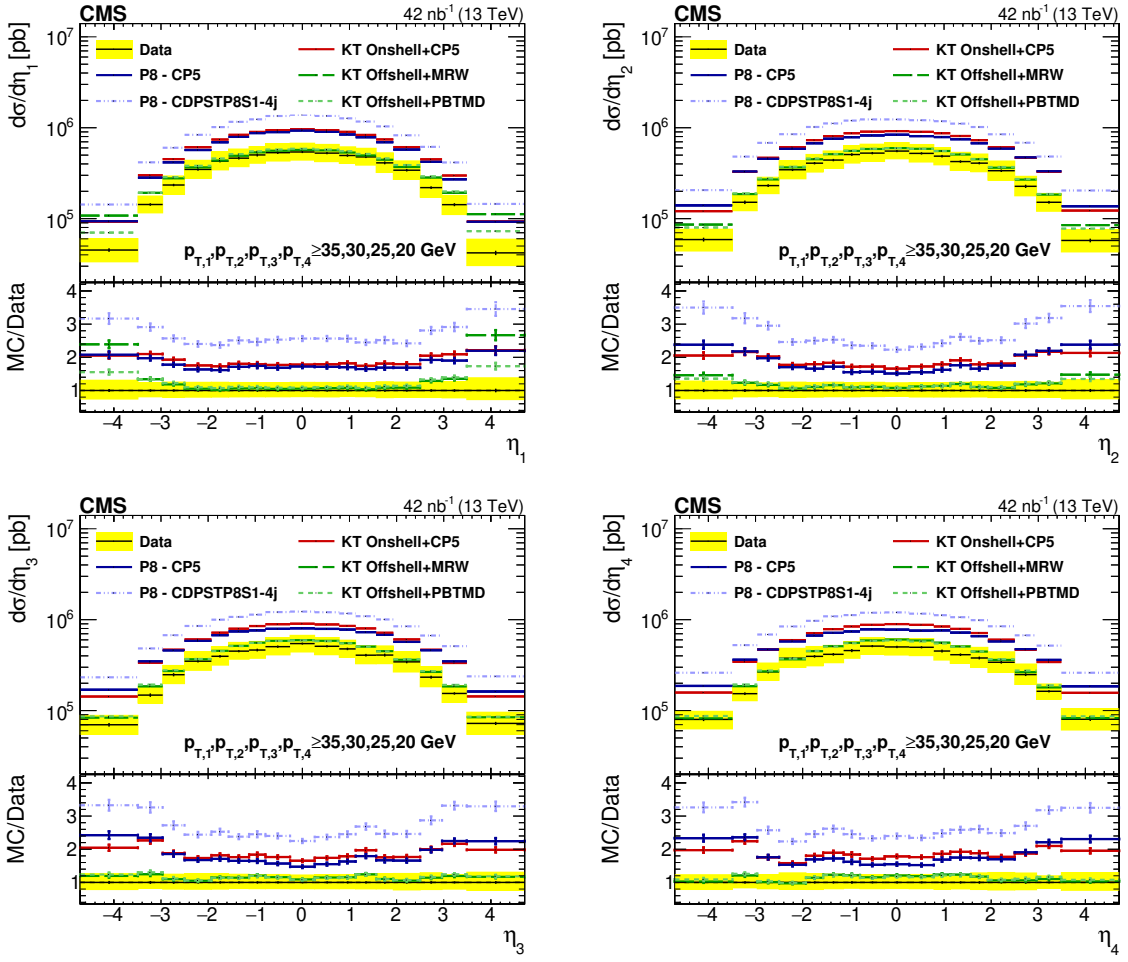

Figure 11. Comparison of the unfolded η spectra of data with different SPS+DPS KaTie (KT) and pythia8 (P8) models, for the leading (upper left), subleading (upper right), third leading (lower left), and fourth leading (lower right) jet in *Region* I. The error bars represent the statistical uncertainty, and the yellow band indicates the total (statistical+systematic) uncertainty in the measurement.

using a p_{T}-ordered parton shower show too large a decorrelation, whereas predictions using higher-order matrix element calculations perform better, demonstrated by the KaTie distributions.

8.4 Extraction of the effective cross section

As demonstrated in the above sections, the ΔS observable exhibits the most robust sensitivity to DPS. Other observables are either less sensitive to DPS or suffer from large variations induced by different parton shower models. Therefore, the ΔS distribution is used in the extraction of σ_{eff}. The DPS cross section is determined and the effective cross section, σ_{eff}, is extracted using different SPS MC event samples with and without the hard MPI removed following the template method laid out in section 6. The pythia8 sample with the CUETP8M1 tune yields a DPS fraction lower compared to all other tunes, while

JHEP01(2022)177

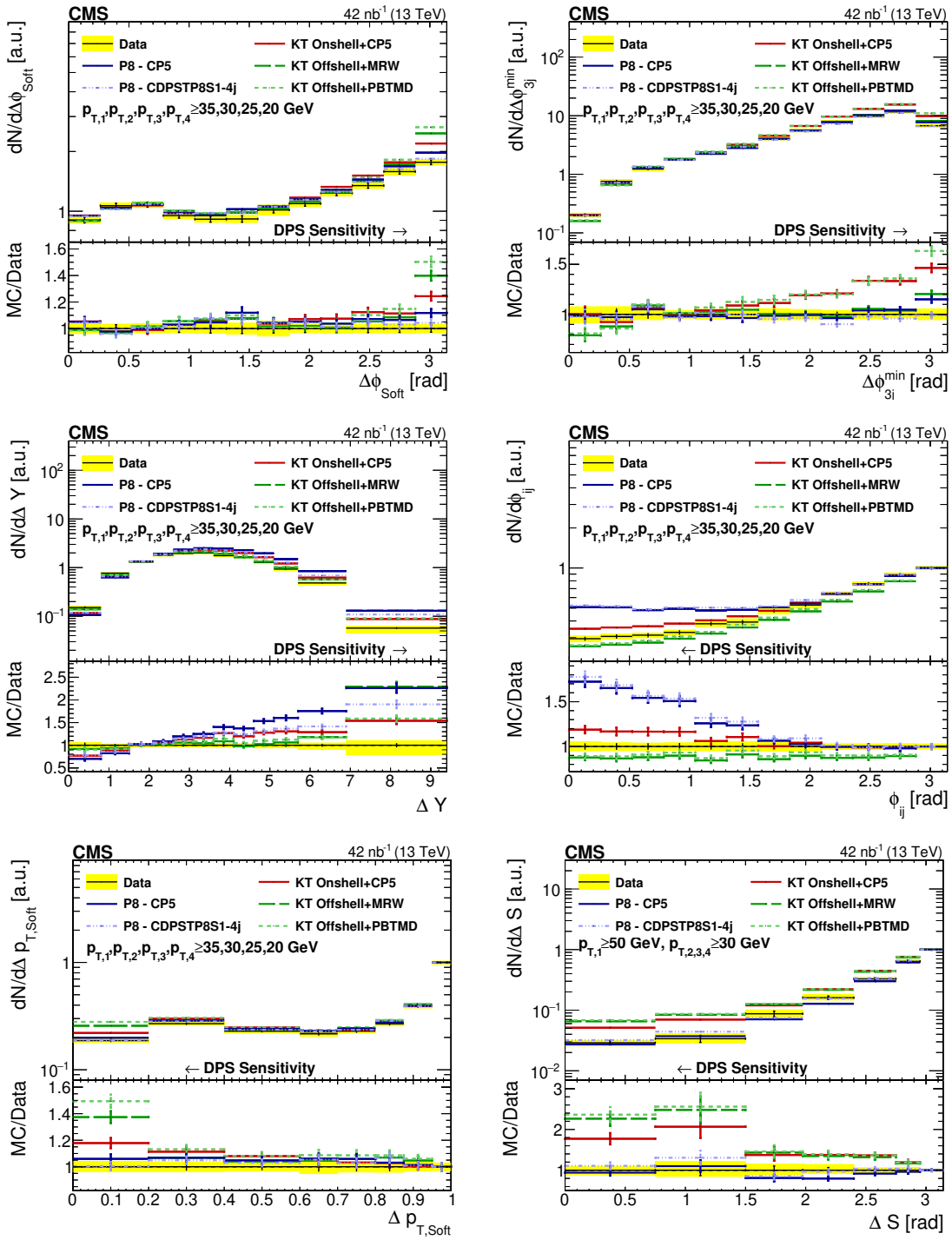

Figure 12. Comparison of the distributions in DPS-sensitive observables obtained from data to different SPS+DPS KaTie (KT) and pythia8 (P8) models. All distributions have been determined in *Region* I, except for the ΔS distribution which has been measured in *Region* II. All distributions have been normalized to the region where a reduced DPS contribution is expected. The error bars represent the statistical uncertainty, and the yellow band indicates the total (statistical+systematic) uncertainty on the measurement.

JHEP01(2022)177

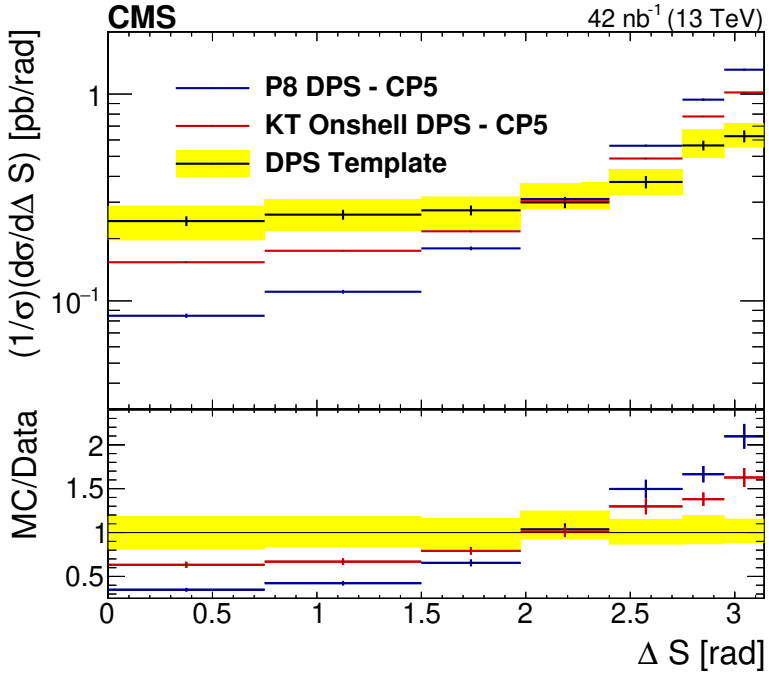

Figure 13. The ΔS distribution obtained from the mixed data sample compared to predictions from the pure DPS sample in PYTHIA8 (P8) and KaTie (KT). The distributions are normalized to unity. The error bars represent the statistical uncertainty, and the yellow band indicates the total (statistical+systematic) uncertainty on the data.

the HERWIG++ sample with the CUETHS1 tune gives similar results as when HERWIG7 with the CH3 tune is used, and therefore both are omitted below. The PYTHIA8 sample interfaced with the CDPSTP8S1-4j tune without the hard MPI removed already contains a DPS contribution, scaled with an effective cross section equal to 21.3 mb [51]. Therefore, the extracted DPS fraction for this model is expected to be close to zero. The extraction is still performed as a consistency check and to test the performance of the tune at a center-of-mass energy of $\sqrt{s} = 13$ TeV. The multijet KaTie models are not considered; they significantly overshoot the DPS-sensitive slope of the ΔS observable and using them would result in a negative DPS contribution.

The mixed event sample obtained from data, as described in section 6, is used to get the ΔS distributions for pure DPS events and is corrected by means of unfolding in the same way as the other distributions. This corrected ΔS distribution is shown in figure 13, along with the ΔS distributions obtained from the DPS component of the PYTHIA8 and on-shell KaTie generators, both interfaced with the CP5 tune. All distributions have been normalized to unity. The distributions show a maximum at $\Delta S = \pi$ because of jet pairs with overlapping p_{T} values such that the two softest and the two hardest jets do not coincide with the jet pairs from separate events or parton collisions. The DPS data sample exhibits a larger decorrelation as compared to the DPS MC samples, which can be attributed to disparities in the p_{T} spectra observed in data and for MC events.

The template fitter program [76] takes the SPS MC distributions along with the DPS data sample as input, and uses the template method to determine the fraction of DPS

JHEP01(2022)177

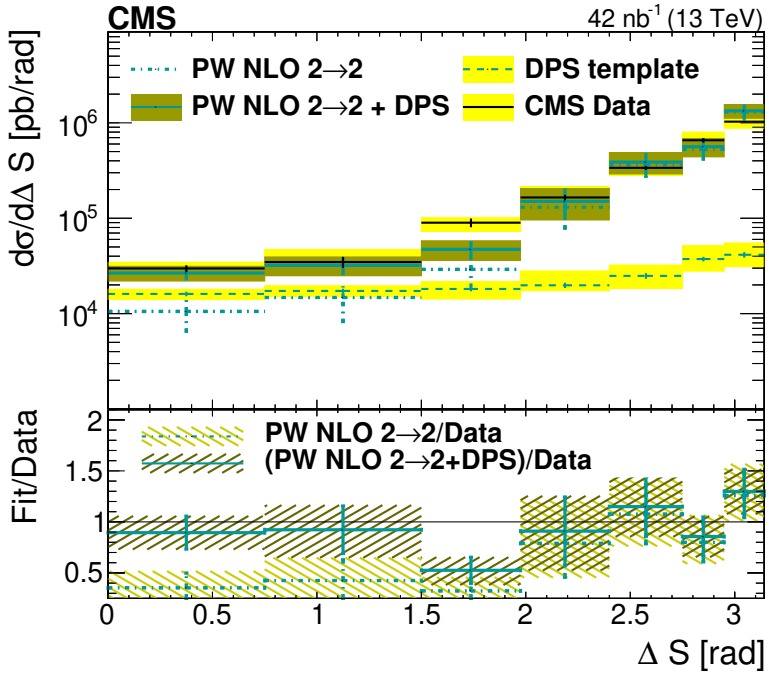

Figure 14. The results of the template fit for the POWHEG (PW) NLO $2 \to 2$ model without the hard MPI removed. The yellow bands represent the total uncertainty of the distribution. The ratio of the scaled MC model and of the total fitted result over the data are shown in the bottom plot. Since the ΔS distribution obtained from the mixed data sample carries a statistical and systematic uncertainty, so does the total fitted sample. The total uncertainty in the ratio is shown on the plot.

events, f_{DPS}. The results for the extracted values of f_{DPS} are shown in table 6. Equations (6.4) and (6.3) are used to determine the DPS cross sections and values for σ_{eff} shown in tables 7 and 8, respectively. The results for both sets of samples (with and without the hard MPI removed) are shown, along with the net difference between both cross sections since this can be interpreted as the amount of DPS inherent to the tune. An example of the template fit is presented in figure 14, where the fitted distributions using the POWHEG NLO $2 \to 2$ model without the hard MPI removed along with its statistical and systematic uncertainties are shown.

The DPS cross section obtained for all models with and without the hard MPI removed range from 14.6 to 70 mb, yielding values for σ_{eff} between 7.7 and 34.8 mb. The exception is PYTHIA8 with the CDPSTP8S1-4j tune without the hard MPI removed where an excess of DPS events is found, resulting in a negative DPS cross section. Therefore, the effective cross section for this model has not been calculated because it would yield a nonphysical result.

In the case of the LO $2 \to 2$ models, 2 final state jets originate from the ME, and 2 additional jets stem from the parton shower. A distinction between two groups of models using a LO $2 \to 2$ matrix element can be made. On the one hand, the PYTHIA8 and HERWIG7 models using the CP5 and CH3 tunes, respectively, use the latest underlying event tune and up-to-date PDFs. On the other hand, both PYTHIA8+VINCIA and HERWIG7 with the SoftTune rely on an older underlying event tune and older PDFs. The extracted

JHEP01(2022)177

values for the DPS cross section for the former two models are 38.5 and 38.2 mb, whereas for the latter two models values of 23.3 and 29.5 mb were obtained where events containing one or more hard partons originating from MPI have been removed. The results indicate that it might be the different underlying event tunes and the usage of older PDFs that are responsible for the more DPS-like topology in both PYTHIA8+VINCIA and HERWIG7 with the SoftTune.

Introducing higher multiplicity MEs reduces the effect of the underlying event tune, parton showers, and the PDFs since more jets will originate from the ME. The dominating contribution to the event sample comes from $2 \to 4$ ME, where the 4 final state jets all stem from the ME. The extracted DPS cross section with hard MPI removed is 31 mb for both PYTHIA8 with the CP5 tune and PYTHIA8+VINCIA, confirming that the effect of the different underlying event tunes, parton showers, and PDFs is suppressed. In the case of PYTHIA8 with the CP5 tune, the higher multiplicity MEs reduce the need for additional DPS, whereas in the case of PYTHIA8+VINCIA more room for additional DPS exists. For both models, about half of the DPS cross section that is needed to describe the data can be covered by the MPI that are intrinsic to the tune.

The NLO $2 \to 2$ models contain a combination of exclusive NLO $2 \to 2$ and LO $2 \to 3$ ME. One or more parton-shower jets are required to produce a 4-jet final state, with a ME/parton-shower matching algorithm applied to avoid double counting. Large DPS cross sections of up to 70 mb are needed to describe the data if events containing hard MPI partons originating from the underlying event description, provided by the CP5 tune, are removed. Compared with the other models, the NLO $2 \to 2$ models are outliers. If events with hard MPI partons from the underlying event description are included, they can again account for about half of the DPS cross section needed to describe the data.

For the POWHEG NLO $2 \to 3$ sample, NLO $2 \to 3$ and LO $2 \to 4$ MEs are combined, leaving room for zero or one additional jets from the parton shower. The extracted DPS cross section approaches the one obtained for the models with a LO $2 \to 2, 3, 4$ ME. Contrary to the LO $2 \to 2, 3, 4$ ME models, however, the NLO $2 \to 3$ models do not allow events containing hard MPI partons to contribute as much to the DPS cross section.

Figure 15 shows the results for σ_{eff} extracted with the models that are based on the recent CP5 and CH3 tunes where the hard MPI have been removed. The extracted σ_{eff} values show agreement with the results from the UA2 and CDF experiments, which set a lower bound on $\sigma_{\text{eff}} > 8.3$ mb [21] and found a σ_{eff} value of $12.1^{+10.7}_{-5.4}$ mb, respectively. All results, except for the values obtained with the NLO $2 \to 2$ models, agree with the measurement performed by the ATLAS collaboration [25] at a center-of-mass energy of 7 TeV [22], where a σ_{eff} equal to $14.9^{+1.2}_{-1.0}(\text{stat})^{+5.1}_{-3.8}(\text{syst})$ mb was reported, whereas none agree with the value of $21.3^{+1.2}_{-1.6}$ mb from the CMS measurement at a center-of-mass energy of 7 TeV [51], which is more in line with the results obtained with some of the models based on older UE tunes.

Two other DPS measurements have been performed at a center-of-mass energy $\sqrt{s} = 13$ TeV. A value of σ_{eff} equal to $12.7^{+5.0}_{-2.9}$ mb has been extracted from the same-sign WW measurement in ref. [14]. A σ_{eff} of $7.3 \pm 0.5\,(\text{stat}) \pm 1.0\,(\text{syst})$ mb has been obtained from the J/ψ pair production measurement in ref. [20]. It has been shown that σ_{eff} is expected

JHEP01(2022)177

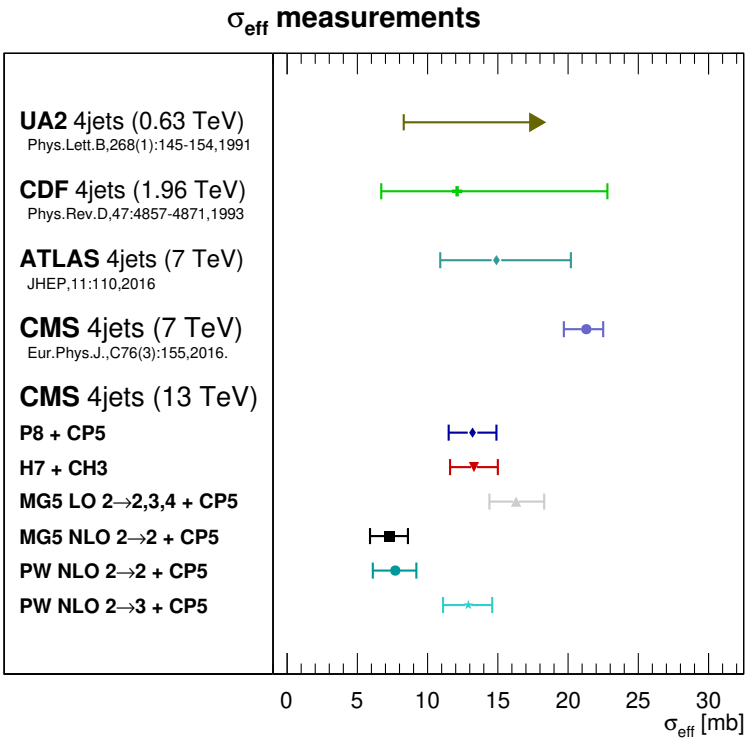

Figure 15. Comparison of the values for σ_{eff} extracted from data using different SPS models where events that have generated one or more hard MPI partons with $p_{\text{T}}^{\text{parton}} \geq 20\,\text{GeV}$, have been removed. The results from four-jet measurements performed at lower center-of-mass energies [7, 21, 25, 51] are shown alongside the newly extracted values. The error bars in each of the values of σ_{eff} represent the total (statistical+systematic) uncertainties.

to be process independent for inclusive final states [78], therefore, it is noteworthy that the result the J/ψ meson pair production measurement shows only agreement with the NLO $2 \to 2$ models. The extracted σ_{eff} of the same-sign WW measurement shows agreement with all models due to the size of the errors in the measurement, indicating that further measurements in this channel are desirable before any further conclusions can be made.

9 Summary

A study of the inclusive production of four-jet events at low transverse momentum has been presented based on data from proton-proton collisions collected with the CMS detector at a center-of-mass energy of 13 TeV. Various observables sensitive to double-parton scattering (DPS) are studied and values for its effective cross section have been extracted.

Models based on leading order (LO) $2 \to 2$ matrix elements significantly overestimate the absolute four-jet cross section in the phase space domains studied in this paper. This excess is related to an abundance of low-p_{T} and forward jets. The predictions of the absolute cross section generally improve when next-to-leading order (NLO) and/or higher-multiplicity matrix elements are used.

JHEP01(2022)177

MC Model	Tune	$f_{\mathrm{DPS}} \pm (\mathrm{stat}) \pm (\mathrm{syst})$ (%)		
—	—	Full tune	Hard MPI removed	Inherent DPS
PYTHIA8	CP5	$3.77 \pm 0.08\,^{+0.45}_{-0.68}$	$6.34 \pm 0.07\,^{+0.32}_{-0.57}$	$2.57 \pm 0.11\,^{+0.36}_{-0.62}$
PYTHIA8+VINCIA	Standard PYTHIA8.3	$2.40 \pm 0.07\,^{+0.41}_{-0.68}$	$3.84 \pm 0.07\,^{+0.34}_{-0.63}$	$1.44 \pm 0.10\,^{+0.37}_{-0.65}$
PYTHIA8	CDPSTP8S1-4j	$-1.30 \pm 0.08\,^{+0.39}_{-0.69}$	$3.06 \pm 0.07\,^{+0.28}_{-0.62}$	$4.36 \pm 0.11\,^{+0.34}_{-0.66}$
HERWIG7	CH3	$3.72 \pm 0.07\,^{+0.38}_{-0.68}$	$6.28 \pm 0.08\,^{+0.29}_{-0.58}$	$2.56 \pm 0.11\,^{+0.33}_{-0.63}$
HERWIG7	SoftTune	$2.67 \pm 0.07\,^{+0.42}_{-0.71}$	$4.85 \pm 0.08\,^{+0.31}_{-0.52}$	$2.18 \pm 0.11\,^{+0.36}_{-0.61}$
MADGRAPH5_AMC@NLO LO $2 \to 2,3,4$, PYTHIA8	CP5	$2.50 \pm 0.08\,^{+0.38}_{-0.69}$	$5.14 \pm 0.08\,^{+0.30}_{-0.56}$	$2.64 \pm 0.11\,^{+0.35}_{-0.62}$
MADGRAPH5_AMC@NLO LO $2 \to 2,3,4$, PYTHIA8+VINCIA	Standard PYTHIA8.3	$2.55 \pm 0.09\,^{+0.38}_{-0.66}$	$5.23 \pm 0.08\,^{+0.27}_{-0.53}$	$2.68 \pm 0.12\,^{+0.33}_{-0.60}$
MADGRAPH5_AMC@NLO NLO $2 \to 2$, PYTHIA8	CP5	$7.13 \pm 0.08\,^{+0.28}_{-0.42}$	$11.45 \pm 0.08\,^{+0.22}_{-0.27}$	$4.32 \pm 0.11\,^{+0.25}_{-0.36}$
POWHEG NLO $2 \to 2$, PYTHIA8	CP5	$4.77 \pm 0.08\,^{+0.32}_{-0.64}$	$10.89 \pm 0.08\,^{+0.24}_{-0.48}$	$6.12 \pm 0.11\,^{+0.28}_{-0.53}$
POWHEG NLO $2 \to 3$, PYTHIA8	CP5	$5.40 \pm 0.07\,^{+0.36}_{-0.67}$	$6.51 \pm 0.07\,^{+0.29}_{-0.51}$	$1.11 \pm 0.10\,^{+0.33}_{-0.59}$

Table 6. The values of the DPS fraction f_{DPS} extracted from data using different SPS models, along with their statistical and systematic uncertainties. The results are shown for the model where the full tune is used, and for the same models where the hard MPI have been removed. The last column shows the net difference between the two first columns, and is interpreted as the fraction of DPS inherent to the tune.

The azimuthal angle between the jets with the largest separation in η, ϕ_{ij}, has a strong discriminating power for different parton-shower approaches and the data favor the angular-ordered and dipole-antenna parton-shower models over those with a p_{T}-ordered parton shower. The yield of jet pairs with large rapidity separation ΔY is, however, overestimated by all models, although models based on NLO and/or higher-multiplicity matrix elements are closer to the data.

The distribution of the minimal combined azimuthal angular range of three jets, $\Delta\phi_{3\mathrm{j}}^{\mathrm{min}}$, also exhibits sensitivity to the parton-shower implementation, with data favoring p_{T}-ordered parton showers with the LO $2 \to 2$ models for this observable. In the case of models based on NLO and/or higher-multiplicity matrix elements the comparisons are less conclusive.

Other observables, such as the azimuthal angle between the two softest jets, $\Delta\phi_{\mathrm{Soft}}$, and their transverse momentum balance, $\Delta p_{\mathrm{T,Soft}}$, indicate the need for a DPS contribution in the models to various degrees, as confirmed by the extracted values of σ_{eff}.

The distribution of the azimuthal angle between the hard and soft jet pairs, ΔS, is the least sensitive to the details of the parton-shower modeling, and it is used for the extraction of the effective cross section, σ_{eff}.

A dependence is observed in the extracted values of σ_{eff} in the model used to describe the SPS contribution. Models based on NLO $2 \to 2$ matrix elements yield the smallest

JHEP01(2022)177

MC Model	Tune	$\sigma_{A,B}^{DPS} \pm (stat) \pm (syst)$ (nb)		
—	—	Full tune	Hard MPI removed	Inherent DPS
PYTHIA8	CP5	$22.9 \pm 0.7\,^{+5.7}_{-7.3}$	$38.5 \pm 0.9\,^{+6.5}_{-9.4}$	$15.6 \pm 1.1\,^{+6.1}_{-8.4}$
PYTHIA8+VINCIA	Standard PYTHIA8.3	$14.6 \pm 0.6\,^{+4.4}_{-5.9}$	$23.3 \pm 0.7\,^{+4.9}_{-7.1}$	$8.7 \pm 0.9\,^{+4.7}_{-6.5}$
PYTHIA8	CDPSTP8S1-4j	$-7.9 \pm 0.5\,^{+2.3}_{-2.9}$	$18.6 \pm 0.6\,^{+4.6}_{-6.5}$	$26.5 \pm 0.8\,^{+3.5}_{-4.7}$
HERWIG7	CH3	$22.6 \pm 0.7\,^{+5.1}_{-7.3}$	$38.2 \pm 0.9\,^{+6.4}_{-9.4}$	$15.6 \pm 1.1\,^{+5.8}_{-8.4}$
HERWIG7	SoftTune	$16.2 \pm 0.6\,^{+4.6}_{-6.3}$	$29.5 \pm 0.8\,^{+5.6}_{-8.6}$	$13.3 \pm 1.0\,^{+5.1}_{-7.5}$
MADGRAPH5_AMC@NLO LO $2 \to 2,3,4$, PYTHIA8	CP5	$15.2 \pm 0.6\,^{+4.2}_{-6.1}$	$31.2 \pm 0.8\,^{+5.5}_{-8.1}$	$16.0 \pm 1.0\,^{+4.9}_{-7.1}$
MADGRAPH5_AMC@NLO LO $2 \to 2,3,4$, PYTHIA8+VINCIA	Standard PYTHIA8.3	$15.5 \pm 0.6\,^{+4.3}_{-6.0}$	$31.8 \pm 0.8\,^{+5.3}_{-8.0}$	$16.3 \pm 1.0\,^{+4.8}_{-7.0}$
MADGRAPH5_AMC@NLO NLO $2 \to 2$, PYTHIA8	CP5	$43.3 \pm 1.0\,^{+4.5}_{-9.4}$	$70 \pm 2\,^{+8}_{-13}$	$26.7 \pm 2\,^{+6}_{-11}$
POWHEG NLO $2 \to 2$, PYTHIA8	CP5	$29.0 \pm 0.9\,^{+5.3}_{-6.1}$	$66 \pm 3\,^{+7}_{-12}$	$37.0 \pm 3.1\,^{+6.2}_{-9.1}$
POWHEG NLO $2 \to 3$, PYTHIA8	CP5	$32.8 \pm 0.9\,^{+5.9}_{-8.3}$	$39.5 \pm 1.0\,^{+6.3}_{-9.2}$	$6.7 \pm 1.3\,^{+6.1}_{-8.8}$

Table 7. The values of the DPS cross section $\sigma_{A,B}^{DPS}$ extracted from data using different SPS models, along with their statistical and systematic uncertainties. The results are shown for the model where the full tune is used, and for the same models where the hard MPI have been removed. The last column shows the net difference between the two first columns, and is interpreted as the amount of DPS inherent to the tune.

($\sim$7 mb) values of σ_{eff} and need the largest DPS contribution. However, models using a $2 \to 2$ matrix element along with older underlying event descriptions and older PDFs, tend to need the smallest DPS contribution. The sensitivity to the underlying event description, parton showers, and the PDFs is observed to be small when including higher-order matrix elements, since both models using the $2 \to 2,3,4$ matrix elements show agreement with each other.

These results demonstrate the need for further development of models to accurately describe final states with multiple jets in phase space regions with large potential DPS contributions.

Acknowledgments

We congratulate our colleagues in the CERN accelerator departments for the excellent performance of the LHC and thank the technical and administrative staffs at CERN and at other CMS institutes for their contributions to the success of the CMS effort. In addition, we gratefully acknowledge the computing centers and personnel of the Worldwide LHC Computing Grid and other centers for delivering so effectively the computing infrastructure essential to our analyses. Finally, we acknowledge the enduring support for the construction and operation of the LHC, the CMS detector, and the supporting computing infrastructure provided by the following funding agencies: BMBWF and FWF (Austria);

JHEP01(2022)177

MC Model	Tune	$\sigma_{\text{eff}} \pm (\text{stat}) \pm (\text{syst})$ (mb)	
—	—	Full tune	Hard MPI removed
PYTHIA8	CP5	$22.2 \pm 0.7\,^{+1.2}_{-0.8}$	$13.2 \pm 0.3\,^{+1.6}_{-1.7}$
PYTHIA8+VINCIA	Standard PYTHIA8.3	$34.8 \pm 1.3\,^{+0.9}_{-3.5}$	$21.8 \pm 0.7\,^{+1.9}_{-1.2}$
PYTHIA8	CDPSTP8S1-4j	-	$27.3 \pm 0.9\,^{+1.5}_{-0.5}$
HERWIG7	CH3	$22.5 \pm 0.7\,^{+1.7}_{-0.7}$	$13.3 \pm 0.3\,^{+1.7}_{-1.7}$
HERWIG7	SoftTune	$31.4 \pm 1.1\,^{+1.1}_{-2.4}$	$17.2 \pm 0.5\,^{+1.8}_{-1.5}$
MADGRAPH5_aMC@NLO LO $2 \to 2, 3, 4$, PYTHIA8	CP5	$33.4 \pm 1.3\,^{+1.1}_{-3.1}$	$16.3 \pm 0.5\,^{+1.9}_{-1.8}$
MADGRAPH5_aMC@NLO LO $2 \to 2, 3, 4$, PYTHIA8+VINCIA	Standard PYTHIA8.3	$32.8 \pm 1.3\,^{+1.2}_{-2.1}$	$16.0 \pm 0.4\,^{+2.0}_{-1.9}$
MADGRAPH5_aMC@NLO NLO $2 \to 2$, PYTHIA8	CP5	$11.7 \pm 0.3\,^{+2.3}_{-1.9}$	$7.3 \pm 0.2\,^{+1.3}_{-1.4}$
POWHEG NLO $2 \to 2$, PYTHIA8	CP5	$17.5 \pm 0.9\,^{+1.6}_{-1.7}$	$7.7 \pm 0.3\,^{+1.5}_{-1.6}$
POWHEG NLO $2 \to 3$, PYTHIA8	CP5	$15.5 \pm 0.5\,^{+1.8}_{-1.8}$	$12.9 \pm 0.3\,^{+1.7}_{-1.8}$

Table 8. The values of the effective cross section σ_{eff} extracted from data using different SPS models, along with their statistical and systematic uncertainties. The results are shown for the model where the full tune is used, and for the same models where the hard MPI have been removed

FNRS and FWO (Belgium); CNPq, CAPES, FAPERJ, FAPERGS, and FAPESP (Brazil); MES and BNSF (Bulgaria); CERN; CAS, MoST, and NSFC (China); MINCIENCIAS (Colombia); MSES and CSF (Croatia); RIF (Cyprus); SENESCYT (Ecuador); MoER, ERC PUT and ERDF (Estonia); Academy of Finland, MEC, and HIP (Finland); CEA and CNRS/IN2P3 (France); BMBF, DFG, and HGF (Germany); GSRI (Greece); NKFIA (Hungary); DAE and DST (India); IPM (Iran); SFI (Ireland); INFN (Italy); MSIP and NRF (Republic of Korea); MES (Latvia); LAS (Lithuania); MOE and UM (Malaysia); BUAP, CINVESTAV, CONACYT, LNS, SEP, and UASLP-FAI (Mexico); MOS (Montenegro); MBIE (New Zealand); PAEC (Pakistan); MSHE and NSC (Poland); FCT (Portugal); JINR (Dubna); MON, RosAtom, RAS, RFBR, and NRC KI (Russia); MESTD (Serbia); SEIDI, CPAN, PCTI, and FEDER (Spain); MOSTR (Sri Lanka); Swiss Funding Agencies (Switzerland); MST (Taipei); ThEPCenter, IPST, STAR, and NSTDA (Thailand); TUBITAK and TAEK (Turkey); NASU (Ukraine); STFC (United Kingdom); DOE and NSF (U.S.A.).

Individuals have received support from the Marie-Curie program and the European Research Council and Horizon 2020 Grant, contract Nos. 675440, 724704, 752730, 758316, 765710, 824093, 884104, and COST Action CA16108 (European Union); the Leventis Foundation; the Alfred P. Sloan Foundation; the Alexander von Humboldt Foundation; the Belgian Federal Science Policy Office; the Fonds pour la Formation à la Recherche dans l'Industrie et dans l'Agriculture (FRIA-Belgium); the Agentschap voor Innovatie

JHEP01(2022)177

door Wetenschap en Technologie (IWT-Belgium); the F.R.S.-FNRS and FWO (Belgium) under the "Excellence of Science — EOS" — be.h project n. 30820817; the Beijing Municipal Science & Technology Commission, No. Z191100007219010; the Ministry of Education, Youth and Sports (MEYS) of the Czech Republic; the Deutsche Forschungsgemeinschaft (DFG), under Germany's Excellence Strategy — EXC 2121 "Quantum Universe" — 390833306, and under project number 400140256 - GRK2497; the Lendület ("Momentum") Program and the János Bolyai Research Scholarship of the Hungarian Academy of Sciences, the New National Excellence Program ÚNKP, the NKFIA research grants 123842, 123959, 124845, 124850, 125105, 128713, 128786, and 129058 (Hungary); the Council of Science and Industrial Research, India; the Latvian Council of Science; the Ministry of Science and Higher Education and the National Science Center, contracts Opus 2014/15/B/ST2/03998 and 2015/19/B/ST2/02861 (Poland); the Fundação para a Ciência e a Tecnologia, grant CEECIND/01334/2018 (Portugal); the National Priorities Research Program by Qatar National Research Fund; the Ministry of Science and Higher Education, project no. 14.W03.31.0026 (Russia); the Programa Estatal de Fomento de la Investigación Científica y Técnica de Excelencia María de Maeztu, grant MDM-2015-0509 and the Programa Severo Ochoa del Principado de Asturias; the Stavros Niarchos Foundation (Greece); the Rachadapisek Sompot Fund for Postdoctoral Fellowship, Chulalongkorn University and the Chulalongkorn Academic into Its 2nd Century Project Advancement Project (Thailand); the Kavli Foundation; the Nvidia Corporation; the SuperMicro Corporation; the Welch Foundation, contract C-1845; and the Weston Havens Foundation (U.S.A.).

References

[1] CMS collaboration, *Measurement of the ratio of inclusive jet cross sections using the anti-k_T algorithm with radius parameters $R = 0.5$ and 0.7 in pp collisions at $\sqrt{s} = 7$ TeV*, *Phys. Rev. D* **90** (2014) 072006 [arXiv:1406.0324] [INSPIRE].

[2] CMS collaboration, *Measurement and QCD analysis of double-differential inclusive jet cross sections in pp collisions at $\sqrt{s} = 8$ TeV and cross section ratios to 2.76 and 7 TeV*, *JHEP* **03** (2017) 156 [arXiv:1609.05331] [INSPIRE].

[3] CMS collaboration, *Measurement of the double-differential inclusive jet cross section in proton-proton collisions at $\sqrt{s} = 13$ TeV*, *Eur. Phys. J. C* **76** (2016) 451 [arXiv:1605.04436] [INSPIRE].

[4] CMS collaboration, *Measurement of four-jet production in proton-proton collisions at $\sqrt{s} = 7$ TeV*, *Phys. Rev. D* **89** (2014) 092010 [arXiv:1312.6440] [INSPIRE].

[5] M. Diehl, D. Ostermeier and A. Schafer, *Elements of a theory for multiparton interactions in QCD*, *JHEP* **03** (2012) 089 [*Erratum ibid.* **03** (2016) 001] [arXiv:1111.0910] [INSPIRE].

[6] CDF collaboration, *Measurement of double parton scattering in $\bar{p}p$ collisions at $\sqrt{s} = 1.8$ TeV*, *Phys. Rev. Lett.* **79** (1997) 584 [INSPIRE].

JHEP01(2022)177

[7] CDF collaboration, *Double parton scattering in $\bar{p}p$ collisions at $\sqrt{s} = 1.8$ TeV*, *Phys. Rev. D* **56** (1997) 3811 [INSPIRE].

[8] D0 collaboration, *Double parton interactions in $\gamma + 3$ jet events in pp^- bar collisions $\sqrt{s} = 1.96$ TeV*, *Phys. Rev. D* **81** (2010) 052012 [arXiv:0912.5104] [INSPIRE].

[9] D0 collaboration, *Double parton interactions in $\gamma + 3$ jet and $\gamma + b/cjet + 2$ jet events in $p\bar{p}$ collisions at $\sqrt{s} = 1.96$ TeV*, *Phys. Rev. D* **89** (2014) 072006 [arXiv:1402.1550] [INSPIRE].

[10] D0 collaboration, *Study of double parton interactions in diphoton + dijet events in $p\bar{p}$ collisions at $\sqrt{s} = 1.96$ TeV*, *Phys. Rev. D* **93** (2016) 052008 [arXiv:1512.05291] [INSPIRE].

[11] ATLAS collaboration, *Measurement of hard double-parton interactions in $W(\rightarrow l\nu) + 2$ jet events at $\sqrt{s} = 7$ TeV with the ATLAS detector*, *New J. Phys.* **15** (2013) 033038 [arXiv:1301.6872] [INSPIRE].

[12] CMS collaboration, *Study of double parton scattering using $W + 2$-jet events in proton-proton collisions at $\sqrt{s} = 7$ TeV*, *JHEP* **03** (2014) 032 [arXiv:1312.5729] [INSPIRE].

[13] CMS collaboration, *Constraints on the double-parton scattering cross section from same-sign W boson pair production in proton-proton collisions at $\sqrt{s} = 8$ TeV*, *JHEP* **02** (2018) 032 [arXiv:1712.02280] [INSPIRE].

[14] CMS collaboration, *Evidence for WW production from double-parton interactions in proton-proton collisions at $\sqrt{s} = 13$ TeV*, *Eur. Phys. J. C* **80** (2020) 41 [arXiv:1909.06265] [INSPIRE].

[15] CMS collaboration, *Study of Z boson plus jets events using variables sensitive to double-parton scattering in pp collisions at* 13 *TeV*, *JHEP* **10** (2021) 176 [arXiv:2105.14511] [INSPIRE].

[16] LHCb collaboration, *Observation of double charm production involving open charm in pp collisions at $\sqrt{s} = 7$ TeV*, *JHEP* **06** (2012) 141 [*Addendum ibid.* **03** (2014) 108] [arXiv:1205.0975] [INSPIRE].

[17] LHCb collaboration, *Observation of associated production of a Z boson with a D meson in the forward region*, *JHEP* **04** (2014) 091 [arXiv:1401.3245] [INSPIRE].

[18] D0 collaboration, *Observation and studies of double J/ψ production at the Tevatron*, *Phys. Rev. D* **90** (2014) 111101 [arXiv:1406.2380] [INSPIRE].

[19] LHCb collaboration, *Production of associated Y and open charm hadrons in pp collisions at $\sqrt{s} = 7$ and 8 TeV via double parton scattering*, *JHEP* **07** (2016) 052 [arXiv:1510.05949] [INSPIRE].

[20] LHCb collaboration, *Measurement of the J/ψ pair production cross-section in pp collisions at $\sqrt{s} = 13$ TeV*, *JHEP* **06** (2017) 047 [*Erratum ibid.* **10** (2017) 068] [arXiv:1612.07451] [INSPIRE].

[21] UA2 collaboration, *A study of multi-jet events at the CERN $\bar{p}p$ collider and a search for double parton scattering*, *Phys. Lett. B* **268** (1991) 145 [INSPIRE].

[22] CDF collaboration, *Study of four jet events and evidence for double parton interactions in $p\bar{p}$ collisions at $\sqrt{s} = 1.8$ TeV*, *Phys. Rev. D* **47** (1993) 4857 [INSPIRE].

[23] ATLAS collaboration, *Measurement of four-jet differential cross sections in $\sqrt{s} = 8$ TeV proton-proton collisions using the ATLAS detector*, *JHEP* **12** (2015) 105 [arXiv:1509.07335] [INSPIRE].

JHEP01(2022)177

[24] I. Sadeh, *Double parton scattering in four-jet events in pp collisions at 7 TeV with the ATLAS experiment at the LHC*, Ph.D. thesis, Tel Aviv University (2013), arXiv:1308.0587 [INSPIRE].

[25] ATLAS collaboration, *Study of hard double-parton scattering in four-jet events in pp collisions at $\sqrt{s} = 7$ TeV with the ATLAS experiment*, *JHEP* **11** (2016) 110 [arXiv:1608.01857] [INSPIRE].

[26] CMS collaboration, *Studies of inclusive four-jet production with two b-tagged jets in proton-proton collisions at 7 TeV*, *Phys. Rev. D* **94** (2016) 112005 [arXiv:1609.03489] [INSPIRE].

[27] *HEPData record for this analysis*, http://dx.doi.org/10.17182/hepdata.102460 (2021).

[28] S. Domdey, H.-J. Pirner and U.A. Wiedemann, *Testing the scale dependence of the scale factor $\sigma_{\rm eff}$) in double dijet production at the LHC*, *Eur. Phys. J. C* **65** (2010) 153 [arXiv:0906.4335] [INSPIRE].

[29] E.L. Berger, C.B. Jackson and G. Shaughnessy, *Characteristics and estimates of double parton scattering at the Large Hadron Collider*, *Phys. Rev. D* **81** (2010) 014014 [arXiv:0911.5348] [INSPIRE].

[30] R. Maciuła and A. Szczurek, *Searching for and exploring double-parton scattering effects in four-jet production at the LHC*, *Phys. Lett. B* **749** (2015) 57 [arXiv:1503.08022] [INSPIRE].

[31] K. Kutak, R. Maciula, M. Serino, A. Szczurek and A. van Hameren, *Four-jet production in single- and double-parton scattering within high-energy factorization*, *JHEP* **04** (2016) 175 [arXiv:1602.06814] [INSPIRE].

[32] K. Kutak, *Production of four-jets in single- and double-parton scattering within high-energy factorization*, *PoS* **ICHEP2016** (2016) 610 [arXiv:1701.00410] [INSPIRE].

[33] K. Kutak, R. Maciuła, M. Serino, A. Szczurek and A. van Hameren, *Search for optimal conditions for exploring double-parton scattering in four-jet production: k_t-factorization approach*, *Phys. Rev. D* **94** (2016) 014019 [arXiv:1605.08240] [INSPIRE].

[34] CMS collaboration, *Performance of the CMS Level-1 trigger in proton-proton collisions at $\sqrt{s} = 13$ TeV*, 2020 *JINST* **15** P10017 [arXiv:2006.10165] [INSPIRE].

[35] CMS collaboration, *The CMS trigger system*, 2017 *JINST* **12** P01020 [arXiv:1609.02366] [INSPIRE].

[36] CMS collaboration, *Particle-flow reconstruction and global event description with the CMS detector*, 2017 *JINST* **12** P10003 [arXiv:1706.04965] [INSPIRE].

[37] M. Cacciari, G.P. Salam and G. Soyez, *The anti-k_t jet clustering algorithm*, *JHEP* **04** (2008) 063 [arXiv:0802.1189] [INSPIRE].

[38] M. Cacciari, G.P. Salam and G. Soyez, *FastJet user manual*, *Eur. Phys. J. C* **72** (2012) 1896 [arXiv:1111.6097] [INSPIRE].

[39] CMS collaboration, *Jet energy scale and resolution in the CMS experiment in pp collisions at 8 TeV*, 2017 *JINST* **12** P02014 [arXiv:1607.03663] [INSPIRE].

[40] CMS collaboration, *The CMS experiment at the CERN LHC*, 2008 *JINST* **3** S08004 [INSPIRE].

[41] T. Sjöstrand et al., *An introduction to PYTHIA 8.2*, *Comput. Phys. Commun.* **191** (2015) 159 [arXiv:1410.3012] [INSPIRE].

JHEP01(2022)177

[42] M. Bahr et al., *HERWIG++ physics and manual*, *Eur. Phys. J. C* **58** (2008) 639 [arXiv:0803.0883] [INSPIRE].

[43] J. Bellm et al., *Herwig 7.0/Herwig++ 3.0 release note*, *Eur. Phys. J. C* **76** (2015) 196 [arXiv:1512.0117].

[44] V.N. Gribov and L.N. Lipatov, *Deep inelastic ep scattering in perturbation theory*, *Sov. J. Nucl. Phys.* **15** (1972) 438 [*Yad. Fiz.* **15** (1972) 781] [INSPIRE].

[45] Y.L. Dokshitzer, *Calculation of the structure functions for deep inelastic scattering and e^+e^- annihilation by perturbation theory in quantum chromodynamics*, *Sov. Phys. JETP* **46** (1977) 641 [*Zh. Eksp. Teor. Fiz.* **73** (1977) 1216] [INSPIRE].

[46] G. Altarelli and G. Parisi, *Asymptotic freedom in parton language*, *Nucl. Phys. B* **126** (1977) 298 [INSPIRE].

[47] B. Andersson, G. Gustafson, G. Ingelman and T. Sjöstrand, *Parton fragmentation and string dynamics*, *Phys. Rept.* **97** (1983) 31 [INSPIRE].

[48] D. Amati and G. Veneziano, *Preconfinement as a property of perturbative QCD*, *Phys. Lett. B* **83** (1979) 87 [INSPIRE].

[49] GEANT4 collaboration, *GEANT4 — a simulation toolkit*, *Nucl. Instrum. Meth. A* **506** (2003) 250 [INSPIRE].

[50] P. Skands, S. Carrazza and J. Rojo, *Tuning PYTHIA 8.1: the Monash 2013 tune*, *Eur. Phys. J. C* **74** (2014) 3024 [arXiv:1404.5630] [INSPIRE].

[51] CMS collaboration, *Event generator tunes obtained from underlying event and multiparton scattering measurements*, *Eur. Phys. J. C* **76** (2016) 155 [arXiv:1512.00815] [INSPIRE].

[52] CMS collaboration, *Extraction and validation of a new set of CMS PYTHIA8 tunes from underlying-event measurements*, *Eur. Phys. J. C* **80** (2020) 4 [arXiv:1903.12179] [INSPIRE].

[53] NNPDF collaboration, *Parton distributions from high-precision collider data*, *Eur. Phys. J. C* **77** (2017) 663 [arXiv:1706.00428] [INSPIRE].

[54] R. Corke and T. Sjöstrand, *Interleaved parton showers and tuning prospects*, *JHEP* **03** (2011) 032 [arXiv:1011.1759] [INSPIRE].

[55] J. Pumplin, D.R. Stump, J. Huston, H.L. Lai, P.M. Nadolsky and W.K. Tung, *New generation of parton distributions with uncertainties from global QCD analysis*, *JHEP* **07** (2002) 012 [hep-ph/0201195] [INSPIRE].

[56] N. Fischer, S. Prestel, M. Ritzmann and P. Skands, *Vincia for hadron colliders*, *Eur. Phys. J. C* **76** (2016) 589 [arXiv:1605.06142] [INSPIRE].

[57] L.A. Harland-Lang, A.D. Martin, P. Motylinski and R.S. Thorne, *Parton distributions in the LHC era: MMHT 2014 PDFs*, *Eur. Phys. J. C* **75** (2015) 204 [arXiv:1412.3989] [INSPIRE].

[58] CMS collaboration, *Development and validation of HERWIG 7 tunes from CMS underlying-event measurements*, *Eur. Phys. J. C* **81** (2021) 312 [arXiv:2011.03422] [INSPIRE].

[59] H. Jung et al., *The CCFM Monte Carlo generator CASCADE version 2.2.03*, *Eur. Phys. J. C* **70** (2010) 1237 [arXiv:1008.0152] [INSPIRE].

[60] J. Alwall et al., *The automated computation of tree-level and next-to-leading order differential cross sections, and their matching to parton shower simulations*, *JHEP* **07** (2014) 079 [arXiv:1405.0301] [INSPIRE].

JHEP01(2022)177

[61] J. Alwall et al., *Comparative study of various algorithms for the merging of parton showers and matrix elements in hadronic collisions*, *Eur. Phys. J. C* **53** (2008) 473 [arXiv:0706.2569] [INSPIRE].

[62] P. Nason, *A new method for combining NLO QCD with shower Monte Carlo algorithms*, *JHEP* **11** (2004) 040 [hep-ph/0409146] [INSPIRE].

[63] S. Frixione, P. Nason and C. Oleari, *Matching NLO QCD computations with Parton Shower simulations: the POWHEG method*, *JHEP* **11** (2007) 070 [arXiv:0709.2092] [INSPIRE].

[64] S. Alioli, P. Nason, C. Oleari and E. Re, *A general framework for implementing NLO calculations in shower Monte Carlo programs: the POWHEG BOX*, *JHEP* **06** (2010) 043 [arXiv:1002.2581] [INSPIRE].

[65] S. Alioli, K. Hamilton, P. Nason, C. Oleari and E. Re, *Jet pair production in POWHEG*, *JHEP* **04** (2011) 081 [arXiv:1012.3380] [INSPIRE].

[66] A. Kardos, P. Nason and C. Oleari, *Three-jet production in POWHEG*, *JHEP* **04** (2014) 043 [arXiv:1402.4001] [INSPIRE].

[67] A. van Hameren, *KaTie: for parton-level event generation with k_T-dependent initial states*, *Comput. Phys. Commun.* **224** (2018) 371 [arXiv:1611.00680] [INSPIRE].

[68] S. Catani and F. Hautmann, *High-energy factorization and small x deep inelastic scattering beyond leading order*, *Nucl. Phys. B* **427** (1994) 475 [hep-ph/9405388] [INSPIRE].

[69] M. Deak, F. Hautmann, H. Jung and K. Kutak, *Forward jet production at the Large Hadron Collider*, *JHEP* **09** (2009) 121 [arXiv:0908.0538] [INSPIRE].

[70] S. Sapeta, *QCD and jets at hadron colliders*, *Prog. Part. Nucl. Phys.* **89** (2016) 1 [arXiv:1511.09336] [INSPIRE].

[71] M. Bury, A. van Hameren, H. Jung, K. Kutak, S. Sapeta and M. Serino, *Calculations with off-shell matrix elements, TMD parton densities and TMD parton showers*, *Eur. Phys. J. C* **78** (2018) 137 [arXiv:1712.05932] [INSPIRE].

[72] A. Bermudez Martinez et al., *Collinear and TMD parton densities from fits to precision DIS measurements in the parton branching method*, *Phys. Rev. D* **99** (2019) 074008 [arXiv:1804.11152] [INSPIRE].

[73] S. Schmitt, *TUnfold: an algorithm for correcting migration effects in high energy physics*, 2012 *JINST* **7** T10003 [arXiv:1205.6201] [INSPIRE].

[74] S. Schmitt, *Data unfolding methods in high energy physics*, *EPJ Web Conf.* **137** (2017) 11008 [arXiv:1611.01927] [INSPIRE].

[75] A.N. Tikhonov, *Solution of incorrectly formulated problems and the regularization method*, *Sov. Math. Dokl.* **4** (1963) 1035.

[76] R. Brun and F. Rademakers, *ROOT: an object oriented data analysis framework*, *Nucl. Instrum. Meth. A* **389** (1997) 81 [INSPIRE].

[77] CMS collaboration, *Precision luminosity measurement in proton-proton collisions at $\sqrt{s} = 13$ TeV in 2015 and 2016 at CMS*, *Eur. Phys. J. C* **81** (2021) 800 [arXiv:2104.01927] [INSPIRE].

[78] M.H. Seymour and A. Siodmok, *Extracting $\sigma_{\text{effective}}$ from the LHCb double-charm measurement*, arXiv:1308.6749 [INSPIRE].

JHEP01(2022)177

The CMS collaboration

Yerevan Physics Institute, Yerevan, Armenia

A. Tumasyan

Institut für Hochenergiephysik, Vienna, Austria

W. Adam, J.W. Andrejkovic, T. Bergauer, S. Chatterjee, M. Dragicevic, A. Escalante Del Valle, R. Frühwirth[1], M. Jeitler[1], N. Krammer, L. Lechner, D. Liko, I. Mikulec, P. Paulitsch, F.M. Pitters, J. Schieck[1], R. Schöfbeck, M. Spanring, S. Templ, W. Waltenberger, C.-E. Wulz[1]

Institute for Nuclear Problems, Minsk, Belarus

V. Chekhovsky, A. Litomin, V. Makarenko

Universiteit Antwerpen, Antwerpen, Belgium

M.R. Darwish[2], E.A. De Wolf, X. Janssen, T. Kello[3], A. Lelek, M. Pieters, H. Rejeb Sfar, H. Van Haevermaet, P. Van Mechelen, S. Van Putte, N. Van Remortel

Vrije Universiteit Brussel, Brussel, Belgium

F. Blekman, E.S. Bols, J. D'Hondt, J. De Clercq, M. Delcourt, H. El Faham, S. Lowette, S. Moortgat, A. Morton, D. Müller, A.R. Sahasransu, S. Tavernier, W. Van Doninck, P. Van Mulders

Université Libre de Bruxelles, Bruxelles, Belgium

D. Beghin, B. Bilin, B. Clerbaux, G. De Lentdecker, L. Favart, A. Grebenyuk, A.K. Kalsi, K. Lee, M. Mahdavikhorrami, I. Makarenko, L. Moureaux, L. Pétré, A. Popov, N. Postiau, E. Starling, L. Thomas, M. Vanden Bemden, C. Vander Velde, P. Vanlaer, D. Vannerom, L. Wezenbeek

Ghent University, Ghent, Belgium

T. Cornelis, D. Dobur, J. Knolle, L. Lambrecht, G. Mestdach, M. Niedziela, C. Roskas, A. Samalan, K. Skovpen, M. Tytgat, W. Verbeke, B. Vermassen, M. Vit

Université Catholique de Louvain, Louvain-la-Neuve, Belgium

A. Bethani, G. Bruno, F. Bury, C. Caputo, P. David, C. Delaere, I.S. Donertas, A. Giammanco, K. Jaffel, Sa. Jain, V. Lemaitre, K. Mondal, J. Prisciandaro, A. Taliercio, M. Teklishyn, T.T. Tran, P. Vischia, S. Wertz, S. Wuyckens

Centro Brasileiro de Pesquisas Fisicas, Rio de Janeiro, Brazil

G.A. Alves, C. Hensel, A. Moraes

Universidade do Estado do Rio de Janeiro, Rio de Janeiro, Brazil

W.L. Aldá Júnior, M. Alves Gallo Pereira, M. Barroso Ferreira Filho, H. BRANDAO MALBOUISSON, W. Carvalho, J. Chinellato[4], E.M. Da Costa, G.G. Da Silveira[5], D. De Jesus Damiao, S. Fonseca De Souza, D. Matos Figueiredo, C. Mora Herrera, K. Mota Amarilo, L. Mundim, H. Nogima, P. Rebello Teles, A. Santoro, S.M. Silva Do Amaral, A. Sznajder, M. Thiel, F. Torres Da Silva De Araujo, A. Vilela Pereira

JHEP01(2022)177

Universidade Estadual Paulista[a], Universidade Federal do ABC[b], São Paulo, Brazil

C.A. Bernardes[a], L. Calligaris[a], T.R. Fernandez Perez Tomei[a], E.M. Gregores[a,b], D.S. Lemos[a], P.G. Mercadante[a,b], S.F. Novaes[a], Sandra S. Padula[a]

Institute for Nuclear Research and Nuclear Energy, Bulgarian Academy of Sciences, Sofia, Bulgaria

A. Aleksandrov, G. Antchev, R. Hadjiiska, P. Iaydjiev, M. Misheva, M. Rodozov, M. Shopova, G. Sultanov

University of Sofia, Sofia, Bulgaria

A. Dimitrov, T. Ivanov, L. Litov, B. Pavlov, P. Petkov, A. Petrov

Beihang University, Beijing, China

T. Cheng, W. Fang[3], Q. Guo, T. Javaid[6], M. Mittal, H. Wang, L. Yuan

Department of Physics, Tsinghua University

M. Ahmad, G. Bauer, C. Dozen[7], Z. Hu, J. Martins[8], Y. Wang, K. Yi[9,10]

Institute of High Energy Physics, Beijing, China

E. Chapon, G.M. Chen[6], H.S. Chen[6], M. Chen, F. Iemmi, A. Kapoor, D. Leggat, H. Liao, Z.-A. LIU[6], V. Milosevic, F. Monti, R. Sharma, J. Tao, J. Thomas-wilsker, J. Wang, H. Zhang, S. Zhang[6], J. Zhao

State Key Laboratory of Nuclear Physics and Technology, Peking University, Beijing, China

A. Agapitos, Y. Ban, C. Chen, Q. Huang, A. Levin, Q. Li, X. Lyu, Y. Mao, S.J. Qian, D. Wang, Q. Wang, J. Xiao

Sun Yat-Sen University, Guangzhou, China

M. Lu, Z. You

Institute of Modern Physics and Key Laboratory of Nuclear Physics and Ion-beam Application (MOE) - Fudan University, Shanghai, China

X. Gao[3], H. Okawa

Zhejiang University, Hangzhou, China

Z. Lin, M. Xiao

Universidad de Los Andes, Bogota, Colombia

C. Avila, A. Cabrera, C. Florez, J. Fraga, A. Sarkar, M.A. Segura Delgado

Universidad de Antioquia, Medellin, Colombia

J. Mejia Guisao, F. Ramirez, J.D. Ruiz Alvarez, C.A. Salazar González

University of Split, Faculty of Electrical Engineering, Mechanical Engineering and Naval Architecture, Split, Croatia

D. Giljanovic, N. Godinovic, D. Lelas, I. Puljak

JHEP01(2022)177

University of Split, Faculty of Science, Split, Croatia
Z. Antunovic, M. Kovac, T. Sculac

Institute Rudjer Boskovic, Zagreb, Croatia
V. Brigljevic, D. Ferencek, D. Majumder, M. Roguljic, A. Starodumov[11], T. Susa

University of Cyprus, Nicosia, Cyprus
A. Attikis, K. Christoforou, E. Erodotou, A. Ioannou, G. Kole, M. Kolosova, S. Konstantinou, J. Mousa, C. Nicolaou, F. Ptochos, P.A. Razis, H. Rykaczewski, H. Saka

Charles University, Prague, Czech Republic
M. Finger[12], M. Finger Jr.[12], A. Kveton

Escuela Politecnica Nacional, Quito, Ecuador
E. Ayala

Universidad San Francisco de Quito, Quito, Ecuador
E. Carrera Jarrin

Academy of Scientific Research and Technology of the Arab Republic of Egypt, Egyptian Network of High Energy Physics, Cairo, Egypt
A.A. Abdelalim[13,14], S. Elgammal[15]

Center for High Energy Physics (CHEP-FU), Fayoum University, El-Fayoum, Egypt
A. Lotfy, M.A. Mahmoud

National Institute of Chemical Physics and Biophysics, Tallinn, Estonia
S. Bhowmik, A. Carvalho Antunes De Oliveira, R.K. Dewanjee, K. Ehataht, M. Kadastik, S. Nandan, C. Nielsen, J. Pata, M. Raidal, L. Tani, C. Veelken

Department of Physics, University of Helsinki, Helsinki, Finland
P. Eerola, L. Forthomme, H. Kirschenmann, K. Osterberg, M. Voutilainen

Helsinki Institute of Physics, Helsinki, Finland
S. Bharthuar, E. Brücken, F. Garcia, J. Havukainen, M.S. Kim, R. Kinnunen, T. Lampén, K. Lassila-Perini, S. Lehti, T. Lindén, M. Lotti, L. Martikainen, J. Ott, H. Siikonen, E. Tuominen, J. Tuominiemi

Lappeenranta University of Technology, Lappeenranta, Finland
P. Luukka, H. Petrow, T. Tuuva

IRFU, CEA, Université Paris-Saclay, Gif-sur-Yvette, France
C. Amendola, M. Besancon, F. Couderc, M. Dejardin, D. Denegri, J.L. Faure, F. Ferri, S. Ganjour, A. Givernaud, P. Gras, G. Hamel de Monchenault, P. Jarry, B. Lenzi, E. Locci, J. Malcles, J. Rander, A. Rosowsky, M.Ö. Sahin, A. Savoy-Navarro[16], M. Titov, G.B. Yu

Laboratoire Leprince-Ringuet, CNRS/IN2P3, Ecole Polytechnique, Institut Polytechnique de Paris, Palaiseau, France
S. Ahuja, F. Beaudette, M. Bonanomi, A. Buchot Perraguin, P. Busson, A. Cappati, C. Charlot, O. Davignon, B. Diab, G. Falmagne, S. Ghosh, R. Granier de Cassagnac,

JHEP01(2022)177

A. Hakimi, I. Kucher, M. Nguyen, C. Ochando, P. Paganini, J. Rembser, R. Salerno, J.B. Sauvan, Y. Sirois, A. Zabi, A. Zghiche

Université de Strasbourg, CNRS, IPHC UMR 7178, Strasbourg, France
J.-L. Agram[17], J. Andrea, D. Apparu, D. Bloch, G. Bourgatte, J.-M. Brom, E.C. Chabert, C. Collard, D. Darej, J.-C. Fontaine[17], U. Goerlach, C. Grimault, A.-C. Le Bihan, E. Nibigira, P. Van Hove

Institut de Physique des 2 Infinis de Lyon (IP2I), Villeurbanne, France
E. Asilar, S. Beauceron, C. Bernet, G. Boudoul, C. Camen, A. Carle, N. Chanon, D. Contardo, P. Depasse, H. El Mamouni, J. Fay, S. Gascon, M. Gouzevitch, B. Ille, I.B. Laktineh, H. Lattaud, A. Lesauvage, M. Lethuillier, L. Mirabito, S. Perries, K. Shchablo, V. Sordini, L. Torterotot, G. Touquet, M. Vander Donckt, S. Viret

Georgian Technical University, Tbilisi, Georgia
I. Lomidze, T. Toriashvili[18], Z. Tsamalaidze[12]

RWTH Aachen University, I. Physikalisches Institut, Aachen, Germany
L. Feld, K. Klein, M. Lipinski, D. Meuser, A. Pauls, M.P. Rauch, N. Röwert, J. Schulz, M. Teroerde

RWTH Aachen University, III. Physikalisches Institut A, Aachen, Germany
A. Dodonova, D. Eliseev, M. Erdmann, P. Fackeldey, B. Fischer, S. Ghosh, T. Hebbeker, K. Hoepfner, F. Ivone, H. Keller, L. Mastrolorenzo, M. Merschmeyer, A. Meyer, G. Mocellin, S. Mondal, S. Mukherjee, D. Noll, A. Novak, T. Pook, A. Pozdnyakov, Y. Rath, H. Reithler, J. Roemer, A. Schmidt, S.C. Schuler, A. Sharma, S. Wiedenbeck, S. Zaleski

RWTH Aachen University, III. Physikalisches Institut B, Aachen, Germany
C. Dziwok, G. Flügge, W. Haj Ahmad[19], O. Hlushchenko, T. Kress, A. Nowack, C. Pistone, O. Pooth, D. Roy, H. Sert, A. Stahl[20], T. Ziemons

Deutsches Elektronen-Synchrotron, Hamburg, Germany
H. Aarup Petersen, M. Aldaya Martin, P. Asmuss, I. Babounikau, S. Baxter, O. Behnke, A. Bermúdez Martínez, S. Bhattacharya, A.A. Bin Anuar, K. Borras[21], V. Botta, D. Brunner, A. Campbell, A. Cardini, C. Cheng, F. Colombina, S. Consuegra Rodríguez, G. Correia Silva, V. Danilov, L. Didukh, G. Eckerlin, D. Eckstein, L.I. Estevez Banos, O. Filatov, E. Gallo[22], A. Geiser, A. Giraldi, A. Grohsjean, M. Guthoff, A. Jafari[23], N.Z. Jomhari, H. Jung, A. Kasem[21], M. Kasemann, H. Kaveh, C. Kleinwort, D. Krücker, W. Lange, J. Lidrych, K. Lipka, W. Lohmann[24], R. Mankel, I.-A. Melzer-Pellmann, J. Metwally, A.B. Meyer, M. Meyer, J. Mnich, A. Mussgiller, Y. Otarid, D. Pérez Adán, D. Pitzl, A. Raspereza, B. Ribeiro Lopes, J. Rübenach, A. Saggio, A. Saibel, M. Savitskyi, M. Scham, V. Scheurer, C. Schwanenberger[22], A. Singh, R.E. Sosa Ricardo, D. Stafford, N. Tonon, O. Turkot, M. Van De Klundert, R. Walsh, D. Walter, Y. Wen, K. Wichmann, L. Wiens, C. Wissing, S. Wuchterl

University of Hamburg, Hamburg, Germany
R. Aggleton, S. Albrecht, S. Bein, L. Benato, A. Benecke, P. Connor, K. De Leo, M. Eich, F. Feindt, A. Fröhlich, C. Garbers, E. Garutti, P. Gunnellini, J. Haller, A. Hinzmann,

JHEP01(2022)177

G. Kasieczka, R. Klanner, R. Kogler, T. Kramer, V. Kutzner, J. Lange, T. Lange, A. Lobanov, A. Malara, A. Nigamova, K.J. Pena Rodriguez, O. Rieger, P. Schleper, M. Schröder, J. Schwandt, D. Schwarz, J. Sonneveld, H. Stadie, G. Steinbrück, A. Tews, B. Vormwald, I. Zoi

Karlsruher Institut fuer Technologie, Karlsruhe, Germany

J. Bechtel, T. Berger, E. Butz, R. Caspart, T. Chwalek, W. De Boer[†], A. Dierlamm, A. Droll, K. El Morabit, N. Faltermann, M. Giffels, J.o. Gosewisch, A. Gottmann, F. Hartmann[20], C. Heidecker, U. Husemann, I. Katkov[25], P. Keicher, R. Koppenhöfer, S. Maier, M. Metzler, S. Mitra, Th. Müller, M. Neukum, A. Nürnberg, G. Quast, K. Rabbertz, J. Rauser, D. Savoiu, M. Schnepf, D. Seith, I. Shvetsov, H.J. Simonis, R. Ulrich, J. Van Der Linden, R.F. Von Cube, M. Wassmer, M. Weber, S. Wieland, R. Wolf, S. Wozniewski, S. Wunsch

Institute of Nuclear and Particle Physics (INPP), NCSR Demokritos, Aghia Paraskevi, Greece

G. Anagnostou, P. Asenov, G. Daskalakis, T. Geralis, A. Kyriakis, D. Loukas, A. Stakia

National and Kapodistrian University of Athens, Athens, Greece

M. Diamantopoulou, D. Karasavvas, G. Karathanasis, P. Kontaxakis, C.K. Koraka, A. Manousakis-katsikakis, A. Panagiotou, I. Papavergou, N. Saoulidou, K. Theofilatos, E. Tziaferi, K. Vellidis, E. Vourliotis

National Technical University of Athens, Athens, Greece

G. Bakas, K. Kousouris, I. Papakrivopoulos, G. Tsipolitis, A. Zacharopoulou

University of Ioánnina, Ioánnina, Greece

I. Evangelou, C. Foudas, P. Gianneios, P. Katsoulis, P. Kokkas, N. Manthos, I. Papadopoulos, J. Strologas

MTA-ELTE Lendület CMS Particle and Nuclear Physics Group, Eötvös Loránd University

M. Csanad, K. Farkas, M.M.A. Gadallah[26], S. Lökös[27], P. Major, K. Mandal, A. Mehta, G. Pasztor, A.J. Rádl, O. Surányi, G.I. Veres

Wigner Research Centre for Physics, Budapest, Hungary

M. Bartók[28], G. Bencze, C. Hajdu, D. Horvath[29], F. Sikler, V. Veszpremi, G. Vesztergombi[†]

Institute of Nuclear Research ATOMKI, Debrecen, Hungary

S. Czellar, J. Karancsi[28], J. Molnar, Z. Szillasi, D. Teyssier

Institute of Physics, University of Debrecen

P. Raics, Z.L. Trocsanyi[30], B. Ujvari

Karoly Robert Campus, MATE Institute of Technology

T. Csorgo[31], F. Nemes[31], T. Novak

Indian Institute of Science (IISc), Bangalore, India

J.R. Komaragiri, D. Kumar, L. Panwar, P.C. Tiwari

JHEP01(2022)177

National Institute of Science Education and Research, HBNI, Bhubaneswar, India

S. Bahinipati[32], D. Dash, C. Kar, P. Mal, T. Mishra, V.K. Muraleedharan Nair Bindhu[33], A. Nayak[33], P. Saha, N. Sur, S.K. Swain, D. Vats[33]

Panjab University, Chandigarh, India

S. Bansal, S.B. Beri, V. Bhatnagar, G. Chaudhary, S. Chauhan, N. Dhingra[34], R. Gupta, A. Kaur, M. Kaur, S. Kaur, P. Kumari, M. Meena, K. Sandeep, J.B. Singh, A.K. Virdi

University of Delhi, Delhi, India

A. Ahmed, A. Bhardwaj, B.C. Choudhary, M. Gola, S. Keshri, A. Kumar, M. Naimuddin, P. Priyanka, K. Ranjan, A. Shah

Saha Institute of Nuclear Physics, HBNI, Kolkata, India

M. Bharti[35], R. Bhattacharya, S. Bhattacharya, D. Bhowmik, S. Dutta, S. Dutta, B. Gomber[36], M. Maity[37], P. Palit, P.K. Rout, G. Saha, B. Sahu, S. Sarkar, M. Sharan, B. Singh[35], S. Thakur[35]

Indian Institute of Technology Madras, Madras, India

P.K. Behera, S.C. Behera, P. Kalbhor, A. Muhammad, R. Pradhan, P.R. Pujahari, A. Sharma, A.K. Sikdar

Bhabha Atomic Research Centre, Mumbai, India

D. Dutta, V. Jha, V. Kumar, D.K. Mishra, K. Naskar[38], P.K. Netrakanti, L.M. Pant, P. Shukla

Tata Institute of Fundamental Research-A, Mumbai, India

T. Aziz, S. Dugad, M. Kumar, U. Sarkar

Tata Institute of Fundamental Research-B, Mumbai, India

S. Banerjee, R. Chudasama, M. Guchait, S. Karmakar, S. Kumar, G. Majumder, K. Mazumdar, S. Mukherjee

Indian Institute of Science Education and Research (IISER), Pune, India

K. Alpana, S. Dube, B. Kansal, A. Laha, S. Pandey, A. Rane, A. Rastogi, S. Sharma

Isfahan University of Technology, Isfahan, Iran

H. Bakhshiansohi[39], M. Zeinali[40]

Institute for Research in Fundamental Sciences (IPM), Tehran, Iran

S. Chenarani[41], S.M. Etesami, M. Khakzad, M. Mohammadi Najafabadi

University College Dublin, Dublin, Ireland

M. Grunewald

INFN Sezione di Bari[a], Università di Bari[b], Politecnico di Bari[c], Bari, Italy

M. Abbrescia[a,b], R. Aly[a,b,42], C. Aruta[a,b], A. Colaleo[a], D. Creanza[a,c], N. De Filippis[a,c], M. De Palma[a,b], A. Di Florio[a,b], A. Di Pilato[a,b], W. Elmetenawee[a,b], L. Fiore[a], A. Gelmi[a,b], M. Gul[a], G. Iaselli[a,c], M. Ince[a,b], S. Lezki[a,b], G. Maggi[a,c], M. Maggi[a], I. Margjeka[a,b],

JHEP01(2022)177

V. Mastrapasqua[a,b], J.A. Merlin[a], S. My[a,b], S. Nuzzo[a,b], A. Pellecchia[a,b], A. Pompili[a,b], G. Pugliese[a,c], A. Ranieri[a], G. Selvaggi[a,b], L. Silvestris[a], F.M. Simone[a,b], R. Venditti[a], P. Verwilligen[a]

INFN Sezione di Bologna[a], Università di Bologna[b], Bologna, Italy
G. Abbiendi[a], C. Battilana[a,b], D. Bonacorsi[a,b], L. Borgonovi[a], L. Brigliadori[a], R. Campanini[a,b], P. Capiluppi[a,b], A. Castro[a,b], F.R. Cavallo[a], M. Cuffiani[a,b], G.M. Dallavalle[a], T. Diotalevi[a,b], F. Fabbri[a], A. Fanfani[a,b], P. Giacomelli[a], L. Giommi[a,b], C. Grandi[a], L. Guiducci[a,b], S. Lo Meo[a,43], L. Lunerti[a,b], S. Marcellini[a], G. Masetti[a], F.L. Navarria[a,b], A. Perrotta[a], F. Primavera[a,b], A.M. Rossi[a,b], T. Rovelli[a,b], G.P. Siroli[a,b]

INFN Sezione di Catania[a], Università di Catania[b], Catania, Italy
S. Albergo[a,b,44], S. Costa[a,b,44], A. Di Mattia[a], R. Potenza[a,b], A. Tricomi[a,b,44], C. Tuve[a,b]

INFN Sezione di Firenze[a], Università di Firenze[b], Firenze, Italy
G. Barbagli[a], A. Cassese[a], R. Ceccarelli[a,b], V. Ciulli[a,b], C. Civinini[a], R. D'Alessandro[a,b], E. Focardi[a,b], G. Latino[a,b], P. Lenzi[a,b], M. Lizzo[a,b], M. Meschini[a], S. Paoletti[a], R. Seidita[a,b], G. Sguazzoni[a], L. Viliani[a]

INFN Laboratori Nazionali di Frascati, Frascati, Italy
L. Benussi, S. Bianco, D. Piccolo

INFN Sezione di Genova[a], Università di Genova[b], Genova, Italy
M. Bozzo[a,b], F. Ferro[a], R. Mulargia[a,b], E. Robutti[a], S. Tosi[a,b]

INFN Sezione di Milano-Bicocca[a], Università di Milano-Bicocca[b], Milano, Italy
A. Benaglia[a], F. Brivio[a,b], F. Cetorelli[a,b], V. Ciriolo[a,b,20], F. De Guio[a,b], M.E. Dinardo[a,b], P. Dini[a], S. Gennai[a], A. Ghezzi[a,b], P. Govoni[a,b], L. Guzzi[a,b], M. Malberti[a], S. Malvezzi[a], A. Massironi[a], D. Menasce[a], L. Moroni[a], M. Paganoni[a,b], D. Pedrini[a], S. Ragazzi[a,b], N. Redaelli[a], T. Tabarelli de Fatis[a,b], D. Valsecchi[a,b,20], D. Zuolo[a,b]

INFN Sezione di Napoli[a], Università di Napoli 'Federico II'[b], Napoli, Italy, Università della Basilicata[c], Potenza, Italy, Università G. Marconi[d], Roma, Italy
S. Buontempo[a], F. Carnevali[a,b], N. Cavallo[a,c], A. De Iorio[a,b], F. Fabozzi[a,c], A.O.M. Iorio[a,b], L. Lista[a,b], S. Meola[a,d,20], P. Paolucci[a,20], B. Rossi[a], C. Sciacca[a,b]

INFN Sezione di Padova[a], Università di Padova[b], Padova, Italy, Università di Trento[c], Trento, Italy
P. Azzi[a], N. Bacchetta[a], D. Bisello[a,b], P. Bortignon[a], A. Bragagnolo[a,b], R. Carlin[a,b], P. Checchia[a], T. Dorigo[a], U. Dosselli[a], F. Gasparini[a,b], U. Gasparini[a,b], S.Y. Hoh[a,b], L. Layer[a,45], M. Margoni[a,b], A.T. Meneguzzo[a,b], J. Pazzini[a,b], M. Presilla[a,b], P. Ronchese[a,b], R. Rossin[a,b], F. Simonetto[a,b], G. Strong[a], M. Tosi[a,b], H. YARAR[a,b], M. Zanetti[a,b], P. Zotto[a,b], A. Zucchetta[a,b], G. Zumerle[a,b]

INFN Sezione di Pavia[a], Università di Pavia[b]
C. Aime'[a,b], A. Braghieri[a], S. Calzaferri[a,b], D. Fiorina[a,b], P. Montagna[a,b], S.P. Ratti[a,b], V. Re[a], C. Riccardi[a,b], P. Salvini[a], I. Vai[a], P. Vitulo[a,b]

JHEP01(2022)177

INFN Sezione di Perugia[a], Università di Perugia[b], Perugia, Italy

G.M. Bilei[a], D. Ciangottini[a,b], L. Fanò[a,b], P. Lariccia[a,b], M. Magherini[b], G. Mantovani[a,b], V. Mariani[a,b], M. Menichelli[a], F. Moscatelli[a], A. Piccinelli[a,b], A. Rossi[a,b], A. Santocchia[a,b], D. Spiga[a], T. Tedeschi[a,b]

INFN Sezione di Pisa[a], Università di Pisa[b], Scuola Normale Superiore di Pisa[c], Pisa Italy, Università di Siena[d], Siena, Italy

P. Azzurri[a], G. Bagliesi[a], V. Bertacchi[a,c], L. Bianchini[a], T. Boccali[a], E. Bossini[a,b], R. Castaldi[a], M.A. Ciocci[a,b], R. Dell'Orso[a], M.R. Di Domenico[a,d], S. Donato[a], A. Giassi[a], M.T. Grippo[a], F. Ligabue[a,c], E. Manca[a,c], G. Mandorli[a,c], A. Messineo[a,b], F. Palla[a], S. Parolia[a,b], G. Ramirez-Sanchez[a,c], A. Rizzi[a,b], G. Rolandi[a,c], S. Roy Chowdhury[a,c], A. Scribano[a], N. Shafiei[a,b], P. Spagnolo[a], R. Tenchini[a], G. Tonelli[a,b], N. Turini[a,d], A. Venturi[a], P.G. Verdini[a]

INFN Sezione di Roma[a], Sapienza Università di Roma[b], Rome, Italy

M. Campana[a,b], F. Cavallari[a], M. Cipriani[a,b], D. Del Re[a,b], E. Di Marco[a], M. Diemoz[a], E. Longo[a,b], P. Meridiani[a], G. Organtini[a,b], F. Pandolfi[a], R. Paramatti[a,b], C. Quaranta[a,b], S. Rahatlou[a,b], C. Rovelli[a], F. Santanastasio[a,b], L. Soffi[a], R. Tramontano[a,b]

INFN Sezione di Torino[a], Università di Torino[b], Torino, Italy, Università del Piemonte Orientale[c], Novara, Italy

N. Amapane[a,b], R. Arcidiacono[a,c], S. Argiro[a,b], M. Arneodo[a,c], N. Bartosik[a], R. Bellan[a,b], A. Bellora[a,b], J. Berenguer Antequera[a,b], C. Biino[a], N. Cartiglia[a], S. Cometti[a], M. Costa[a,b], R. Covarelli[a,b], N. Demaria[a], B. Kiani[a,b], F. Legger[a], C. Mariotti[a], S. Maselli[a], E. Migliore[a,b], E. Monteil[a,b], M. Monteno[a], M.M. Obertino[a,b], G. Ortona[a], L. Pacher[a,b], N. Pastrone[a], M. Pelliccioni[a], G.L. Pinna Angioni[a,b], M. Ruspa[a,c], K. Shchelina[a,b], F. Siviero[a,b], V. Sola[a], A. Solano[a,b], D. Soldi[a,b], A. Staiano[a], M. Tornago[a,b], D. Trocino[a,b], A. Vagnerini

INFN Sezione di Trieste[a], Università di Trieste[b], Trieste, Italy

S. Belforte[a], V. Candelise[a,b], M. Casarsa[a], F. Cossutti[a], A. Da Rold[a,b], G. Della Ricca[a,b], G. Sorrentino[a,b], F. Vazzoler[a,b]

Kyungpook National University, Daegu, Korea

S. Dogra, C. Huh, B. Kim, D.H. Kim, G.N. Kim, J. Kim, J. Lee, S.W. Lee, C.S. Moon, Y.D. Oh, S.I. Pak, B.C. Radburn-Smith, S. Sekmen, Y.C. Yang

Chonnam National University, Institute for Universe and Elementary Particles, Kwangju, Korea

H. Kim, D.H. Moon

Hanyang University, Seoul, Korea

B. Francois, T.J. Kim, J. Park

Korea University, Seoul, Korea

S. Cho, S. Choi, Y. Go, B. Hong, K. Lee, K.S. Lee, J. Lim, J. Park, S.K. Park, J. Yoo

JHEP01(2022)177

Kyung Hee University, Department of Physics, Seoul, Republic of Korea
J. Goh, A. Gurtu

Sejong University, Seoul, Korea
H.S. Kim, Y. Kim

Seoul National University, Seoul, Korea
J. Almond, J.H. Bhyun, J. Choi, S. Jeon, J. Kim, J.S. Kim, S. Ko, H. Kwon, H. Lee, S. Lee, B.H. Oh, M. Oh, S.B. Oh, H. Seo, U.K. Yang, I. Yoon

University of Seoul, Seoul, Korea
W. Jang, D. Jeon, D.Y. Kang, Y. Kang, J.H. Kim, S. Kim, B. Ko, J.S.H. Lee, Y. Lee, I.C. Park, Y. Roh, M.S. Ryu, D. Song, I.J. Watson, S. Yang

Yonsei University, Department of Physics, Seoul, Korea
S. Ha, H.D. Yoo

Sungkyunkwan University, Suwon, Korea
Y. Jeong, H. Lee, Y. Lee, I. Yu

College of Engineering and Technology, American University of the Middle East (AUM), Egaila, Kuwait
T. Beyrouthy, Y. Maghrbi

Riga Technical University
T. Torims, V. Veckalns[46]

Vilnius University, Vilnius, Lithuania
M. Ambrozas, A. Juodagalvis, A. Rinkevicius, G. Tamulaitis, A. Vaitkevicius

National Centre for Particle Physics, Universiti Malaya, Kuala Lumpur, Malaysia
N. Bin Norjoharuddeen, W.A.T. Wan Abdullah, M.N. Yusli, Z. Zolkapli

Universidad de Sonora (UNISON), Hermosillo, Mexico
J.F. Benitez, A. Castaneda Hernandez, M. León Coello, J.A. Murillo Quijada, A. Sehrawat, L. Valencia Palomo

Centro de Investigacion y de Estudios Avanzados del IPN, Mexico City, Mexico
G. Ayala, H. Castilla-Valdez, I. Heredia-De La Cruz[47], R. Lopez-Fernandez, C.A. Mondragon Herrera, D.A. Perez Navarro, A. Sanchez-Hernandez

Universidad Iberoamericana, Mexico City, Mexico
S. Carrillo Moreno, C. Oropeza Barrera, M. Ramirez-Garcia, F. Vazquez Valencia

Benemerita Universidad Autonoma de Puebla, Puebla, Mexico
I. Pedraza, H.A. Salazar Ibarguen, C. Uribe Estrada

University of Montenegro, Podgorica, Montenegro
J. Mijuskovic[48], N. Raicevic

JHEP01(2022)177

University of Auckland, Auckland, New Zealand

D. Krofcheck

University of Canterbury, Christchurch, New Zealand

S. Bheesette, P.H. Butler

National Centre for Physics, Quaid-I-Azam University, Islamabad, Pakistan

A. Ahmad, M.I. Asghar, A. Awais, M.I.M. Awan, H.R. Hoorani, W.A. Khan, M.A. Shah, M. Shoaib, M. Waqas

AGH University of Science and Technology Faculty of Computer Science, Electronics and Telecommunications, Krakow, Poland

V. Avati, L. Grzanka, M. Malawski

National Centre for Nuclear Research, Swierk, Poland

H. Bialkowska, M. Bluj, B. Boimska, M. Górski, M. Kazana, M. Szleper, P. Zalewski

Institute of Experimental Physics, Faculty of Physics, University of Warsaw, Warsaw, Poland

K. Bunkowski, K. Doroba, A. Kalinowski, M. Konecki, J. Krolikowski, M. Walczak

Laboratório de Instrumentação e Física Experimental de Partículas, Lisboa, Portugal

M. Araujo, P. Bargassa, D. Bastos, A. Boletti, P. Faccioli, M. Gallinaro, J. Hollar, N. Leonardo, T. Niknejad, M. Pisano, J. Seixas, O. Toldaiev, J. Varela

Joint Institute for Nuclear Research, Dubna, Russia

S. Afanasiev, D. Budkouski, I. Golutvin, I. Gorbunov, V. Karjavine, V. Korenkov, A. Lanev, A. Malakhov, V. Matveev[49,50], V. Palichik, V. Perelygin, M. Savina, D. Seitova, V. Shalaev, S. Shmatov, S. Shulha, V. Smirnov, O. Teryaev, N. Voytishin, B.S. Yuldashev[51], A. Zarubin, I. Zhizhin

Petersburg Nuclear Physics Institute, Gatchina (St. Petersburg), Russia

G. Gavrilov, V. Golovtcov, Y. Ivanov, V. Kim[52], E. Kuznetsova[53], V. Murzin, V. Oreshkin, I. Smirnov, D. Sosnov, V. Sulimov, L. Uvarov, S. Volkov, A. Vorobyev

Institute for Nuclear Research, Moscow, Russia

Yu. Andreev, A. Dermenev, S. Gninenko, N. Golubev, A. Karneyeu, D. Kirpichnikov, M. Kirsanov, N. Krasnikov, A. Pashenkov, G. Pivovarov, D. Tlisov[†], A. Toropin

Institute for Theoretical and Experimental Physics named by A.I. Alikhanov of NRC 'Kurchatov Institute', Moscow, Russia

V. Epshteyn, V. Gavrilov, N. Lychkovskaya, A. Nikitenko[54], V. Popov, A. Spiridonov, A. Stepennov, M. Toms, E. Vlasov, A. Zhokin

Moscow Institute of Physics and Technology, Moscow, Russia

T. Aushev

JHEP01(2022)177

National Research Nuclear University 'Moscow Engineering Physics Institute' (MEPhI), Moscow, Russia

M. Chadeeva[55], A. Oskin, P. Parygin, E. Popova, V. Rusinov

P.N. Lebedev Physical Institute, Moscow, Russia

V. Andreev, M. Azarkin, I. Dremin, M. Kirakosyan, A. Terkulov

Skobeltsyn Institute of Nuclear Physics, Lomonosov Moscow State University, Moscow, Russia

A. Belyaev, E. Boos, M. Dubinin[56], L. Dudko, A. Ershov, A. Gribushin, V. Klyukhin, O. Kodolova, I. Lokhtin, S. Obraztsov, S. Petrushanko, V. Savrin, A. Snigirev

Novosibirsk State University (NSU), Novosibirsk, Russia

V. Blinov[57], T. Dimova[57], L. Kardapoltsev[57], A. Kozyrev[57], I. Ovtin[57], Y. Skovpen[57]

Institute for High Energy Physics of National Research Centre 'Kurchatov Institute', Protvino, Russia

I. Azhgirey, I. Bayshev, D. Elumakhov, V. Kachanov, D. Konstantinov, P. Mandrik, V. Petrov, R. Ryutin, S. Slabospitskii, A. Sobol, S. Troshin, N. Tyurin, A. Uzunian, A. Volkov

National Research Tomsk Polytechnic University, Tomsk, Russia

A. Babaev, V. Okhotnikov

Tomsk State University, Tomsk, Russia

V. Borchsh, V. Ivanchenko, E. Tcherniaev

University of Belgrade: Faculty of Physics and VINCA Institute of Nuclear Sciences, Belgrade, Serbia

P. Adzic[58], M. Dordevic, P. Milenovic, J. Milosevic

Centro de Investigaciones Energéticas Medioambientales y Tecnológicas (CIEMAT), Madrid, Spain

M. Aguilar-Benitez, J. Alcaraz Maestre, A. Álvarez Fernández, I. Bachiller, M. Barrio Luna, Cristina F. Bedoya, C.A. Carrillo Montoya, M. Cepeda, M. Cerrada, N. Colino, B. De La Cruz, A. Delgado Peris, J.P. Fernández Ramos, J. Flix, M.C. Fouz, O. Gonzalez Lopez, S. Goy Lopez, J.M. Hernandez, M.I. Josa, J. León Holgado, D. Moran, Á. Navarro Tobar, A. Pérez-Calero Yzquierdo, J. Puerta Pelayo, I. Redondo, L. Romero, S. Sánchez Navas, L. Urda Gómez, C. Willmott

Universidad Autónoma de Madrid, Madrid, Spain

J.F. de Trocóniz, R. Reyes-Almanza

Universidad de Oviedo, Instituto Universitario de Ciencias y Tecnologías Espaciales de Asturias (ICTEA), Oviedo, Spain

B. Alvarez Gonzalez, J. Cuevas, C. Erice, J. Fernandez Menendez, S. Folgueras, I. Gonzalez Caballero, E. Palencia Cortezon, C. Ramón Álvarez, J. Ripoll Sau, V. Rodríguez Bouza, A. Trapote, N. Trevisani

JHEP01(2022)177

Instituto de Física de Cantabria (IFCA), CSIC-Universidad de Cantabria, Santander, Spain

J.A. Brochero Cifuentes, I.J. Cabrillo, A. Calderon, J. Duarte Campderros, M. Fernandez, C. Fernandez Madrazo, P.J. Fernández Manteca, A. García Alonso, G. Gomez, C. Martinez Rivero, P. Martinez Ruiz del Arbol, F. Matorras, P. Matorras Cuevas, J. Piedra Gomez, C. Prieels, T. Rodrigo, A. Ruiz-Jimeno, L. Scodellaro, I. Vila, J.M. Vizan Garcia

University of Colombo, Colombo, Sri Lanka

MK Jayananda, B. Kailasapathy[59], D.U.J. Sonnadara, DDC Wickramarathna

University of Ruhuna, Department of Physics, Matara, Sri Lanka

W.G.D. Dharmaratna, K. Liyanage, N. Perera, N. Wickramage

CERN, European Organization for Nuclear Research, Geneva, Switzerland

T.K. Aarrestad, D. Abbaneo, J. Alimena, E. Auffray, G. Auzinger, J. Baechler, P. Baillon[†], D. Barney, J. Bendavid, M. Bianco, A. Bocci, T. Camporesi, M. Capeans Garrido, G. Cerminara, S.S. Chhibra, L. Cristella, D. d'Enterria, A. Dabrowski, N. Daci, A. David, A. De Roeck, M.M. Defranchis, M. Deile, M. Dobson, M. Dünser, N. Dupont, A. Elliott-Peisert, N. Emriskova, F. Fallavollita[60], D. Fasanella, S. Fiorendi, A. Florent, G. Franzoni, W. Funk, S. Giani, D. Gigi, K. Gill, F. Glege, L. Gouskos, M. Haranko, J. Hegeman, Y. Iiyama, V. Innocente, T. James, P. Janot, J. Kaspar, J. Kieseler, M. Komm, N. Kratochwil, C. Lange, S. Laurila, P. Lecoq, K. Long, C. Lourenço, L. Malgeri, S. Mallios, M. Mannelli, A.C. Marini, F. Meijers, S. Mersi, E. Meschi, F. Moortgat, M. Mulders, S. Orfanelli, L. Orsini, F. Pantaleo, L. Pape, E. Perez, M. Peruzzi, A. Petrilli, G. Petrucciani, A. Pfeiffer, M. Pierini, D. Piparo, M. Pitt, H. Qu, T. Quast, D. Rabady, A. Racz, G. Reales Gutiérrez, M. Rieger, M. Rovere, H. Sakulin, J. Salfeld-Nebgen, S. Scarfi, C. Schäfer, C. Schwick, M. Selvaggi, A. Sharma, P. Silva, W. Snoeys, P. Sphicas[61], S. Summers, V.R. Tavolaro, D. Treille, A. Tsirou, G.P. Van Onsem, M. Verzetti, J. Wanczyk[62], K.A. Wozniak, W.D. Zeuner

Paul Scherrer Institut, Villigen, Switzerland

L. Caminada[63], A. Ebrahimi, W. Erdmann, R. Horisberger, Q. Ingram, H.C. Kaestli, D. Kotlinski, U. Langenegger, M. Missiroli, T. Rohe

ETH Zurich - Institute for Particle Physics and Astrophysics (IPA), Zurich, Switzerland

K. Androsov[62], M. Backhaus, P. Berger, A. Calandri, N. Chernyavskaya, A. De Cosa, G. Dissertori, M. Dittmar, M. Donegà, C. Dorfer, F. Eble, T.A. Gómez Espinosa, C. Grab, D. Hits, W. Lustermann, A.-M. Lyon, R.A. Manzoni, C. Martin Perez, M.T. Meinhard, F. Micheli, F. Nessi-Tedaldi, J. Niedziela, F. Pauss, V. Perovic, G. Perrin, S. Pigazzini, M.G. Ratti, M. Reichmann, C. Reissel, T. Reitenspiess, B. Ristic, D. Ruini, D.A. Sanz Becerra, M. Schönenberger, V. Stampf, J. Steggemann[62], R. Wallny, D.H. Zhu

JHEP01(2022)177

Universität Zürich, Zurich, Switzerland
C. Amsler[64], P. Bärtschi, C. Botta, D. Brzhechko, M.F. Canelli, K. Cormier, A. De Wit, R. Del Burgo, J.K. Heikkilä, M. Huwiler, A. Jofrehei, B. Kilminster, S. Leontsinis, A. Macchiolo, P. Meiring, V.M. Mikuni, U. Molinatti, I. Neutelings, A. Reimers, P. Robmann, S. Sanchez Cruz, K. Schweiger, Y. Takahashi

National Central University, Chung-Li, Taiwan
C. Adloff[65], C.M. Kuo, W. Lin, A. Roy, T. Sarkar[37], S.S. Yu

National Taiwan University (NTU), Taipei, Taiwan
L. Ceard, Y. Chao, K.F. Chen, P.H. Chen, W.-S. Hou, Y.y. Li, R.-S. Lu, E. Paganis, A. Psallidas, A. Steen, H.y. Wu, E. Yazgan, P.r. Yu

Chulalongkorn University, Faculty of Science, Department of Physics, Bangkok, Thailand
B. Asavapibhop, C. Asawatangtrakuldee, N. Srimanobhas

Çukurova University, Physics Department, Science and Art Faculty, Adana, Turkey
F. Boran, S. Damarseckin[66], Z.S. Demiroglu, F. Dolek, I. Dumanoglu[67], E. Eskut, Y. Guler, E. Gurpinar Guler[68], I. Hos[69], C. Isik, O. Kara, A. Kayis Topaksu, U. Kiminsu, G. Onengut, K. Ozdemir[70], A. Polatoz, A.E. Simsek, B. Tali[71], U.G. Tok, S. Turkcapar, I.S. Zorbakir, C. Zorbilmez

Middle East Technical University, Physics Department, Ankara, Turkey
B. Isildak[72], G. Karapinar[73], K. Ocalan[74], M. Yalvac[75]

Bogazici University, Istanbul, Turkey
B. Akgun, I.O. Atakisi, E. Gülmez, M. Kaya[76], O. Kaya[77], Ö. Özçelik, S. Tekten[78], E.A. Yetkin[79]

Istanbul Technical University, Istanbul, Turkey
A. Cakir, K. Cankocak[67], Y. Komurcu, S. Sen[80]

Istanbul University, Istanbul, Turkey
S. Cerci[71], B. Kaynak, S. Ozkorucuklu, D. Sunar Cerci[71]

Institute for Scintillation Materials of National Academy of Science of Ukraine, Kharkov, Ukraine
B. Grynyov

National Scientific Center, Kharkov Institute of Physics and Technology, Kharkov, Ukraine
L. Levchuk

University of Bristol, Bristol, United Kingdom
D. Anthony, E. Bhal, S. Bologna, J.J. Brooke, A. Bundock, E. Clement, D. Cussans, H. Flacher, J. Goldstein, G.P. Heath, H.F. Heath, L. Kreczko, B. Krikler, S. Paramesvaran, S. Seif El Nasr-Storey, V.J. Smith, N. Stylianou[81], R. White

JHEP01(2022)177

Rutherford Appleton Laboratory, Didcot, United Kingdom

K.W. Bell, A. Belyaev[82], C. Brew, R.M. Brown, D.J.A. Cockerill, K.V. Ellis, K. Harder, S. Harper, J. Linacre, K. Manolopoulos, D.M. Newbold, E. Olaiya, D. Petyt, T. Reis, T. Schuh, C.H. Shepherd-Themistocleous, I.R. Tomalin, T. Williams

Imperial College, London, United Kingdom

R. Bainbridge, P. Bloch, S. Bonomally, J. Borg, S. Breeze, O. Buchmuller, V. Cepaitis, G.S. Chahal[83], D. Colling, P. Dauncey, G. Davies, M. Della Negra, S. Fayer, G. Fedi, G. Hall, M.H. Hassanshahi, G. Iles, J. Langford, L. Lyons, A.-M. Magnan, S. Malik, A. Martelli, J. Nash[84], M. Pesaresi, D.M. Raymond, A. Richards, A. Rose, E. Scott, C. Seez, A. Shtipliyski, A. Tapper, K. Uchida, T. Virdee[20], N. Wardle, S.N. Webb, D. Winterbottom, A.G. Zecchinelli

Brunel University, Uxbridge, United Kingdom

K. Coldham, J.E. Cole, A. Khan, P. Kyberd, I.D. Reid, L. Teodorescu, S. Zahid

Baylor University, Waco, U.S.A.

S. Abdullin, A. Brinkerhoff, B. Caraway, J. Dittmann, K. Hatakeyama, A.R. Kanuganti, B. McMaster, N. Pastika, S. Sawant, C. Sutantawibul, J. Wilson

Catholic University of America, Washington, DC, U.S.A.

R. Bartek, A. Dominguez, R. Uniyal, A.M. Vargas Hernandez

The University of Alabama, Tuscaloosa, U.S.A.

A. Buccilli, S.I. Cooper, D. Di Croce, S.V. Gleyzer, C. Henderson, C.U. Perez, P. Rumerio[85], C. West

Boston University, Boston, U.S.A.

A. Akpinar, A. Albert, D. Arcaro, C. Cosby, Z. Demiragli, E. Fontanesi, D. Gastler, J. Rohlf, K. Salyer, D. Sperka, D. Spitzbart, I. Suarez, A. Tsatsos, S. Yuan, D. Zou

Brown University, Providence, U.S.A.

G. Benelli, B. Burkle, X. Coubez[21], D. Cutts, M. Hadley, U. Heintz, J.M. Hogan[86], G. Landsberg, K.T. Lau, M. Lukasik, J. Luo, M. Narain, S. Sagir[87], E. Usai, W.Y. Wong, X. Yan, D. Yu, W. Zhang

University of California, Davis, Davis, U.S.A.

J. Bonilla, C. Brainerd, R. Breedon, M. Calderon De La Barca Sanchez, M. Chertok, J. Conway, P.T. Cox, R. Erbacher, G. Haza, F. Jensen, O. Kukral, R. Lander, M. Mulhearn, D. Pellett, B. Regnery, D. Taylor, Y. Yao, F. Zhang

University of California, Los Angeles, U.S.A.

M. Bachtis, R. Cousins, A. Datta, D. Hamilton, J. Hauser, M. Ignatenko, M.A. Iqbal, T. Lam, N. Mccoll, W.A. Nash, S. Regnard, D. Saltzberg, B. Stone, V. Valuev

University of California, Riverside, Riverside, U.S.A.

K. Burt, Y. Chen, R. Clare, J.W. Gary, M. Gordon, G. Hanson, G. Karapostoli, O.R. Long, N. Manganelli, M. Olmedo Negrete, W. Si, S. Wimpenny, Y. Zhang

JHEP01(2022)177

University of California, San Diego, La Jolla, U.S.A.

J.G. Branson, P. Chang, S. Cittolin, S. Cooperstein, N. Deelen, J. Duarte, R. Gerosa, L. Giannini, D. Gilbert, J. Guiang, R. Kansal, V. Krutelyov, R. Lee, J. Letts, M. Masciovecchio, S. May, M. Pieri, B.V. Sathia Narayanan, V. Sharma, M. Tadel, A. Vartak, F. Würthwein, Y. Xiang, A. Yagil

University of California, Santa Barbara - Department of Physics, Santa Barbara, U.S.A.

N. Amin, C. Campagnari, M. Citron, A. Dorsett, V. Dutta, J. Incandela, M. Kilpatrick, J. Kim, B. Marsh, H. Mei, M. Oshiro, M. Quinnan, J. Richman, U. Sarica, D. Stuart, S. Wang

California Institute of Technology, Pasadena, U.S.A.

A. Bornheim, O. Cerri, I. Dutta, J.M. Lawhorn, N. Lu, J. Mao, H.B. Newman, J. Ngadiuba, T.Q. Nguyen, M. Spiropulu, J.R. Vlimant, C. Wang, S. Xie, Z. Zhang, R.Y. Zhu

Carnegie Mellon University, Pittsburgh, U.S.A.

J. Alison, S. An, M.B. Andrews, P. Bryant, T. Ferguson, A. Harilal, C. Liu, T. Mudholkar, M. Paulini, A. Sanchez

University of Colorado Boulder, Boulder, U.S.A.

J.P. Cumalat, W.T. Ford, A. Hassani, E. MacDonald, R. Patel, A. Perloff, C. Savard, K. Stenson, K.A. Ulmer, S.R. Wagner

Cornell University, Ithaca, U.S.A.

J. Alexander, S. Bright-thonney, Y. Cheng, D.J. Cranshaw, S. Hogan, J. Monroy, J.R. Patterson, D. Quach, J. Reichert, M. Reid, A. Ryd, W. Sun, J. Thom, P. Wittich, R. Zou

Fermi National Accelerator Laboratory, Batavia, U.S.A.

M. Albrow, M. Alyari, G. Apollinari, A. Apresyan, A. Apyan, S. Banerjee, L.A.T. Bauerdick, D. Berry, J. Berryhill, P.C. Bhat, K. Burkett, J.N. Butler, A. Canepa, G.B. Cerati, H.W.K. Cheung, F. Chlebana, M. Cremonesi, K.F. Di Petrillo, V.D. Elvira, Y. Feng, J. Freeman, Z. Gecse, L. Gray, D. Green, S. Grünendahl, O. Gutsche, R.M. Harris, R. Heller, T.C. Herwig, J. Hirschauer, B. Jayatilaka, S. Jindariani, M. Johnson, U. Joshi, T. Klijnsma, B. Klima, K.H.M. Kwok, S. Lammel, D. Lincoln, R. Lipton, T. Liu, C. Madrid, K. Maeshima, C. Mantilla, D. Mason, P. McBride, P. Merkel, S. Mrenna, S. Nahn, V. O'Dell, V. Papadimitriou, K. Pedro, C. Pena[56], O. Prokofyev, F. Ravera, A. Reinsvold Hall, L. Ristori, B. Schneider, E. Sexton-Kennedy, N. Smith, A. Soha, W.J. Spalding, L. Spiegel, S. Stoynev, J. Strait, L. Taylor, S. Tkaczyk, N.V. Tran, L. Uplegger, E.W. Vaandering, H.A. Weber

University of Florida, Gainesville, U.S.A.

D. Acosta, P. Avery, D. Bourilkov, L. Cadamuro, V. Cherepanov, F. Errico, R.D. Field, D. Guerrero, B.M. Joshi, M. Kim, E. Koenig, J. Konigsberg, A. Korytov, K.H. Lo, K. Matchev, N. Menendez, G. Mitselmakher, A. Muthirakalayil Madhu, N. Rawal, D. Rosenzweig, S. Rosenzweig, K. Shi, J. Sturdy, J. Wang, E. Yigitbasi, X. Zuo

JHEP01(2022)177

Florida State University, Tallahassee, U.S.A.

T. Adams, A. Askew, D. Diaz, R. Habibullah, V. Hagopian, K.F. Johnson, R. Khurana, T. Kolberg, G. Martinez, H. Prosper, C. Schiber, R. Yohay, J. Zhang

Florida Institute of Technology, Melbourne, U.S.A.

M.M. Baarmand, S. Butalla, T. Elkafrawy[88], M. Hohlmann, R. Kumar Verma, D. Noonan, M. Rahmani, M. Saunders, F. Yumiceva

University of Illinois at Chicago (UIC), Chicago, U.S.A.

M.R. Adams, H. Becerril Gonzalez, R. Cavanaugh, X. Chen, S. Dittmer, O. Evdokimov, C.E. Gerber, D.A. Hangal, D.J. Hofman, A.H. Merrit, C. Mills, G. Oh, T. Roy, S. Rudrabhatla, M.B. Tonjes, N. Varelas, J. Viinikainen, X. Wang, Z. Wu, Z. Ye

The University of Iowa, Iowa City, U.S.A.

M. Alhusseini, K. Dilsiz[89], R.P. Gandrajula, O.K. Köseyan, J.-P. Merlo, A. Mestvirishvili[90], J. Nachtman, H. Ogul[91], Y. Onel, A. Penzo, C. Snyder, E. Tiras[92]

Johns Hopkins University, Baltimore, U.S.A.

O. Amram, B. Blumenfeld, L. Corcodilos, J. Davis, M. Eminizer, A.V. Gritsan, S. Kyriacou, P. Maksimovic, J. Roskes, M. Swartz, T.Á. Vámi

The University of Kansas, Lawrence, U.S.A.

J. Anguiano, C. Baldenegro Barrera, P. Baringer, A. Bean, A. Bylinkin, T. Isidori, S. Khalil, J. King, G. Krintiras, A. Kropivnitskaya, C. Lindsey, N. Minafra, M. Murray, C. Rogan, C. Royon, R. Salvatico, S. Sanders, E. Schmitz, C. Smith, J.D. Tapia Takaki, Q. Wang, J. Williams, G. Wilson

Kansas State University, Manhattan, U.S.A.

S. Duric, A. Ivanov, K. Kaadze, D. Kim, Y. Maravin, T. Mitchell, A. Modak, K. Nam

Lawrence Livermore National Laboratory, Livermore, U.S.A.

F. Rebassoo, D. Wright

University of Maryland, College Park, U.S.A.

E. Adams, A. Baden, O. Baron, A. Belloni, S.C. Eno, N.J. Hadley, S. Jabeen, R.G. Kellogg, T. Koeth, A.C. Mignerey, S. Nabili, M. Seidel, A. Skuja, L. Wang, K. Wong

Massachusetts Institute of Technology, Cambridge, U.S.A.

D. Abercrombie, G. Andreassi, R. Bi, S. Brandt, W. Busza, I.A. Cali, Y. Chen, M. D'Alfonso, J. Eysermans, G. Gomez Ceballos, M. Goncharov, P. Harris, M. Hu, M. Klute, D. Kovalskyi, J. Krupa, Y.-J. Lee, B. Maier, C. Mironov, C. Paus, D. Rankin, C. Roland, G. Roland, Z. Shi, G.S.F. Stephans, K. Tatar, J. Wang, Z. Wang, B. Wyslouch

University of Minnesota, Minneapolis, U.S.A.

R.M. Chatterjee, A. Evans, P. Hansen, J. Hiltbrand, Sh. Jain, M. Krohn, Y. Kubota, J. Mans, M. Revering, R. Rusack, R. Saradhy, N. Schroeder, N. Strobbe, M.A. Wadud

JHEP01(2022)177

University of Nebraska-Lincoln, Lincoln, U.S.A.

K. Bloom, M. Bryson, S. Chauhan, D.R. Claes, C. Fangmeier, L. Finco, F. Golf, J.R. González Fernández, C. Joo, I. Kravchenko, M. Musich, I. Reed, J.E. Siado, G.R. Snow[†], W. Tabb, F. Yan

State University of New York at Buffalo, Buffalo, U.S.A.

G. Agarwal, H. Bandyopadhyay, L. Hay, I. Iashvili, A. Kharchilava, C. McLean, D. Nguyen, J. Pekkanen, S. Rappoccio, A. Williams

Northeastern University, Boston, U.S.A.

G. Alverson, E. Barberis, C. Freer, Y. Haddad, A. Hortiangtham, J. Li, G. Madigan, B. Marzocchi, D.M. Morse, V. Nguyen, T. Orimoto, A. Parker, L. Skinnari, A. Tishelman-Charny, T. Wamorkar, B. Wang, A. Wisecarver, D. Wood

Northwestern University, Evanston, U.S.A.

S. Bhattacharya, J. Bueghly, Z. Chen, A. Gilbert, T. Gunter, K.A. Hahn, N. Odell, M.H. Schmitt, M. Velasco

University of Notre Dame, Notre Dame, U.S.A.

R. Band, R. Bucci, A. Das, N. Dev, R. Goldouzian, M. Hildreth, K. Hurtado Anampa, C. Jessop, K. Lannon, N. Loukas, N. Marinelli, I. Mcalister, T. McCauley, F. Meng, K. Mohrman, Y. Musienko[49], R. Ruchti, P. Siddireddy, M. Wayne, A. Wightman, M. Wolf, M. Zarucki, L. Zygala

The Ohio State University, Columbus, U.S.A.

B. Bylsma, B. Cardwell, L.S. Durkin, B. Francis, C. Hill, M. Nunez Ornelas, K. Wei, B.L. Winer, B.R. Yates

Princeton University, Princeton, U.S.A.

F.M. Addesa, B. Bonham, P. Das, G. Dezoort, P. Elmer, A. Frankenthal, B. Greenberg, N. Haubrich, S. Higginbotham, A. Kalogeropoulos, G. Kopp, S. Kwan, D. Lange, M.T. Lucchini, D. Marlow, K. Mei, I. Ojalvo, J. Olsen, C. Palmer, D. Stickland, C. Tully

University of Puerto Rico, Mayaguez, U.S.A.

S. Malik, S. Norberg

Purdue University, West Lafayette, U.S.A.

A.S. Bakshi, V.E. Barnes, R. Chawla, S. Das, L. Gutay, M. Jones, A.W. Jung, S. Karmarkar, M. Liu, G. Negro, N. Neumeister, G. Paspalaki, C.C. Peng, S. Piperov, A. Purohit, J.F. Schulte, M. Stojanovic[16], J. Thieman, F. Wang, R. Xiao, W. Xie

Purdue University Northwest, Hammond, U.S.A.

J. Dolen, N. Parashar

Rice University, Houston, U.S.A.

A. Baty, M. Decaro, S. Dildick, K.M. Ecklund, S. Freed, P. Gardner, F.J.M. Geurts, A. Kumar, W. Li, B.P. Padley, R. Redjimi, W. Shi, A.G. Stahl Leiton, S. Yang, L. Zhang, Y. Zhang

JHEP01(2022)177

University of Rochester, Rochester, U.S.A.
A. Bodek, P. de Barbaro, R. Demina, J.L. Dulemba, C. Fallon, T. Ferbel, M. Galanti, A. Garcia-Bellido, O. Hindrichs, A. Khukhunaishvili, E. Ranken, R. Taus

Rutgers, The State University of New Jersey, Piscataway, U.S.A.
B. Chiarito, J.P. Chou, A. Gandrakota, Y. Gershtein, E. Halkiadakis, A. Hart, M. Heindl, E. Hughes, S. Kaplan, O. Karacheban[24], I. Laflotte, A. Lath, R. Montalvo, K. Nash, M. Osherson, S. Salur, S. Schnetzer, S. Somalwar, R. Stone, S.A. Thayil, S. Thomas, H. Wang

University of Tennessee, Knoxville, U.S.A.
H. Acharya, A.G. Delannoy, S. Spanier

Texas A&M University, College Station, U.S.A.
O. Bouhali[93], M. Dalchenko, A. Delgado, R. Eusebi, J. Gilmore, T. Huang, T. Kamon[94], H. Kim, S. Luo, S. Malhotra, R. Mueller, D. Overton, D. Rathjens, A. Safonov

Texas Tech University, Lubbock, U.S.A.
N. Akchurin, J. Damgov, V. Hegde, S. Kunori, K. Lamichhane, S.W. Lee, T. Mengke, S. Muthumuni, T. Peltola, I. Volobouev, Z. Wang, A. Whitbeck

Vanderbilt University, Nashville, U.S.A.
E. Appelt, S. Greene, A. Gurrola, W. Johns, A. Melo, H. Ni, K. Padeken, F. Romeo, P. Sheldon, S. Tuo, J. Velkovska

University of Virginia, Charlottesville, U.S.A.
M.W. Arenton, B. Cox, G. Cummings, J. Hakala, R. Hirosky, M. Joyce, A. Ledovskoy, A. Li, C. Neu, B. Tannenwald, S. White, E. Wolfe

Wayne State University, Detroit, U.S.A.
N. Poudyal

University of Wisconsin - Madison, Madison, WI, U.S.A.
K. Black, T. Bose, J. Buchanan, C. Caillol, S. Dasu, I. De Bruyn, P. Everaerts, F. Fienga, C. Galloni, H. He, M. Herndon, A. Hervé, U. Hussain, A. Lanaro, A. Loeliger, R. Loveless, J. Madhusudanan Sreekala, A. Mallampalli, A. Mohammadi, D. Pinna, A. Savin, V. Shang, V. Sharma, W.H. Smith, D. Teague, S. Trembath-reichert, W. Vetens

†: Deceased
1: Also at TU Wien, Wien, Austria
2: Also at Institute of Basic and Applied Sciences, Faculty of Engineering, Arab Academy for Science, Technology and Maritime Transport, Alexandria, Egypt
3: Also at Université Libre de Bruxelles, Bruxelles, Belgium
4: Also at Universidade Estadual de Campinas, Campinas, Brazil
5: Also at Federal University of Rio Grande do Sul, Porto Alegre, Brazil
6: Also at University of Chinese Academy of Sciences, Beijing, China
7: Also at Department of Physics, Tsinghua University, Beijing, China
8: Also at UFMS, Nova Andradina, Brazil

JHEP01(2022)177

9: Also at Nanjing Normal University Department of Physics, Nanjing, China
10: Now at The University of Iowa, Iowa City, U.S.A.
11: Also at Institute for Theoretical and Experimental Physics named by A.I. Alikhanov of NRC 'Kurchatov Institute', Moscow, Russia
12: Also at Joint Institute for Nuclear Research, Dubna, Russia
13: Also at Helwan University, Cairo, Egypt
14: Now at Zewail City of Science and Technology, Zewail, Egypt
15: Now at British University in Egypt, Cairo, Egypt
16: Also at Purdue University, West Lafayette, U.S.A.
17: Also at Université de Haute Alsace, Mulhouse, France
18: Also at Tbilisi State University, Tbilisi, Georgia
19: Also at Erzincan Binali Yildirim University, Erzincan, Turkey
20: Also at CERN, European Organization for Nuclear Research, Geneva, Switzerland
21: Also at RWTH Aachen University, III. Physikalisches Institut A, Aachen, Germany
22: Also at University of Hamburg, Hamburg, Germany
23: Also at Isfahan University of Technology, Isfahan, Iran
24: Also at Brandenburg University of Technology, Cottbus, Germany
25: Also at Skobeltsyn Institute of Nuclear Physics, Lomonosov Moscow State University, Moscow, Russia
26: Also at Physics Department, Faculty of Science, Assiut University, Assiut, Egypt
27: Also at Karoly Robert Campus, MATE Institute of Technology, Gyongyos, Hungary
28: Also at Institute of Physics, University of Debrecen, Debrecen, Hungary
29: Also at Institute of Nuclear Research ATOMKI, Debrecen, Hungary
30: Also at MTA-ELTE Lendület CMS Particle and Nuclear Physics Group, Eötvös Loránd University, Budapest, Hungary
31: Also at Wigner Research Centre for Physics, Budapest, Hungary
32: Also at IIT Bhubaneswar, Bhubaneswar, India
33: Also at Institute of Physics, Bhubaneswar, India
34: Also at G.H.G. Khalsa College, Punjab, India
35: Also at Shoolini University, Solan, India
36: Also at University of Hyderabad, Hyderabad, India
37: Also at University of Visva-Bharati, Santiniketan, India
38: Also at Indian Institute of Technology (IIT), Mumbai, India
39: Also at Deutsches Elektronen-Synchrotron, Hamburg, Germany
40: Also at Sharif University of Technology, Tehran, Iran
41: Also at Department of Physics, University of Science and Technology of Mazandaran, Behshahr, Iran
42: Now at INFN Sezione di Bari, Università di Bari, Politecnico di Bari, Bari, Italy
43: Also at Italian National Agency for New Technologies, Energy and Sustainable Economic Development, Bologna, Italy
44: Also at Centro Siciliano di Fisica Nucleare e di Struttura Della Materia, Catania, Italy
45: Also at Università di Napoli 'Federico II', Napoli, Italy
46: Also at Riga Technical University, Riga, Latvia
47: Also at Consejo Nacional de Ciencia y Tecnología, Mexico City, Mexico
48: Also at IRFU, CEA, Université Paris-Saclay, Gif-sur-Yvette, France
49: Also at Institute for Nuclear Research, Moscow, Russia
50: Now at National Research Nuclear University 'Moscow Engineering Physics Institute' (MEPhI), Moscow, Russia

JHEP01(2022)177

51: Also at Institute of Nuclear Physics of the Uzbekistan Academy of Sciences, Tashkent, Uzbekistan
52: Also at St. Petersburg State Polytechnical University, St. Petersburg, Russia
53: Also at University of Florida, Gainesville, U.S.A.
54: Also at Imperial College, London, United Kingdom
55: Also at P.N. Lebedev Physical Institute, Moscow, Russia
56: Also at California Institute of Technology, Pasadena, U.S.A.
57: Also at Budker Institute of Nuclear Physics, Novosibirsk, Russia
58: Also at Faculty of Physics, University of Belgrade, Belgrade, Serbia
59: Also at Trincomalee Campus, Eastern University, Sri Lanka, Nilaveli, Sri Lanka
60: Also at INFN Sezione di Pavia, Università di Pavia, Pavia, Italy
61: Also at National and Kapodistrian University of Athens, Athens, Greece
62: Also at Ecole Polytechnique Fédérale Lausanne, Lausanne, Switzerland
63: Also at Universität Zürich, Zurich, Switzerland
64: Also at Stefan Meyer Institute for Subatomic Physics, Vienna, Austria
65: Also at Laboratoire d'Annecy-le-Vieux de Physique des Particules, IN2P3-CNRS, Annecy-le-Vieux, France
66: Also at Şırnak University, Sirnak, Turkey
67: Also at Near East University, Research Center of Experimental Health Science, Nicosia, Turkey
68: Also at Konya Technical University, Konya, Turkey
69: Also at Istanbul University - Cerrahpasa, Faculty of Engineering, Istanbul, Turkey
70: Also at Piri Reis University, Istanbul, Turkey
71: Also at Adiyaman University, Adiyaman, Turkey
72: Also at Ozyegin University, Istanbul, Turkey
73: Also at Izmir Institute of Technology, Izmir, Turkey
74: Also at Necmettin Erbakan University, Konya, Turkey
75: Also at Bozok Universitetesi Rektörlügü, Yozgat, Turkey
76: Also at Marmara University, Istanbul, Turkey
77: Also at Milli Savunma University, Istanbul, Turkey
78: Also at Kafkas University, Kars, Turkey
79: Also at Istanbul Bilgi University, Istanbul, Turkey
80: Also at Hacettepe University, Ankara, Turkey
81: Also at Vrije Universiteit Brussel, Brussel, Belgium
82: Also at School of Physics and Astronomy, University of Southampton, Southampton, United Kingdom
83: Also at IPPP Durham University, Durham, United Kingdom
84: Also at Monash University, Faculty of Science, Clayton, Australia
85: Also at Università di Torino, Torino, Italy
86: Also at Bethel University, St. Paul, Minneapolis, U.S.A.
87: Also at Karamanoğlu Mehmetbey University, Karaman, Turkey
88: Also at Ain Shams University, Cairo, Egypt
89: Also at Bingol University, Bingol, Turkey
90: Also at Georgian Technical University, Tbilisi, Georgia
91: Also at Sinop University, Sinop, Turkey
92: Also at Erciyes University, Kayseri, Turkey
93: Also at Texas A&M University at Qatar, Doha, Qatar
94: Also at Kyungpook National University, Daegu, Korea

JHEP01(2022)177